

THE DESIGN OF HIGH-POWER
ACCELERATOR TARGETS

A thesis submitted in fulfilment of the requirements
for the degree of Master of Philosophy by

JOHN RICHARD WILKINSON

April 1977

University of Aston
in Birmingham

SUMMARY

Activation analysis using (P, γ) resonances has hitherto been largely restricted to the assay of fluorine. With a view to extending this technique to other elements, computer programs have been developed for calculating the temperature distribution in an accelerator target, and hence the maximum permissible beam power. Attempts were made to verify these calculations by experiment. Graphical results of these calculations, for various target shapes and materials, are given, with particular regard to targets suitable for use on the 3 Mev Dynamitron accelerator of the Birmingham Radiation Centre.

ACKNOWLEDGEMENTS

My thanks are due , first and foremost, to Professor S. E. HUNT , for suggesting and supervising this project ; and to Dr. L. G. EARWAKER and his staff for allowing me to use their facilities at the Birmingham Radiation Centre.

I would also like to thank Dr. M. R. HAWKESWORTH for allowing me to work on his beam line on the Dynamitron ; and Dr. B. O'CONNELL for permitting me to 'sit in' on his fluorine experiments.

Finally, I must extend my thanks to Dr. Bill LAKIN and Mrs. Sandra DILLON , both formerly at the Radiation Centre, for their help and advice on all matters relating to the computing ; and, in particular, to Mr. John DOWN, for many helpful discussions.

CONTENTS

INTRODUCTION	I
FACTORS AFFECTING SENSITIVITY	5
TARGET DESIGN	8
COMPARISON WITH EXPERIMENT	19
RESULTS	25
APPLICATIONS TO SPECIFIC TARGET DESIGNS	28
Appendix : HP ALGOL PROGRAMS RWCON, RWELB & RWELS	31
REFERENCES	47
TABLES	51
DIAGRAMS	54

INTRODUCTION

Until fairly recently, non-destructive activation analysis has been entirely carried out by neutron irradiation, using either nuclear reactors or accelerator sources. In contrast to chemical separation methods, this can take advantage of very short half-life induced activities, and leaves the sample intact (1,2). This purely instrumental technique has been applied to charged particle activation for some purposes.

The range of charged particles in solids is quite short : typically, for protons of a few Mev energy, no more than 50μ . So, whereas neutron activation analysis measures the impurity level throughout the bulk of the specimen, charged particle activation analysis (CPAA) is more suitable for surface or thin-film studies (3).

Conventional (i.e. neutron) activation analysis is mainly concerned with long-life induced activity, and usually involves separation of the active species from its' matrix. Many nuclear transitions, however, are rapid : e.g. γ -radiation emitted during de-excitation of excited nuclear states. The study of such prompt radiation does not permit chemical separation, but must be carried out on the intact sample, often even during the irradiation. Penetrating radiation or charged particles can be used for this purpose. Charged particles are particularly suitable for assaying light elements, as the Coulomb barrier militates against reactions with heavier nuclei ; indeed, yields are small beyond calcium and negligible beyond iron. This results in fewer interferences and simpler spectra. CPAA is therefore complementary to X-ray fluorescence, which is unsuitable for elements at the lower end of the periodic table (4). The Coulomb barrier increases with the charge of the incident ion, so protons and deuterons are favoured as bombarding particles, rather than helium ions (5). By contrast, neutron activation analysis must contend with interferences arising from elements of all atomic weights, modified only by the variable reaction cross-sections.

Due to the high Q-value of many reactions, even low energy particles can, on bombardment, form highly excited states, whose decay can be complex. However, many transitions are of low yield. Much information on the characteristics of (p, γ) reactions is available in the literature (6,7,8,9,10,11).

Various bombarding particles and nuclear reactions can be used for CPAA. RUBIN et al (12) used the elastic scattering of 2 Mev protons for surface analysis. They also assayed fluorine in opal glass by means of the $^{19}\text{F}(p,\alpha)^{16}\text{O}$ reaction, and examined (d,p) reactions, reaching a sensitivity of $0.01\mu\text{g}/\text{cm}^2$. SIPPEL and GLOVER (4) assayed geochemical samples for several light elements by bombardment with protons, deuterons and alpha particles to a sensitivity greater than 0.1%.

Deuterons have been much used : e.g. by PIERCE et al (13) and ENGLAND et al (14) for the measurement of carbon in steel using the (d, γ) reaction ; the former established a linear relationship between γ -ray yield and carbon concentration, which ranged from 0.04% to 0.69%. AMSEL et al (15,16,17) used the charged particles resulting from the (d, α) and (d,p) reactions for the estimation of oxygen in metal or oxide substrates. ANDERS (18) also used the (d,p) reaction, as well as elastic scattering of deuterons, with a variety of samples, achieving a sensitivity of $10\mu\text{g}/\text{cm}^2$. MÖLLER et al (19) monitored neutrons from (d,n) reactions with carbon, nitrogen and oxygen in steel substrates. They measured the neutron energy by the time-of-flight method, and obtained information on the depth distribution of the impurities. A sensitivity of $0.1\mu\text{g}/\text{cm}^2$ was claimed.

Helium-3 ions have also been used as bombarding particles, notably by RICCI and HAHN (20), who obtained a sensitivity greater than 1ppm for oxygen in various matrices.

Protons have perhaps been more widely used as an analytic tool than other charged particles (5). The techniques used cover both elastic scattering (3,12,18) and nuclear reactions. Among the latter, the $^{19}\text{F}(p,\alpha)^{16}\text{O}$ reaction, because of its' huge cross-section, has been the most used,

usually by monitoring the prompt γ -ray emission. Thus, it has been used for the determination of fluorine in opal glass (12), reactor graphite (21), polythene sheeting (22) (sensitivity 250 ppm), tantalum (17,23), and various other materials (24) (sensitivity 10 ppm). BEWERS and FLACK assayed liquids and gases as well as solids (25) (sensitivity 27 ppm). The same technique has been applied to some other elements : e.g. carbon in steel (26,27) ; geological samples (28) ; and light elements such as beryllium, boron, sodium, magnesium, aluminium and phosphorus, in various substrates (6,10,11,29,30). Because of the lower cross-sections, the sensitivities obtained for these elements were generally poorer : aluminium (29) 10-100 ppm at 10 μ A beam current; phosphorus (30) 50-1000 ppm; beryllium (11) 10,000 ppm; compared with 0.5 ppm for fluorine. Oxygen has also been assayed by monitoring the emitted alpha-particles (31).

Monitoring the emergent alpha-particles has been used to determine the depth distribution of an element in its' matrix. The initially mono-energetic alpha-particles will be slowed down in the substrate ; their emergent energies, coupled with information on the stopping power of the medium, will indicate the depth at which the reaction took place. AMSEL and SAMUEL (31) were the first to do this, using implanted ^{18}O in oxide films, and aluminium in tantalum. It has also been applied to oxygen in other matrices : quartz (32), gallium phosphide (33), titanium dioxide (34) and chromium (35). A variety of de-convolution techniques for extracting the concentration profile from the yield were used. A similar technique has been used by ZIEGLER (36,37) with the (n,α) and (α,α) reactions of boron.

The cross-sections for (p,γ) reactions in light elements, expressed as a function of incident proton energy, usually exhibit sharp resonances. These, too, can be employed to determine the depth distribution of the target element in a substrate by bombarding the sample with protons at an energy above resonance. When the protons slow down to the resonance energy, the (p,γ) reaction will be excited in the impurity atoms. The

γ -ray yield will be a measure of the elemental concentration at the depth corresponding to that energy value. Thus, in principle, concentration as a function of depth can be computed from the curve of yield against incident proton energy.

In practice, the computation is not straightforward. Usually there are several resonances, not just one. Often they are not intrinsically very sharp, and are effectively broadened further by the energy spread in the beam. This is increased by 'straggling', a statistical result of the random collision events in the matrix; hence the depth resolution obtained decreases with depth. The complexities of the resulting calculation have been one of the limiting factors hindering wider application of this technique (42).

Nonetheless, it has been applied by several groups, principally to the determination of fluorine in e.g. tooth enamel (36,37), Zircaloy (38), chromium plate (41,42) and other metals (43). The attraction of the $^{19}\text{F}(p,\alpha\gamma)^{16}\text{O}$ reaction has been its very large cross-section: up to 661 mb at the 872 keV resonance (10), with smaller resonances of 300, 180 and 102 mb. Only some low-abundance isotopes exhibit stronger resonances: ^{13}C (340 mb); ^{15}N (800, 425, 340, 300 mb). The common isotopes of other elements exhibit resonances at least two orders of magnitude smaller. Nevertheless, some work has been done on them e.g. aluminium (31,44,45) and sodium (45). Similarly, other proton reactions can be used: e.g. $(p,p'\gamma)$ for silicon and sulphur in semiconductors (46).

FACTORS AFFECTING SENSITIVITY

The sensitivity of activation analysis is determined by the cross-section of the element being analysed for the reaction being used, the efficiency of the detection system, and the time rate of the nuclear reactions occurring in the target i.e. the ion beam current.

The cross-section for many reactions increases rapidly as the ion beam energy approaches that needed to produce an excitation energy equal to an excited state of the compound nucleus. In other words, the gamma-ray yield curve exhibits sharp resonances, whose cross-section may be of the order of hundreds of millibarns, as compared to perhaps tens of microbarns away from a resonance (38). Obviously, it is advantageous to operate at an energy above a big resonance in a thick target to maximise yield.

The detection systems used have usually been thallium-doped sodium iodide crystal scintillators, which offer higher sensitivity than solid-state detectors, although with much poorer resolution. Naturally, the larger the crystal used, the more sensitive the assay will be. HENSHAW, using a 3" x 3" NaI (ThI) crystal, achieved a sensitivity of about 200 ppm for a beam current of 200 nA for the determination of fluorine in polythene sheeting (22). WORMLEY, using a 5" x 5" crystal, obtained a sensitivity of about 100 ppm for a current of less than 100 nA for fluorine in tooth enamel (38); while CHEN, with a similar detector, reached 10 ppm for a current of 10 nA with ammonium fluoride (24).

For a given detection system and target element, sensitivity is limited only by ion beam current. Beam currents in the experiments mentioned above have often been no more than a few nano-amperes, which is adequate for some work with fluorine; and rarely more than a few micro-amperes, which still permits only insensitive analysis of other elements. GOLICHEFF et al (10) have calculated theoretical detection sensitivities for a number of elements. They assumed an aluminium matrix, and a beam current of 1 nA. For fluorine, easily the most favourable case, they find a detection sensitivity of one part in 333,000 by weight. Lithium and nitrogen are

more than two orders of magnitude less accessible, one part in 2000 and 1000 respectively ; while beryllium, boron and carbon are fully three orders of magnitude lower than fluorine, at one part in 333, 285 and 143 respectively. But clearly, if the beam current could be increased to the region of 1 mA, impurity levels of those elements could be determined to a level of sensitivity comparable to that now possible with fluorine. This would be desirable in semi-conductor studies, for example.

For neutron activation analysis, high currents are also clearly desirable, the neutron yield being proportional to beam current. However, the necessity for an elaborate cooling system, consisting, as it may do, of low atomic weight material, will tend to soften the neutron spectrum. For thermal neutron activation analysis, of course, this would present no problem.

In recent years, high current accelerators have become available : e.g. the 3 Mev Dynamitron of the Birmingham Radiation Centre, which can deliver proton beams of up to 2 mA current.

The limiting factor in high-current operation is target heating. A 2 mA beam of 3 Mev protons carries 6 kW of power, the greater part of which is to be dissipated in a target at the end of a 2" flight tube, i.e. in an area of no more than 20 cm²; in practice, less. Clearly, beam power densities of 1 kW/cm² or more, with their attendant heating problems, will be met with. Power densities of this order are sometimes encountered in accelerator targets for neutron generation. These are usually made of tritiated titanium, or of lithium or beryllium metal. The target face is usually very thin (<1mm) and cooled with fast-flowing water on the back face. Beam power densities of up to 10 kW/cm² have been reported for such arrangements (47,48,49,50,51,52). Increasingly, rotating neutron targets are being used to alleviate heating problems (53,54,55,56,57,58). Usually, of course, this solution cannot be adopted when the target is a sample for analysis, though it has been used in a special case (30). The limiting temperature for neutron-generating targets is usually taken as being

only a little below that at which actual structural damage or melting (i.e. 'burnout') would occur (45,46). In analytical samples, such severe heating cannot normally be tolerated, as the elemental distribution under investigation might change during the course of the irradiation (22).

Hitherto, most work in the literature on the design of target cooling systems has been based on empirical data rather than calculation (48,49); the latter has usually been based on simplified analytical or semi-analytical methods (47,59,60,61).

TARGET DESIGN

Introduction

In the work which follows, an attempt has been made to devise computer programs which enable one to determine the temperature distribution in a liquid-cooled target of fairly general geometric configuration. To this end, the following simplifying assumptions have been made :

1 The shape of the target is a right circular cylinder with one face (not necessarily flat) exposed to the ion beam in vacuum. Some, or all, of the other surfaces are cooled by a circulating fluid. Provision must be made for indented coolant channels in the sides.

2 The beam is circular in cross-section, and axial.

3 The incident beam power is converted entirely to thermal power on the target surface. That this assumption is valid can be seen by considering a flat plate of conductivity K , area A and thickness L , heated uniformly by a power input of Q watts at one side, and cooled on the other. The temperature drop across the plate will be, by Fourier's law :

$$\Delta T_1 = \frac{QL}{KA}$$

if all the beam power is converted to heat at the surface. However, if the power is generated within a thickness l below the incident surface (59) :

$$\Delta T_2 = \frac{Q}{KA} \left(L - \frac{l}{2} \right)$$

Here, l will be simply the range of the beam particles in the target material ; for 3 MeV protons, this will typically be 20 - 30 μ , much smaller than L , the target thickness. So, in practice, ΔT_2 is virtually equal to ΔT_1 ; thus we may indeed assume that the beam yields its' power entirely at the target face.

4 The power density in the beam is assumed to be uniform over the cross-sectional area i.e. a 'top hat' power distribution.

5 The thermal conductivity K is assumed constant and isotropic throughout the target, and to be independent of temperature. Similarly, the heat transfer coefficient H between target and coolant is assumed to be uniform over the cooled surfaces of the target.

6 Radiation losses are assumed to be from the top face (i.e. the face exposed to the beam) only. Such losses are likely to be comparatively small in any case, and, given the strong temperature dependence of radiation, radiation loss from the cooled surfaces can be neglected.

Such a configuration, like most problems in heat transfer, is not simple enough to permit a practicable analytic solution. One must therefore resort to numerical methods. These are of essentially two types : a normal iterative method, the Gauss-Seidel process ; and the relaxation method, due to Southwell.

Southwell's Relaxation Method

This method was attempted first, as it is particularly suited to manual calculation, and the course of the computation can be visualised more clearly in physical terms. It was originally devised for calculating stresses in networks of rods, but is readily applicable to any problem which reduces to solving Laplace's equation, such as steady-state heat flow (62,63).

As applied to heat flow, Laplace's equation is

$$\nabla^2 T = 0 \quad (1)$$

where T is the temperature at a point (x,y,z) .

In a practical problem, we may be presented with boundary conditions in the form of fixed temperatures, or in the form of heat inputs or outputs (e.g. the power in a beam, or the heat transfer coefficient and temperature of a coolant).

The initial step in any relaxation solution is to divide the body up by a uniform grid, so defining a three-dimensional mesh of points of spacing h (fig.1).

At any point O , the temperature T can be Taylor-expanded thus :

$$\begin{aligned} T_1 = T_0 + \left(\frac{dT}{dx}\right)_0 (x-x_0) + \frac{1}{2!} \left(\frac{d^2T}{dx^2}\right)_0 (x-x_0)^2 + \frac{1}{3!} \left(\frac{d^3T}{dx^3}\right)_0 (x-x_0)^3 + \dots + \text{higher terms} \\ + \dots \dots \text{analogous terms in } y \\ + \dots \dots \text{analogous terms in } z. \end{aligned}$$

If, for x , we substitute x_0+h (for point 1), or x_0-h (for point 3), we obtain :

$$T_1 = T_0 + h\left(\frac{dT}{dx}\right)_0 + \frac{h^2}{2}\left(\frac{d^2T}{dx^2}\right)_0 + \frac{h^3}{6}\left(\frac{d^3T}{dx^3}\right)_0 + \dots$$

$$T_3 = T_0 - h\left(\frac{dT}{dx}\right)_0 + \frac{h^2}{2}\left(\frac{d^2T}{dx^2}\right)_0 - \frac{h^3}{6}\left(\frac{d^3T}{dx^3}\right)_0 + \dots$$

So :

$$T_1 + T_3 = 2 \cdot T_0 + h^2\left(\frac{d^2T}{dx^2}\right)_0 + \dots \text{ higher terms } \dots$$

Neglecting the higher terms, which rapidly become smaller as the grid spacing h is made finer, we obtain the finite difference approximation of $\frac{d^2T}{dx^2}$:

$$h^2\left(\frac{d^2T}{dx^2}\right) = T_1 + T_3 - 2 \cdot T_0$$

Similarly, for the y and z axes :

$$h^2\left(\frac{d^2T}{dy^2}\right) = T_2 + T_4 - 2 \cdot T_0$$

$$h^2\left(\frac{d^2T}{dz^2}\right) = T_5 + T_6 - 2 \cdot T_0$$

Substituting in Laplace's equation (1) :

$$T_1 + T_2 + T_3 + T_4 + T_5 + T_6 - 6 \cdot T_0 = 0$$

We now define a residual, Q , such that :

$$Q = T_1 + T_2 + T_3 + T_4 + T_5 + T_6 - 6 \cdot T_0 \quad (2)$$

$$\text{or : } Q = \sum_{n=1}^6 T_n - 6 \cdot T_0$$

For any arbitrary guesses at the temperatures T_0, T_n , a value of Q can be calculated. In general, it will be non-zero. The problem is to reduce the residual Q to zero at every point, when Laplace's equation will be satisfied.

In physical terms, equation (2) can be regarded as the thermal budget for the point 0 : each difference $T_n - T_0$ is a measure of the heat flow from point N to point 0. Clearly, for a system in thermal equilibrium, the net heat flow into or out of any point in the system must be zero, hence $Q = 0$.

The relaxation procedure consists of : first, imposing a uniform mesh of points on the target ; then, guessing the temperatures at each node of the grid ; then, calculating the residuals at each node using eq.(2) ;

finally, 'relaxing' (i.e. systematically reducing) the residuals until they all become zero, or as close to zero as the required accuracy demands.

This last stage can best be carried out by selecting the point with the largest residual, say a point with co-ordinates i, j, k and residual Q . This residual is then set equal to zero, and its' excess heat inflow or outflow shared between its' neighbours in accordance with the residual equation (2) at that point. For a point deep inside a body, this will be

$$Q_{ijk} = T_{i-1,j,k} + T_{i+1,j,k} + T_{i,j-1,k} + T_{i,j+1,k} + T_{i,j,k-1} + T_{i,j,k+1} - 6 \cdot T_{i,j,k}$$

A unit change of temperature at this point will clearly result in a change of -6 to the residual. A relaxation pattern can be drawn up as shown in fig. 2 : i.e. one-sixth of the value of Q is added to each of the neighbouring residuals, and to the temperature T . For the boundaries of a body, e.g. the faces, edges and corners of a cubical block, the relaxation patterns are somewhat different (fig. 3).

The patterns shown above apply to a cubical mesh. For a rectangular mesh, the patterns can be expressed using the parameter P , the ratio of cell height to cell breadth (fig. 4).

The residual equations for a point on the boundary of the body, in contact with the coolant fluid, will contain an added term for heat output from the body, expressed in terms of the coolant bulk temperature and a heat transfer coefficient between solid and liquid. Likewise, for a point on the top face, under the beam, there will be an added numerical term expressing the beam power.

When the residual equation for each point has been set up, the relaxation procedure is started in accordance with the patterns given above. The mechanics of the computation involve solely the residuals ; the alterations in temperature are incidental.

For computer operation, two three-dimensional arrays are used, one for the temperatures (T), the other for the residuals (Q), the dimensions of both being the same as the number of points into which the target is subdivided. An arbitrary guess is made of the temperatures, and the

residuals are calculated. This takes up the bulk of the program, though only a small part of the execution time. A sub-routine then scans the residuals to find the highest one. The corresponding point is then relaxed in accordance with the appropriate pattern above. This is repeated until the highest value of Q is below a pre-ordained level, when the temperatures are read off to the output device.

This technique was originally devised with manual operation in mind, and it is the best method for this if a reasonably small number of points is used. It offers opportunities for judgement to be exercised by a practised calculator, in that a faster solution can be obtained by such techniques as over-relaxation, block relaxation and the like. It is virtually impossible, however, to program a computer to take advantage of these features of the method ; it is cumbersome to set up on a computer, and therefore really no better than a standard iterative solution. Nor does it readily lend itself to handling non-rectangular geometries; e.g. a cylinder. A rectangular grid would have to be imposed on this, making for extremely cumbersome border relaxations.

The Gauss-Seidel Iterative Process

This is a more direct method for machine computation. Consider a point a , in thermal contact by conduction with another point, or points, b , and by convection with a point, or points, c . There may also be heat generated, or incident on a surface, which may be represented as q_g . So the total heat input to a is given by :

$$q_a = K_{ba}(t_b - t_a) + K_{ca}(t_c - t_a) + q_g$$

where K_{ba} , K_{ca} are the conductances between the points b, c and a . In a steady-state system, q_a will be zero at every point ; i.e.

$$K_{ba}t_b + K_{ca}t_c - \sum K_a t_a + q_g = 0$$

where $\sum K_a$ represents the summation of the conductances between point a and its' various adjacent points.

For the temperature at a , we get :

$$t_a = \frac{K_{ca}}{\sum K_a} t_c + \frac{K_{ba}}{\sum K_a} t_b + \frac{q_g}{\sum K_a} \quad (3)$$

This states that the temperature at any point in equilibrium is given by a weighted mean of the temperatures of the surrounding points, plus an appropriate term for direct heat inputs.

In the Gauss-Seidel method, the system is divided up by a mesh as before, and initial temperatures are guessed. Then the temperature at each point is replaced by a weighted mean, as in equation (3) above, of the adjacent temperatures. This is repeated indefinitely (63).

In a rectangular mesh, the conductances would be KA/L and HA for conduction and convection respectively, where A and L are the area and length of each mesh cell. If the target under consideration is a cylindrical block, with a circular, axial beam spot on the top face, the problem can be reduced from three dimensions to two dimensions because of radial symmetry. In such a case, each cell of the mesh would be, not a parallelepiped, but a circular ring of rectangular cross-section ; centred on, and normal to, the beam axis. The target is divided into a number of these, each one characterised by a radius R and a height above the back face Z . The temperature at any point will in general vary with R and Z , but can be assumed constant throughout the ring.

Each ring interacts thermally with its' immediate neighbours, usually four in number (except at a face or edge). The conductances determining the heat flow between them are more complex than for the rectangular case, being dependent on R for the ring in question.

For example, in fig. 5 we have, for the conductance $K_{\bar{z}}$ between interior rings (R,Z) and $(R,Z+I)$ (or $(R,Z-I)$) :

$$K_{\bar{z}} = 2\pi KR(\Delta R)^2 / \Delta Z$$

where K is the thermal conductivity of the material. Using the well-known formula for the conductance of an annulus (67) we have, for the conductances $K_{R\uparrow}$, $K_{R\downarrow}$ between ring (R,Z) and rings $(R+I,Z)$, $(R-I,Z)$ respectively:

$$K_{R\uparrow} = \frac{2\pi K \cdot \Delta Z}{\ln\left(\frac{R+I}{R}\right)} \quad ; \quad K_{R\downarrow} = \frac{2\pi K \cdot \Delta Z}{\ln\left(\frac{R}{R-I}\right)}$$

Clearly, for $R = 0, I$ these two expressions are undefined. It is therefore

necessary to ignore the two innermost points in the computation. Naturally this will distort the resulting temperature distribution, but the distortion can be made tolerably small by using a sufficiently fine mesh division. In practice, the the temperatures at these two values of R were set equal to those at (2,Z) at the end of each iteration.

A more satisfactory formulation, which obviates the need for logarithmic terms in the expression for the radial conductance, is to use the definition of conductance for a small element : conductivity x area / length, taking the effective area of the annulus as the average between the areas of the inner and outer faces. This yields :

$$K_{\uparrow\uparrow} = 2\pi K \left(R + \frac{1}{2}\right) \cdot \Delta Z \quad ; \quad K_{\downarrow\downarrow} = 2\pi K \left(R - \frac{1}{2}\right) \cdot \Delta Z \quad (4)$$

These formulae are satisfactory for all values of R. Equations (4) are for complete internal rings. Similar expressions may be easily derived for rings at boundaries or edges. For a completely general treatment, the number of different ring types is quite large, about 54. However, by imposing not very onerous restrictions on the geometries to be treated, this number can be reduced to 24. Table I displays schematic cross-sections of these rings. Fig. 6 indicates the conductances involved for a completely general point. From this, the radial and vertical conductances for any point in table I may be found. When this has been done an equation may be drawn up for each ring type, setting its' temperature equal to the sum of the temperatures in the adjacent rings, suitably weighted by the appropriate conductance. The resulting equations are given in Table II. These equations are for annuli with no heat input; for equations corresponding to points on the top face, there is an additive term for the heat input from the beam.

Radiation, varying as it does non-linearly with temperature, presents difficulties for numerical calculation. In this program, it has been treated as a negative heat input term. As each point on the top surface is scanned, as well as adding in any beam power term that might be required, a radiative term Q_R is subtracted :

$$Q_R = \sigma \epsilon S A (T_{s,z}^4 - T_c^4)$$

where σ is Stefan's constant, ϵ is the emissivity of the surface, S is the shape factor, and $T_{s,z}$ and T_c are the absolute temperatures of the surface point and surrounding environment.

When these equations have been drawn up, a control matrix is required to command the computer to read the correct equation for each point as it scans the matrix during each iteration. This is generated by a separate program, RWCON. The input for RWCON is a tape (paper or magnetic) giving in sequence a number for each point (ring) (R,Z) of the target geometry, in accordance with the following convention : any point outside the target is given the value -I ; any point in or on the target is given the value I, except at a cooled boundary, where it takes the value 0. Such a tape is easily generated by a simple program for even quite complicated geometries. Using this input, RWCON generates the control matrix by 'looking' at each point on the input matrix, and its' adjacent points, and sorting the point into an appropriate category according to which type of ring it is seen to represent : e.g. a point in the middle of the top face, on a cooled edge, an uncooled back face &c. (see Table I). These categories are given different integral numerical values, corresponding to the labelling of the equations in the main iterative program RWEL. Thus a control matrix is generated onto paper or magnetic tape. This forms the input for RWEL, which performs the iterative computation proper (see Appendix).

The control matrix embodies the geometric shape of the target. In addition, RWEL requires certain physical data before proceeding : the overall dimensions (radius, thickness) of the target, the radius of the ion beam, the thermal conductivity of the target material, the heat transfer coefficient at cooled boundaries, the coolant temperature, and the beam power (beam voltage x ion current); also, a value for the initial guess to which the temperatures are to be first set.

Given these data, the computer scans the control matrix, and at each

point executes the equation corresponding to the numerical value at that point. It repeats this until directed to stop ; it then feeds the resulting temperature distribution to an output device (line printer or magnetic tape recorder).

The computer can be directed to stop after a given number of iterations has been performed. This is not a flexible procedure, as there is no way of predicting how many iterations will be sufficient. A more satisfactory method consists of monitoring the outflow of heat from the target. In a steady-state, when the final temperature distribution has been attained, this must equal the heat input from the ion beam. A sub-routine in the program periodically calculates the quantity of heat flowing into the coolant, using the conductances for the relevant boundary points. If it falls within a certain percentage value of the beam power, the computation stops. The total radiated power is monitored along with the heat outflow to the coolant ; the former must be added to the latter when testing for heat balance to terminate the program.

Accelerating the Convergence

The Gauss-Seidel method outlined above tends to take a great deal of computer time. Typically, several thousand iterations, perhaps taking as long as two hours altogether, may be necessary. Therefore, it is desirable to accelerate the convergence, if possible. There are two methods of achieving this.

The first is analogous to over-relaxation in the Southwellian relaxation method. In the Gauss-Seidel process, we have, for an interior point:

$$T_{i,j}^{n+1} = f(T')$$

i.e. the value of T at the $(n+1)$ th iteration is given by some function of the surrounding points T' , so that we have, for the difference in T between two successive iterations :

$$T_{i,j}^{n+1} - T_{i,j}^n = \beta (f(T') - T_{i,j}^n)$$

where $\beta = 1$.

If, instead, β takes a value between 1 and 2, the values will converge

faster. β is known as the relaxation coefficient. The resulting iterative process is the extrapolated Liebmann method ; the Gauss-Seidel process is a special case of it (64). Thus, we obtain :

$$T_{i,j}^{n+1} = \beta f(T^i) + (I - \beta) T_{i,j}^n \quad (5)$$

The higher the value of β , the more rapid the convergence, but instability may occur if $\beta \cong 1.8$. Normally, β was set at 1.75 .

The dramatic effect of over-relaxation is shown in fig. 7. A tenfold decrease in execution time may result for a high value of β .

Another technique for speeding the convergence is the Aitken \mathcal{S}^2 -process (65,66). If we have three equally spaced successive iterates T^n, T^{n+m}, T^{n+2m} of a variable whose 'true' value is T , it is assumed that successive iterates differ from T by an amount proportional to a factor M .

$$\begin{aligned} \text{i.e.} \quad T - T^n &= M (T - T^{n+m}) \\ T - T^{n+m} &= M (T - T^{n+2m}) \end{aligned}$$

Eliminating M , we find :

$$T = \frac{T^n T^{n+2m} - (T^{n+m})^2}{T^n + T^{n+2m} - 2 \cdot T^{n+m}} \quad (6)$$

This will generally be a better guess. Clearly, the iterates need not be consecutive, though they must be separated by the same number of iterations.

A drawback to this method is that it requires considerable computer storage capacity ; for, in addition to the usual matrix for the temperature, two additional matrices are required. Two successive iterations are stored in these. After the next iteration, the values in the temperature matrix are replaced with values given by eq. 6 above. Consequently, on the Hewlett-Packard 2100A computer used, this technique could only be applied to target configurations involving a small control matrix.

It is important not to apply the \mathcal{S}^2 -process too early in a run. The early iterations tend to be atypical, and wildly erratic values might result if the method was applied during this phase. This is because, in a geometry defined by a $N \times N$ matrix, approximately N iterations are required for information about the boundary conditions at one face to

percolate through to the other. Only after this do the temperatures settle down to a smooth path to the final values (see fig.7). The method should therefore be applied only well after the first n iterations.

The S^1 process (fig.8) gives less dramatic results than over-relaxation, but nonetheless confers a very useful saving in computer execution time, when it can be used. Using both techniques, execution time can be reduced to a few minutes.

The mechanics of the programs are described in greater detail in the Appendix, where they are reproduced (pp. 31-46).

COMPARISON WITH EXPERIMENT

While the program was being prepared, attempts were made to test it by submitting to it simple thermal systems with known solutions : e.g. a cylinder whose top and bottom faces are held at uniform, fixed, known temperatures. The program yielded the correct answers. The test could be rendered more exacting by replacing the boundary conditions at the bottom face (i.e. a fixed temperature) by a heat transfer coefficient and coolant temperature. The top face boundary condition could be replaced by a beam power term, the beam being spread right across the face. These tests yielded the correct answers : viz. a uniform increase in temperature from bottom to top, it being constant at any given depth.

However, the computations for these simple systems bring into play only twelve of the twenty-four equations in the program. It was felt that a more searching, experimental test should be carried out on an accelerator target actually being used in the Radiation Centre : namely, a beryllium target used for producing fast neutrons by means of the (p,n) and (d,n) reactions. These neutrons are moderated and used for neutron radiography or activation analysis.

The general layout of the beam line used is shown in fig. 9. The ion beam enters from the left through 2" piping from the magnet room of the Dynamitron accelerator. It passes through two sets of quadrupole magnets, used for focussing and steering, into a larger 4" section of the line, via an adaptor bell and flexible bellows. This section ends with a 1" copper water-cooled collimator in a vacuum box. The beam then enters the target chamber via a 2" bellows. A beam profile monitor is mounted in the 4" section of the pipe, between two 60 l. ion pumps used to maintain vacuum.

The target itself is shown in fig. 10. The beryllium face exposed to the beam has been machined to a 60° cone to minimise thermal loading. Back-cooling of the target was not permitted because of the risk of burnout and subsequent admission of cooling water into the vacuum system. Consequently a coolant channel indented in the side of the target was used.

The whole target was copper-plated, except on the face exposed to the beam. The target is held in the target chamber by a threaded steel backing plate, and two greased 'O'-ring seals.

The target chamber, constructed of stainless steel, has two 2" ports: one to allow the beam access to the target, and a separate angled viewing port which permits optical monitoring through a vacuum-sealed window. The chamber is immersed in a tank of de-ionised water to moderate the neutrons. Ancillary equipment mounted on the tank permits neutron radiography, or thermal neutron activation analysis.

A closed loop, continuous recirculation cooling circuit was used, employing de-ionised water as coolant, fed from a separate tank by a small rotary pump. A heat transfer coefficient of about 0.35 watts/cm.²C was achieved.

The temperature of the target face was measured with a Thermodot infra-red radiometer, mounted on adjustable rails so that it looked directly at the apex of the beryllium cone. Its' distance from the target could be varied. It was focussed visually before an experimental run. A television camera was mounted over the eyepiece for observing any hot-spots. The radiometer employs a lead sulphide detector. It can be adjusted for different target emissivities. The cooling water reservoir temperature was measured with an electronic thermometer.

The system is aligned by means of a laser mounted on a fixed bracket on the Dynamitron, shining through a window along the beam path. The target and tank are disconnected from the beam line and replaced with a window to maintain vacuum, as the beam line must be open to the accelerator in order to give an unimpeded light path to the laser beam. The laser beam is aligned on a datum point on the opposite wall of the beam room. With the target reconnected, it only remains to adjust its' position by means of jacks fitted underneath the tank, until the laser spot is seen to be hitting the apex of the target cone on the monitor screen. Bellows couplings on the beam line take up any flexure during this operation.

During experimental runs, the Dynamitron was operated at energies in excess of 2.5 MeV, the threshold for neutron production in beryllium, at beam currents of up to several hundred micro-amps on target. The beam profile monitor could be used for currents below 100 μ A ; above this, it must be switched off to avoid damage to the collector wire.

The main difficulty in making temperature measurements proved to be false readings resulting from spurious reflections of hot-spots elsewhere in the beam line ; for, inevitably, some of the beam hits other components, such as beam stops or collimators, and the IR emitted reflects off the shiny surface of the beryllium. Sometimes current on a beam stop and radiometer reading could be correlated closely. Sometimes a hot-spot could be seen on the T.V. monitor, and could often be identified with a hot beam stop, rather than a genuine hot-spot on target.

Furthermore, the beam would often be off-axis, causing heating away from the centre of the target where the radiometer was aimed. Hence, if any temperature was registered, it would correspond to an unknown region of the hot-spot. This was complicated by the shape of the target ; for a hot-spot, whether real or reflected from elsewhere, would show reflections from other parts of the cone if it was not centred exactly on the apex. The temperature reading registered was usually far from steady. This might be due to fluctuations in spot size, causing changes in temperature. More probably, it could be due to the beam spot wobbling in a Lissajou pattern : as different parts of the spot crossed the radiometer's field of view, different temperatures would be registered ; similarly, a wobbling hot-spot reflected from elsewhere, or a combination of the two effects, could be responsible.

A further complication was the accumulation of 'crud' on the target surface, presumably consisting of carbonaceous material condensing from oil vapour in the vacuum system. Many of the hot-spots seen on the monitor were clearly due to such deposits, for when the beam was deflected by the operator, the characteristic pattern of glowing spots would remain un-

changed, though sometimes varying in luminosity. This would give wholly spurious readings on the radiometer.

As a consequence of these factors, we obtained no usable results ; i.e. readings which could be confidently identified as the temperature of the target.

Accordingly, it was found necessary to consult the literature for data which might be used to test the program. KAS and NOVAK (60) conducted model experiments to test a calculation method of their own for determining the heat loading on an accelerator target.

Their targets, used for neutron generation, consisted of titanium tritide on thin (0.3 mm) molybdenum backing plates of 4.5 cm. diameter. Heat dissipation was by means of back-cooling by a thin (0.5 mm) water film. They sought the maximum permissible power as a function of water velocity, it having been decided that the maximum permissible temperature of the target was to be 110°C ; this was to suppress steam bubble formation at an over-pressure of 0.5 atmospheres. Their calculation method consisted of dividing the target area into two parts : (a) that comprising the beam spot ; and (b) the annular area around the spot. Thus, the heat transfer consists of two components : heat transfer directly from the spot to the water, easily calculable (it was assumed that temperature was uniform within the spot) ; and a component first conducted radially within the backing and then dissipated in the water over an annular area. This latter component was calculated by analogy with the heat transfer from cooling fins of uniform cross-section. Curves were obtained giving permissible power against cooling water velocity.

As an experimental test for these calculations, Kas and Novak devised a heat test rig consisting of a copper rod, which took the part of the ion beam. It was heated electrically at its' upper end, and insulated over the rest of its' length. Two thermocouples measured the temperature gradient in the rod, from which the heat flow rate could be calculated. To the bottom end of the rod was soldered a molybdenum target backing

plate (0.2 mm. thick). This was mounted in the accelerator target holder. The heat flow rate was increased until a temperature of 110 °C was obtained on the spot, for varying water flow rates, the water temperature being 16 °C. Two rods, giving effectively different beam diameters (0.7 & 1.0 cm) were used. The results they obtained agree well with their calculations.

Their experimental points are reproduced in fig. I2. It was necessary to convert their water velocity values to heat transfer coefficient values by means of the semi-empirical Dittus-Boelter correlation ; viz :

$$H = 0.023 K^{0.6} e^{0.8} \left(\frac{C_p}{\mu} \right)^{0.4} \frac{V^{0.8}}{D^{0.2}} \quad (7)$$

where K, e, C_p, μ and V are, respectively, the thermal conductivity, density, specific heat, viscosity and flow velocity of the coolant, and D is the equivalent diameter of the coolant channel (67). For a thin, narrow channel, the latter may be approximated as $4 \times \frac{\text{cross-section of channel}}{\text{perimeter}}$; or, in the above case, as just twice the actual width of the channel (i.e. 1 mm.).

For the calculated curves shown in fig. I2, RWELB was run with a fixed heat input of 1000 watts, with a coolant temperature of zero, for various values of heat transfer coefficient. From the results, the beam power necessary to give a maximum temperature of 94 °C (i.e. 110 - 16) was obtained by simple proportion. The values obtained are plotted as a function of heat transfer coefficient in fig. I2 (dotted lines). The agreement with the experimental points is quite poor.

However, this may be because the system modelled by the RWELB program does not correspond very closely with the experimental set-up of Kas and Novak. An incident ion beam does not interact thermally with the target, but leaves the latter free to reach an appropriate temperature distribution: namely, some kind of bell-shaped pattern, with temperature decreasing radially outwards from the centre of the beam-spot. It is just such a case that RWELB is designed to simulate. Kas and Novak's heat rig, consisting as it does of a heated, insulated metal rod in direct thermal contact with

the target face, would tend to force a 'top-hat' temperature distribution on the target ; i.e. one with a fairly uniform temperature within the simulated beam spot. This would make the overall temperature pattern, and hence the 'beam power' required to produce a given spot temperature, somewhat different.

RWELB can be readily modified to give a top-hat distribution of an initially assumed temperature (in this case 110°C) by setting the points inside the beam in the control matrix to a new value, which directs the program, during each iteration, to hold those points at the constant temperature. The heat input Q is set at zero, and the program allowed to iterate as before. The sub-routine which monitors the heat outflow from the target can then be used to give the heat input required to produce the given distribution when a steady-state has been reached (consequently, this sub-routine cannot be used to terminate the program ; instead, the program is run for a fixed number of iterations). These values are plotted in fig. 12 (unbroken lines). Considerably better agreement with experiment is obtained.

RESULTS

Computed results from RWELE are given in figs. I6-24.

When designing a target, two thermal considerations have generally to be borne in mind : the need to ensure that maximum target temperature, T_{max} (usually the temperature at the central point on the vacuum face); does not exceed some given limit (usually the melting point of the target material, but possibly lower); and the need to suppress boiling in the coolant channels, to minimise the possibility of 'burn-out' occurring. Accordingly, two curves have been given for each target configuration : one gives T_{max} as a function of various factors ; the other gives a comparable plot for T_{min} the maximum temperature at a cooled surface of the target. Knowing T_{min} the over-pressure in the coolant circuit necessary to avoid boiling can be determined from the vapour pressure curve of the coolant.

Throughout, target radius has been assumed to be 2.5 cm. (I"), this being standard beam tube diameter on many target systems. Coolant temperature was fixed at 0°C, and beam power at I kW. Hence T_{max} and T_{min} for any value of Q can be calculated by simple proportion and adding on the actual coolant temperature.

Two widely used target types were studied for purposes of comparison : A) a flat metal disc uniformly cooled over the back face ; B) a flat metal disc cooled uniformly around the edge. B is often used to minimise the catastrophic effects of 'burn-out' and consequent target rupture, which in A might result in coolant entering the vacuum system.

The heat transfer coefficient, H, for a liquid non-metallic coolant is given by eq. 7 above, the two controlable variables being channel width D and flow velocity V. H increases with V, and decreases slowly with D. Curves of H against V for water, for various D, are given in fig. I3.

Liquid metals have been suggested for use with accelerator targets (5I), as they give much higher heat transfer coefficients. For these, another correlation (67) should be used :

$$H = \left(\frac{K}{D} \right)^{0.6} (ve)^{0.4}$$

This is plotted in fig. I4 for the sodium-potassium alloy NaK. This has the advantage of being liquid at room temperature, but is dangerous to handle. For accelerator targets, a better choice would be mercury, despite its' toxicity (fig. I5).

Various common target materials were considered. From a purely thermal standpoint, copper would be the ideal choice. However, the gamma-ray background of copper under proton bombardment is among the highest for common metals (68). Tantalum, much used for collimators, is a lot better in this regard, but its' conductivity is rather low (0.57). Molybdenum gives a lower background than tantalum at energies below 2.5 MeV, and has quite good conductivity (1.47). Better still is tungsten, which gives a very low gamma-ray yield coupled with good conductivity (1.78), and, moreover, a high melting-point.

Fig. I6 gives results for the A configuration for a copper target, plotted as a function of target thickness, for various beam radii, and a heat transfer coefficient $H=0.5$, a readily obtainable figure. As expected, temperatures rise sharply as beam radius is decreased. It is noteworthy that the very thinnest target plate is not necessarily the best for effective heat dissipation. As thickness is increased, T_{max} at first falls to reach a minimum, beyond which only a modest increase occurs. Clearly, a target should ideally be designed with a thickness near the trough of the curves for the beam radii likely to be encountered. This shifts to lower thicknesses as the beam radius increases to cover the target plate. For a beam fully covering the target, of course, this effect vanishes, and a linear relation is found, the thinner targets giving better performance.

Fig. I7 gives comparable curves for a copper target in the B configuration. As expected, temperature falls steadily with thickness, but less steeply with increasing beam size. The overall temperature levels are also higher. The variation of T_{min} with beam radius is very small over a wide

range of beam sizes. This could be advantageous in an accelerator system which gives fluctuating, unpredictable beam sizes ; in the A configuration, this always entails the risk of a sudden burn-out condition.

Figs. 18-19 give similar curves for the A and B configurations for tungsten, $H = 1.0$. The same general trends are evident, though the general temperature level is higher due to the lower conductivity of tungsten.

Figs. 20 give curves for a back-cooled beryllium plate, such as might be used for neutron generation, for various values of H . Fig. 21 gives curves for a similar aluminium target. Fig. 22 gives curves for a uranium target : these have been used for photonuclear neutron production using the bremsstrahlung gamma-rays from an incident electron beam.(51).

Finally, fig.23 gives curves for a more complex target shape : the beryllium neutron generation target of fig. 10, shown schematically in fig. 11 as it is divided up for the computations. T_{max} and T_{min} are plotted against H for various beam radii. Again, T_{min} varies very little with beam radius, so only one curve has been plotted. This would make the target fairly immune to a 'burn-out' due to a sudden contraction in spot size.

In contrast to the simpler target shapes, the hottest part of the target is not axially under the beam, but forms an axial ring, whose radius increases with beam radius (fig. 24).

APPLICATIONS TO SPECIFIC TARGET DESIGNS

As an application of the above computations, we may address ourselves to the problem of devising a high-current target suitable for use on the Dynamitron accelerator. Nominally, the latter can achieve 2 mA of beam current at energies up to 3 MeV ; i.e. beam powers up to 6 kW. The standard beam tube diameter at the target is 2".

First, it might be useful to consider a target actually in use on this accelerator ; viz. the beryllium target for neutron generation shown in figs. 10 & 11. Computations for this target are plotted in fig. 23. The heat transfer coefficient actually achieved with this target was about 0.35 watts/cm.²°C . In practice, the beam radii experienced on this line, as measured by the beam profile monitor, were usually about 1 cm. We may, rather arbitrarily, define a limiting temperature of 90% of the melting point of beryllium (i.e. 1150 °C) as the maximum allowable. The temperature shown in fig. 23, for 1 kW beam power, is 130 °C. Consequently, if beam spot temperature alone was the limiting factor, this target could tolerate up to 1150/130 kW, i.e. 8.8 kW of beam power.

However, we must also consider the need to avoid boiling in the coolant channel. At a coolant temperature of 10 °C, with no pressurisation in the coolant circuit, T_{min} must not exceed 90 °C. From fig. 23, we see that the maximum permissible power is 90/97 kW, i.e. 0.93 kW.

This figure could be raised by using a pressurised cooling circuit. From fig. 29, it will be seen that at an over-pressure of half an atmosphere (7lb/in²), boiling will not occur until the temperature reaches 110 °C. This would permit a power of 100/97 kW, i.e. 1.03 kW ; while an over-pressure of one atmosphere would allow a power of 110/97 kW, i.e. 1.13 kW. Clearly, no very dramatic improvement is possible by this means without invoking unreasonably high pressures.

Alternatively, the heat transfer coefficient could be increased. A figure of $H = 1.0$ ought to be fairly readily obtainable with water cooling : this need only entail increasing the water flow rate by a factor

of about 4 (see eq.7), which would present little difficulty. A power of 2.2 kW could then be reached. This would give a spot temperature of only 180°C. With an over-pressure of one atmosphere, 2.75 kW could be reached.

The target design above was constrained by the requirement that there be no coolant directly behind the target, in case the target ruptured. If this requirement is abandoned, substantially higher beam powers might be possible. Fig. 20 (a,b) gives the calculated curves for a back-cooled beryllium plate for $H = 0.4$, i.e. comparable to the figure actually obtained with the previous target. The thickness for minimum spot temperature, for a beam radius of 1 cm, is about 0.8 cm. Boiling will occur at a beam power of about 600 watts, so this target is markedly inferior to the conical one above. H would have to be increased to about 1.0 to give a performance to match the latter (fig. 20 g,h).

Consequently, it would be worthwhile examining a system cooled at both the back face and round the edge. Curves for such a beryllium target are shown in fig. 29. As expected, it gives considerably better performance, which improves with increasing target thickness. For a thickness of 1.5 cm and $H=0.5$, a beam power of 1.34 kW is obtainable, entailing a spot temperature of only 180°C. If the heat transfer coefficient is increased to 1.0, 2.14 kW would be possible, always assuming an unpressurised coolant channel. For an over-pressure of one atmosphere, the figure could be increased to 2.6 kW.

The relatively good performance of both the conical target and that with all-round cooling prompts the idea of combining both these features in one target, as in fig. 30, where the target consists of a 60° beryllium cone (which effectively halves the beam loading on the target face) of uniform thickness cooled over all its' back surface. Plots of temperature as a function of thickness and heat transfer coefficient are shown in fig. 31. As before, beam radius is 1 cm; the curves are normalised to a power of 1 kW.

T_{min} decreases with thickness, while T_{max} exhibits a minimum at 2 cm

(for $H = 0.5$), or 1.8 cm ($H = 1.0$). At these thicknesses, powers of 2.9 and 5.0 kW respectively would be attainable without pressurisation. T_{max} would reach 225° and 312° in each case ; as in the conical target examined above, this does not occur at the centre of the target, but in an axial ring around it (see fig. 24).

A beam power of 6 kW might be attainable by a modest further increase in H , or by pressurisation : for a half-atmosphere over-pressure, 3.25 kW ($H = 0.5$) or 5.55 kW ($H = 1.0$) could be expected ; for one atmosphere, 3.55 kW and 6.1 kW. Alternatively, or additionally, it might be possible to use a more diffuse beam spot at these high currents.

Fig. 32 shows curves for an identical target made of copper, such as might be used as a backing for samples for (p, γ) analysis. This exhibits similar behaviour, although the general temperature level is somewhat lower. The minima of T_{max} occur at thicknesses of 2.2 cm ($H = 0.5$) and 2.0 cm ($H = 1.0$). At these thicknesses, powers of 3.21 and 5.62 kW are possible without pressurisation. With half an atmosphere over-pressure, 3.57 and 6.25 kW could be attained, while at one atmosphere 3.93 and 6.88 kW might be reached. In the latter case, values of T_{max} of only 200 and 260 would arise, which might be tolerable in many analytical applications.

It would thus appear that water cooling is adequate for a neutron generating target that will withstand the full rated beam power of the Dynamitron accelerator. It seems unnecessary to incur the technical difficulties associated with liquid-metal coolants.

APPENDIX

HP ALGOL PROGRAMS RWCON , RWELB & RWELSRWCON

The HP ALGOL program RWCON generates a control matrix $H(R,Z)$ from an input matrix $G(R,Z)$. $G(R,Z)$ delineates the geometric shape of the target as an array of numbers defined by co-ordinates R,Z : R is the radius outwards from the centre axis ($R = 0$), Z the distance from the base of the array ($Z = 0$). The target shape is assumed to be a right circular cylinder with the back, or side, or both, cooled ; possibly with indented coolant channels and a non-flat top face. The elements of $G(R,Z)$ take various values according to the following convention : -I for a point outside the target, I for a point in or on the target, except at a cooled boundary, which is given the value 0. In addition the boundaries of the array must take the value -I ; i.e. the target shape must not completely fill the array. Such arrays are shown in figs. 25, 26 & 27 (a) for, respectively, a back-cooled target, a side-cooled target, and the beryllium target shown in figs. IO & II.

The size of the matrices G,H is defined in line 3 of the program (p.36). R takes values from 0 to N , Z from 0 to M . Line 6 defines a format for $H(R,Z)$; the coefficient in this format (6 in this case) must be $M+I$.

Lines II & I2 type requests for the peripheral device required for feeding in $G(R,Z)$, usually paper tape ; and for delivering $H(R,Z)$ as output, usually magnetic or paper tape. The appropriate code numbers are then typed in (usually 5 for tape-reader, 6 for line-printer, 7 for magnetic tape recorder). Lines I4 & I5 command the input device to read $G(R,Z)$.

Having read $G(R,Z)$, the program scans this array ; it considers each point in $G(R,Z)$ in relation to its' immediate neighbours and assigns it a numerical value (from I to 25) in $H(R,Z)$, according to the scheme in Table I, which shows the geometrical configuration of each point in relation to any boundaries. This occupies lines I7 to I44 in the program. Lines I46, I47 command $H(R,Z)$ to be read off on the output device.

Various arrays $H(R,Z)$ are reproduced in figs. 25, 26 & 27 (b).

RWELB

This program, using as input the control matrix $H(R,Z)$ generated by RWCON above, performs the actual thermal computation described in 'Target Design' above.

Lines 3-13 (p.39) formally declare all the variables, arrays and labels to be used in the program. Line 6 defines the size of the matrices $H(R,Z)$, the control matrix, and $T(R,Z)$, the matrix defining the temperature at each point. N and M must take the same values as in RWCON. Likewise, the coefficient in the format declaration (line 14) must be the same, i.e. $M + 1$. Lines 15 & 16 define the input device for $H(R,Z)$ (usually 7, for magnetic tape recorder), and the output device for $T(R,Z)$ (usually 6, for line-printer).

The program requires certain basic data defining the size and properties of the target ; also, certain constants necessary for the computation. These, set in lines 17-30, are :

RADIUS : the radius of the target in cm.

HEIGHT : the total thickness of the target in cm.

BEAM : the radius of the beam spot in cm.

Q : beam power in watts.

K : the thermal conductivity of the target material in watts/cm.².°C .

W : the heat transfer coefficient at the cooled boundaries in watts/cm.².°C

TC : the bulk temperature of the coolant in °C.

EMS : the emissivity of the target face.

SH : the radiation shape factor of the target face, usually set at 1.0.

ST : Stefan's constant : 5.67×10^{-12} watts/cm.².sec.°K⁴ .

B : the relaxation coefficient, β , usually set at 1.75 .

AK : the range of tolerance within which the heat outflow from the target must match Q to terminate the program ; i.e. if $AK = 0.01$, heat output from the target is within 1% of Q.

OMI : output monitoring interval ; this determines the number of

iterations between successive tests for heat balance.

GUESS : the initial estimate of temperature.

Lines 31-37 define some commonly occurring clusters of constants which would otherwise clutter up the equations. Lines 38-39 command the computer to read H(R,Z).

Lines 40-41 set the value of the temperatures T(R,Z) to GUESS.

Line 43 is the start of the iterative cycle.

Line 44 updates two variables, COUNT and KOUNT, which register the number of iterations that have occurred.

Line 45 commands the computer to jump to line 69, the start of the computation proper, unless it is necessary to test for heat balance, i.e. unless KOUNT = OMI. If this is necessary, the block 46-68 is executed. This will be outlined in more detail below.

The computation proper starts at line 70. The control matrix H(R,Z) is scanned, and at each point the computer is commanded to jump to the equation corresponding to that point. That equation is then executed before the program moves on to the next point. When the whole array has been scanned, the program jumps back to line 43 and the process is repeated.

The iterative equations occupy lines 78-193. These equations are derived from the basic thermal equations given in Table 2 by making the following simplifying substitutions (lines 31-34 in RWELB) :

$$A = \pi K \cdot \Delta R^2 / \Delta Z$$

$$C = \pi K \cdot \Delta Z$$

$$D = \pi W \cdot \Delta R^2$$

$$E = \pi W \cdot \Delta R \cdot \Delta Z$$

$$\text{where } R = \frac{\text{RADIUS}}{N-1}, \quad Z = \frac{\text{HEIGHT}}{M-2}, \quad \text{and } W = H.$$

In addition, the relaxation equation (5 above) has been applied.

These equations apply to a target with no heat input. It will be seen from Table I that equations 1, 2, 3, 7 & 17, i.e. those for elements incorporating a flat top face, require in addition a heat input term if

they are covered by the ion beam ; i.e. if $R \leq X$, the value of R at the beam edge, defined as $(N-I) \times \text{BEAM}/\text{RADIUS}$ (line 35). This heat input term consists of $Q/(\pi X^2 \Delta R^2)$, i.e. beam power per unit area, multiplied by the area of the element in question and the relaxation coefficient B, divided by the same weighting factor as in the main equation.

Similarly, equations I, 2, 3 & I7 require a negative heat input term to represent radiation from the top face, denoted by the variable RAD in the equations. As well as being used to adjust the equations, RAD is summed by means of a variable RADSUM as the control matrix is scanned ; at the end of each iteration, RADSUM therefore represents the total heat lost by radiation.

Points corresponding to equation 25 are outside the target and play no part in the computation. Equation 25 sets these ' temperatures' to a large number, e.g. 10^6 . This overloads the format and is printed as a dollar sign in the output ; thus, it can readily be distinguished from 'bona fide' temperature results.

At line 45, if KOUNT = OMI, the block 46-68 tests the temperatures for heat balance. Only elements containing a cooled boundary (i.e. IO-2I) need be considered. The control matrix is again scanned, and these elements are singled out : the variable J represents the heat conductance coefficient across the cooled boundary for the particular element, which when multiplied by the temperature between element and coolant gives the heat lost across that boundary. The variable F sums the various J's at each point in the scan, to finally give total heat lost to the coolant. For heat balance, F must equal $Q - \text{RADSUM}$. This is tested by using the tolerance factor AK ; i.e. to terminate the program :

$$(I - AK) \cdot (Q - \text{RADSUM}) \leq F \leq (I + AK) \cdot (Q - \text{RADSUM}) .$$

If this criterion is satisfied, the program jumps to line I97. Following this are the output commands which yield the matrix T(R,Z) on the specified output device.

RWELS

This program (p.43) is identical to RWELB above, with the addition of lines 45-62 which perform the Aitken δ^2 -technique. Two temperature matrices $T^{(1)}(R,Z)$ and $T^{(2)}(R,Z)$ are required, as well as $T(R,Z)$. After the first $2M$ iterations, the current temperatures in $T(R,Z)$ are stored in $T^{(1)}(R,Z)$. After a further 10 iterations, we have three evenly spaced temperature iterates $T^{(1)}$, $T^{(2)}$, and T . In lines 60-61, the temperatures are then set equal to the expression in eq. 6 above, which will probably be much nearer the final values.

RWELS can only be used for quite small matrices, due to the computer storage capacity required for the three temperature matrices, in addition to the control matrix $H(R,Z)$.


```

0059 IF G[R+1,Z] < 0 THEN BEGIN
0060 IF G[R-1,Z] > 0 THEN BEGIN
0061 IF G[R,Z+1] >= 0 THEN BEGIN
0062 IF G[R,Z-1] >= 0 THEN H[R,Z] + 5;
0063 END; END; END;
0064 IF G[R+1,Z] < 0 THEN BEGIN
0065 IF G[R-1,Z] > 0 THEN BEGIN
0066 IF G[R,Z+1] > 0 THEN BEGIN
0067 IF G[R,Z-1] < 0 THEN H[R,Z] + 6;
0068 END; END; END;
0069 IF G[R+1,Z] < 0 THEN BEGIN
0070 IF G[R-1,Z] > 0 THEN BEGIN
0071 IF G[R,Z+1] < 0 THEN BEGIN
0072 IF G[R,Z-1] > 0 THEN H[R,Z] + 7;
0073 END; END; END;
0074 IF G[R+1,Z] >= 0 THEN BEGIN
0075 IF G[R-1,Z] > 0 THEN BEGIN
0076 IF G[R,Z+1] >= 0 THEN BEGIN
0077 IF G[R-1,Z+1] >= 0 THEN BEGIN
0078 IF G[R,Z-1] >= 0 THEN H[R,Z] + 8;
0079 END; END; END; END;
0080 IF G[R+1,Z] > 0 THEN BEGIN
0081 IF G[R-1,Z] < 0 THEN BEGIN
0082 IF G[R,Z+1] > 0 THEN BEGIN
0083 IF G[R,Z-1] > 0 THEN H[R,Z] + 9;
0084 END; END; END;
0085 END;
0086 IF G[R,Z] = 0 THEN
0087 BEGIN
0088 IF G[R+1,Z] = 0 THEN BEGIN
0089 IF G[R-1,Z] = 0 THEN BEGIN
0090 IF G[R,Z+1] < 0 THEN BEGIN
0091 IF G[R,Z-1] > 0 THEN H[R,Z] + 10;
0092 END; END; END;
0093 IF G[R+1,Z] = 0 THEN BEGIN
0094 IF G[R-1,Z] = 0 THEN BEGIN
0095 IF G[R,Z+1] > 0 THEN BEGIN
0096 IF G[R,Z-1] < 0 THEN H[R,Z] + 11;
0097 END; END; END;
0098 IF G[R+1,Z] < 0 THEN BEGIN
0099 IF G[R-1,Z] > 0 THEN BEGIN
0100 IF G[R,Z+1] = 0 THEN BEGIN
0101 IF G[R,Z-1] = 0 THEN H[R,Z] + 12;
0102 END; END; END;
0103 IF G[R+1,Z] < 0 THEN BEGIN
0104 IF G[R-1,Z] > 0 THEN BEGIN
0105 IF G[R,Z+1] = 0 THEN BEGIN
0106 IF G[R,Z-1] < 0 THEN H[R,Z] + 13;
0107 END; END; END;
0108 IF G[R+1,Z] < 0 THEN BEGIN
0109 IF G[R-1,Z] = 0 THEN BEGIN
0110 IF G[R,Z+1] > 0 THEN BEGIN
0111 IF G[R,Z-1] < 0 THEN H[R,Z] + 14;
0112 END; END; END;
0113 IF G[R+1,Z] < 0 THEN BEGIN
0114 IF G[R-1,Z] = 0 THEN BEGIN
0115 IF G[R,Z+1] = 0 THEN BEGIN
0116 IF G[R,Z-1] < 0 THEN H[R,Z] + 15;
0117 END; END; END;
0118 IF G[R+1,Z] < 0 THEN BEGIN
0119 IF G[R-1,Z] = 0 THEN BEGIN
0120 IF G[R,Z+1] < 0 THEN BEGIN
0121 IF G[R,Z-1] > 0 THEN H[R,Z] + 16;
0122 END; END; END;

```

```

0123     IF G[R+1,Z] < 0 THEN BEGIN
0124     IF G[R-1,Z] > 0 THEN BEGIN
0125     IF G[R,Z+1] < 0 THEN BEGIN
0126     IF G[R,Z-1] = 0 THEN H[R,Z] ← 17;
0127     END; END; END;
0128     IF G[R+1,Z] < 0 THEN BEGIN
0129     IF G[R-1,Z] = 0 THEN BEGIN
0130     IF G[R,Z+1] < 0 THEN BEGIN
0131     IF G[R,Z-1] = 0 THEN H[R,Z] ← 18;
0132     END; END; END;
0133     IF G[R+1,Z] = 0 THEN BEGIN
0134     IF G[R-1,Z] > 0 THEN BEGIN
0135     IF G[R,Z+1] > 0 THEN BEGIN
0136     IF G[R,Z-1] = 0 THEN H[R,Z] ← 19;
0137     END; END; END;
0138     IF G[R+1,Z] = 0 THEN BEGIN
0139     IF G[R-1,Z] > 0 THEN BEGIN
0140     IF G[R,Z+1] = 0 THEN BEGIN
0141     IF G[R,Z-1] > 0 THEN H[R,Z] ← 20;
0142     END; END; END;
0143     END;
0144     END;
0145     &
0146     WRITE(LUO,F1,FOR R←0 TO N DO
0147           FOR Z←0 TO M DO H[R,Z]);
0148     WRITE(1,F4);
0149     ENDS

```


PROGRAM RWELB

```

0001  HPAL,L,"RWELB"
0002  BEGIN
0003  REAL BEAM,AK,RADIUS,HEIGHT,EMS,SH,ST,SB,RAD,RADSUM,TT,F,
0004      A,B,C,D,E,Q,W,K,J,TRZ,TCC?
0005  INTEGER GUESS,LUI,LUO,OMI,COUNT,KOUNT,L,TC,X,R,Z?
0006  EQUATE N←10,M←5?
0007  LABEL START,ITER,NEWON,FINAL,L1,L2,L3,L4,L5,L6,L7,L8,L9,
0008      L10,L11,L12,L13,L14,L15,L16,L17,L18,L19,L20,L21,
0009      L22,L23,L24,L25?
0010  SWITCH S←L1,L2,L3,L4,L5,L6,L7,L8,L9,L10,L11,L12,L13,
0011      L14,L15,L16,L17,L18,L19,L20,L21,L22,L23,L24,L25?
0012  REAL ARRAY T[0:N,0:M]?
0013  INTEGER ARRAY H[0:N,0:M]?
0014  FORMAT F1(6(X,I2))?
0015  LUI←5?
0016  LUO←6?
0017  RADIUS←1.0?
0018  HEIGHT←1.0?
0019  BEAM←0.5?
0020  Q←1?3?
0021  W←1.0?
0022  K←1.0?
0023  TC←0.0?
0024  B←1.5?
0025  OMI←10?
0026  AK←0.005?
0027  EMS←1.0?
0028  SH←1.0?
0029  ST←5.67?1-12?
0030  GUESS←3?2?
0031  A←PI*K*((RADIUS/(N-1))↑2)/(HEIGHT/(M-2));
0032  C←PI*K*HEIGHT/(M-2);
0033  D←PI*W*((RADIUS/(N-1))↑2);
0034  E←PI*W*RADIUS*HEIGHT/((N-1)*(M-2));
0035  X←(N-1)*(BEAM/RADIUS);
0036  SB←EMS*SH*ST?
0037  TCC←TC+273?
0038  READ(LUI,F1,FOR R←0 TO N DO
0039      FOR Z←0 TO M DO H[R,Z]);
0040  FOR R←0 TO N DO
0041      FOR Z←0 TO M DO T[R,Z]←GUESS?
0042  COUNT←0? KOUNT←0?
0043  START:
0044  COUNT←COUNT+1? KOUNT←KOUNT+1?
0045  IF KOUNT#OMI THEN GO TO ITER?
0046  KOUNT←0? F←0? J←0?
0047  FOR R←0 TO N DO
0048  FOR Z←0 TO M DO
0049  BEGIN
0050  J←0?
0051  IF H[R,Z]=10 THEN J←2*D*R?
0052  IF H[R,Z]=11 THEN J←2*D*R?
0053  IF H[R,Z]=12 THEN J←2*E*R?
0054  IF H[R,Z]=13 THEN J←E*R?
0055  IF H[R,Z]=14 THEN J←D*(R-1/4)?
0056  IF H[R,Z]=15 THEN J←2*(E+D)*R?
0057  IF H[R,Z]=16 THEN J←D*(R-1/4)?
0058  IF H[R,Z]=17 THEN J←E*R?
0059  IF H[R,Z]=18 THEN J←2*(E+D)*R?

```



```

0060 IF H[R,Z]=19 THEN J←E*R+D*(R+1/4);
0061 IF H[R,Z]=20 THEN J←E*R+D*(R+1/4);
0062 IF H[R,Z]=21 THEN J←D/4;
0063 F←F+J*(T[R,Z]-TC);
0064 END;
0065 IF F>(1-AK)*Q-RADSUM THEN
0066 BEGIN
0067 IF F<(1+AK)*Q-RADSUM THEN GO TO FINAL;
0068 END;
0069 ITER: RADSUM←0;
0070 FOR R←0 TO N DO
0071 FOR Z←M STEP -1 UNTIL 0 DO
0072 BEGIN
0073 TRZ←T[R,Z]+273;
0074 TT←TRZ↑4-TCC↑4;
0075 L←H[R,Z];
0076 GO TO S[L];
0077
0078 L1 : T[R,Z]←B*(C*(R-1/2)*T[R-1,Z]+C*(R+1/2)*T[R+1,Z]
0079      +2*A*R*T[R,Z-1])/(2*(A+C)*R)
0080      + (1-B)*T[R,Z];
0081      RAD←(2*D*R/W)*SB*TT;
0082      T[R,Z]←T[R,Z]-B*RAD/(2*(A+C)*R);
0083      RADSUM←RADSUM+RAD;
0084      IF R<X THEN T[R,Z]←T[R,Z]+B*Q/((X↑2)*(A+C));
0085      IF R=X THEN T[R,Z]←T[R,Z]+(B*Q*(R-1/4)/(X↑2))/
0086      (2*R*(A+C));
0087      GO TO NEWON;
0088 L2 : T[R,Z]←B*(C*(R-1/2)*T[R-1,Z]+2*C*(R+1/2)*T[R+1,Z]
0089      +2*A*R*T[R,Z-1]+A*(R+1/4)*T[R,Z+1])/
0090      (C*(3*R+1/2)+A*(3*R+1/4)) + (1-B)*T[R,Z];
0091      RAD←(D*(R-1/4)/W)*SB*TT;
0092      T[R,Z]←T[R,Z]-B*RAD/(C*(3*R+1/2)+A*(3*R+1/4));
0093      RADSUM←RADSUM+RAD;
0094      IF R≤X THEN T[R,Z]←T[R,Z]+(B*Q*(R-1/4)/(X↑2))/
0095      (C*(3*R+1/2)+A*(3*R+1/4));
0096      GO TO NEWON;
0097 L3 : T[R,Z]←B*(C*(R+1/2)*T[R+1,Z]+A*(R+1/4)*T[R,Z-1])/
0098      (C*(R+1/2)+A*(R+1/4)) + (1-B)*T[R,Z];
0099      RAD←(D*(R+1/4)/W)*SB*TT;
0100      T[R,Z]←T[R,Z]-B*RAD/(C*(R+1/2)+A*(R+1/4));
0101      RADSUM←RADSUM+RAD;
0102      IF R<X THEN T[R,Z]←T[R,Z]+(B*Q*(R+1/4)/(X↑2))/
0103      (C*(R+1/2)+A*(R+1/4));
0104      GO TO NEWON;
0105 L4 : T[R,Z]←B*(C*(R-1/2)*T[R-1,Z]+C*(R+1/2)*T[R+1,Z]
0106      +2*A*R*T[R,Z+1])/(2*(A+C)*R)+(1-B)*T[R,Z];
0107      GO TO NEWON;
0108 L5 : T[R,Z]←B*(2*C*(R-1/2)*T[R-1,Z]+A*(R-1/4)*(T[R,Z-1]
0109      +T[R,Z+1]))/(2*C*(R-1/2)+2*A*(R-1/4))
0110      + (1-B)*T[R,Z];
0111      GO TO NEWON;
0112 L6 : T[R,Z]←B*(C*(R-1/2)*T[R-1,Z]+A*(R+1/4)*T[R,Z+1])/
0113      (C*(R-1/2)+A*(R+1/4)) + (1-B)*T[R,Z];
0114      GO TO NEWON;
0115 L7 : T[R,Z]←B*(C*(R-1/2)*T[R-1,Z]+A*(R-1/4)*T[R,Z-1])/
0116      (C*(R-1/2)+A*(R-1/4)) + (1-B)*T[R,Z];
0117      RAD←(D*(R-1/4)/W)*SB*TT;
0118      T[R,Z]←T[R,Z]-B*RAD/(C*(R-1/2)+A*(R-1/4));
0119      RADSUM←RADSUM+RAD;
0120      IF X=N-1 THEN T[R,Z]←T[R,Z]+(B*Q*(R-1/4)/(X↑2))/
0121      (C*(R-1/2)+A*(R-1/4));
0122      GO TO NEWON;

```



```

0123 L8 : T[R,Z] ← B*(2*C*(R-1/2)*T[R-1,Z] + 2*C*(R+1/2)*T[R+1,Z]
0124           + 2*A*R*(T[R,Z-1] + T[R,Z+1])) / (4*(A+C)*R)
0125           + (1-B)*T[R,Z];
0126 GO TO NEWON;
0127 L9 : T[R,Z] ← B*(2*C*(R+1/2)*T[R+1,Z] + A*(R+1/4)*(T[R,Z-1]
0128           + T[R,Z+1])) / (2*C*(R+1/2) + 2*A*(R+1/4))
0129           + (1-B)*T[R,Z];
0130 GO TO NEWON;
0131 L10: T[R,Z] ← B*(C*(R-1/2)*T[R-1,Z] + C*(R+1/2)*T[R+1,Z]
0132           + 2*A*R*T[R,Z-1] + 2*D*R*TC) / (2*(A+C+D)*R)
0133           + (1-B)*T[R,Z];
0134 GO TO NEWON;
0135 L11: T[R,Z] ← B*(C*(R-1/2)*T[R-1,Z] + C*(R+1/2)*T[R+1,Z]
0136           + 2*A*R*T[R,Z+1] + 2*D*R*TC) / (2*(A+C+D)*R)
0137           + (1-B)*T[R,Z];
0138 GO TO NEWON;
0139 L12: T[R,Z] ← B*(2*C*(R-1/2)*T[R-1,Z] + A*(R-1/4)*(T[R,Z-1]
0140           + T[R,Z+1]) + 2*E*R*TC) / (2*C*(R-1/2)
0141           + 2*A*(R-1/4) + 2*E*R) + (1-B)*T[R,Z];
0142 GO TO NEWON;
0143 L13: T[R,Z] ← B*(C*(R-1/2)*T[R-1,Z] + A*(R-1/4)*T[R,Z+1]
0144           + E*R*TC) / (C*(R-1/2) + A*(R-1/4) + E*R)
0145           + (1-B)*T[R,Z];
0146 GO TO NEWON;
0147 L14: T[R,Z] ← B*(C*(R-1/2)*T[R-1,Z] + A*(R-1/4)*T[R,Z+1]
0148           + D*(R-1/4)*TC) / (C*(R-1/2) + (A+D)*(R-1/4))
0149           + (1-B)*T[R,Z];
0150 GO TO NEWON;
0151 L15: T[R,Z] ← B*(C*(R-1/2)*T[R-1,Z] + A*(R-1/4)*T[R,Z+1]
0152           + 2*(E+D)*R*TC) / (C*(R-1/2) + A*(R-1/4) + 2*(E
0153           + D)*R) + (1-B)*T[R,Z];
0154 GO TO NEWON;
0155 L16: T[R,Z] ← B*(C*(R-1/2)*T[R-1,Z] + A*(R-1/4)*T[R,Z-1]
0156           + D*(R-1/4)*TC) / (C*(R-1/2) + (A+D)*(R-1/4))
0157           + (1-B)*T[R,Z];
0158 GO TO NEWON;
0159 L17: T[R,Z] ← B*(C*(R-1/2)*T[R-1,Z] + A*(R-1/4)*T[R,Z-1]
0160           + E*R*TC) / (C*(R-1/2) + A*(R-1/4) + E*R)
0161           + (1-B)*T[R,Z];
0162 IF X=N-1 THEN T[R,Z] ← T[R,Z] + (B*Q*(R-1/4)/(X↑2)) /
0163           (C*(R-1/2) + A*(R-1/4) + E*R);
0164 GO TO NEWON;
0165 L18: T[R,Z] ← B*(C*(R-1/2)*T[R-1,Z] + A*(R-1/4)*T[R,Z-1]
0166           + 2*(E+D)*R*TC) / (C*(R-1/2) + A*(R-1/4) + 2*(E+D)
0167           *R) + (1-B)*T[R,Z];
0168 GO TO NEWON;
0169 L19: T[R,Z] ← B*(2*C*(R-1/2)*T[R-1,Z] + C*(R+1/2)*T[R+1,Z]
0170           + 2*A*R*T[R,Z+1] + A*(R-1/4)*T[R,Z-1] + E*R*TC
0171           + D*(R+1/4)*TC) / (C*(3*R-1/2) + A*(3*R-1/4)
0172           + E*R + D*(R+1/4)) + (1-B)*T[R,Z];
0173 GO TO NEWON;
0174 L20: T[R,Z] ← B*(2*C*(R-1/2)*T[R-1,Z] + C*(R+1/2)*T[R+1,Z]
0175           + 2*A*R*T[R,Z-1] + A*(R-1/4)*T[R,Z+1] + E*R*TC
0176           + D*(R+1/4)*TC) / (C*(3*R-1/2) + A*(3*R-1/4)
0177           + E*R + D*(R+1/4)) + (1-B)*T[R,Z];
0178 GO TO NEWON;
0179 L21: T[R,Z] ← B*((C/2)*T[R+1,Z] + (A/4)*T[R,Z+1] + (D/4)*TC) /
0180           (C/2 + A/4 + D/4) + (1-B)*T[R,Z];
0181 GO TO NEWON;
0182 L22: T[R,Z] ← B*((C*T[R+1,Z] + (A/4)*(T[R,Z+1] + T[R,Z-1])) /
0183           (C+A/2)) + (1-B)*T[R,Z];

```

```

0184      GO TO NEWON;
0185 L23:  T[R,Z]←B*((C/2)*T[R+1,Z]+(A/4)*T[R,Z-1]+Q/
0186          (4*(X↑2)))/(C/2+A/4) + (1-B)*T[R,Z];
0187      RAD←(D/(4*W))*SB*TT;
0188      T[R,Z]←T[R,Z]-B*RAD/(C/2+A/4);
0189      RADSUM←RADSUM+RAD;
0190      GO TO NEWON;
0191 L24:  T[R,Z]←B*((C/2)*T[R+1,Z]+(A/4)*T[R,Z+1])/
0192          (C/2+A/4)+(1-B)*T[R,Z];
0193      GO TO NEWON;
0194 L25:  T[R,Z]←1000000;      GO TO NEWON;
0195 NEWON:  END;
0196 GO TO START;
0197 FINAL:
0198 WRITE(LUD,#(X,I5),COUNT);
0199 WRITE(LUD,#(6(X,I3)),FOR R←0 TO N DO
0200 FOR Z←0 TO M DO T[R,Z]);
0201 ENDS

```


PROGRAM RWELS

```

0001 HPAL,L,"RWELS"
0002 BEGIN
0003 REAL BEAM,AK,RADIUS,HEIGHT,EMS,SH,ST,SB,RAD,RADSUM,TT,F,
0004     A,B,C,D,E,Q,W,K,J,TRZ,TCC;
0005 INTEGER GUESS,LUI,LUO,OMI,COUNT,KOUNT,L,TC,X,R,Z;
0006 EQUATE N←10,M←5;
0007 LABEL START,ITER,NEWON,FINAL,L1,L2,L3,L4,L5,L6,L7,L8,L9,
0008     L10,L11,L12,L13,L14,L15,L16,L17,L18,L19,L20,L21,
0009     L22,L23,L24,L25;
0010 SWITCH S←L1,L2,L3,L4,L5,L6,L7,L8,L9,L10,L11,L12,L13,
0011     L14,L15,L16,L17,L18,L19,L20,L21,L22,L23,L24,L25;
0012 REAL ARRAY TTTT,TTT,T[0:N,0:M];
0013 INTEGER ARRAY H[0:N,0:M];
0014 FORMAT F1(6(X,I2));
0015 LUI←5;
0016 LUO←6;
0017 RADIUS←1.0;
0018 HEIGHT←1.0;
0019 BEAM←0.5;
0020 Q←1.3;
0021 W←1.0;
0022 K←1.0;
0023 TC←0.0;
0024 B←1.5;
0025 OMI←10;
0026 AK←0.005;
0027 EMS←1.0;
0028 SH←1.0;
0029 ST←5.67-12;
0030 GUESS←3.2;
0031 A←PI*K*((RADIUS/(N-1))2)/(HEIGHT/(M-2));
0032 C←PI*K*HEIGHT/(M-2);
0033 D←PI*W*((RADIUS/(N-1))2);
0034 E←PI*W*RADIUS*HEIGHT/((N-1)*(M-2));
0035 X←(N-1)*(BEAM/RADIUS);
0036 SB←EMS*SH*ST;
0037 TCC←TC+273;
0038 READ(LUI,F1,FOR R←0 TO N DO
0039     FOR Z←0 TO M DO H[R,Z]);
0040 FOR R←0 TO N DO
0041     FOR Z←0 TO M DO T[R,Z]←GUESS;
0042 COUNT←0; KOUNT←0;
0043 START:
0044 COUNT←COUNT+1; KOUNT←KOUNT+1;
0045 IF COUNT=2*M THEN
0046 BEGIN
0047     FOR R←0 TO N DO
0048     FOR Z←0 TO M DO
0049     TTTT[R,Z]←T[R,Z];
0050 END;
0051 IF COUNT=2*M+10 THEN
0052 BEGIN
0053     FOR R←0 TO N DO
0054     FOR Z←0 TO M DO TTT[R,Z]←T[R,Z];
0055 END;
0056 IF COUNT=2*M+20 THEN
0057 BEGIN
0058     FOR R←0 TO N DO
0059     FOR Z←0 TO M DO
0060     T[R,Z]←(TTTT[R,Z]*T[R,Z]-TTT[R,Z]2)/
0061     (TTTT[R,Z]+T[R,Z]-2*TTT[R,Z]);

```



```

0062 END;
0063 IF KOUNT#OMI THEN GO TO ITER;
0064 KOUNT←0; F←0; J←0;
0065 FOR R←0 TO N DO
0066 FOR Z←0 TO M DO
0067 BEGIN
0068 J←0;
0069 IF H[R,Z]=10 THEN J←2*D*R;
0070 IF H[R,Z]=11 THEN J←2*D*R;
0071 IF H[R,Z]=12 THEN J←2*E*R;
0072 IF H[R,Z]=13 THEN J←E*R;
0073 IF H[R,Z]=14 THEN J←D*(R-1/4);
0074 IF H[R,Z]=15 THEN J←2*(E+D)*R;
0075 IF H[R,Z]=16 THEN J←D*(R-1/4);
0076 IF H[R,Z]=17 THEN J←E*R;
0077 IF H[R,Z]=18 THEN J←2*(E+D)*R;
0078 IF H[R,Z]=19 THEN J←E*R+D*(R+1/4);
0079 IF H[R,Z]=20 THEN J←E*R+D*(R+1/4);
0080 IF H[R,Z]=21 THEN J←D/4;
0081 F←F+J*(T[R,Z]-TC);
0082 END;
0083 IF F>(1-AK)*Q=RADSUM THEN
0084 BEGIN
0085 IF F<(1+AK)*Q=RADSUM THEN GO TO FINAL;
0086 END;
0087 ITER: RADSUM←0;
0088 FOR R←0 TO N DO
0089 FOR Z←M STEP -1 UNTIL 0 DO
0090 BEGIN
0091 TRZ←T[R,Z]+273;
0092 TT←TRZ↑4-TCC↑4;
0093 L←H[R,Z];
0094 GO TO S[L];
0095
0096 L1 : T[R,Z]←B*(C*(R-1/2)*T[R-1,Z]+C*(R+1/2)*T[R+1,Z]
0097 +2*A*R*T[R,Z-1])/(2*(A+C)*R)
0098 + (1-B)*T[R,Z];
0099 RAD←(2*D*R/W)*SB*TT;
0100 T[R,Z]←T[R,Z]-B*RAD/(2*(A+C)*R);
0101 RADSUM←RADSUM+RAD;
0102 IF R<X THEN T[R,Z]←T[R,Z]+B*Q/((X↑2)*(A+C));
0103 IF R=X THEN T[R,Z]←T[R,Z]+(B*Q*(R-1/4)/(X↑2))/
0104 (2*R*(A+C));
0105 GO TO NEWON;
0106 L2 : T[R,Z]←B*(C*(R-1/2)*T[R-1,Z]+2*C*(R+1/2)*T[R+1,Z]
0107 +2*A*R*T[R,Z-1]+A*(R+1/4)*T[R,Z+1])/
0108 (C*(3*R+1/2)+A*(3*R+1/4)) + (1-B)*T[R,Z];
0109 RAD←(D*(R-1/4)/W)*SB*TT;
0110 T[R,Z]←T[R,Z]-B*RAD/(C*(3*R+1/2)+A*(3*R+1/4));
0111 RADSUM←RADSUM+RAD;
0112 IF R<=X THEN T[R,Z]←T[R,Z]+(B*Q*(R-1/4)/(X↑2))/
0113 (C*(3*R+1/2)+A*(3*R+1/4));
0114 GO TO NEWON;
0115 L3 : T[R,Z]←B*(C*(R+1/2)*T[R+1,Z]+A*(R+1/4)*T[R,Z-1])/
0116 (C*(R+1/2)+A*(R+1/4)) + (1-B)*T[R,Z];
0117 RAD←(D*(R+1/4)/W)*SB*TT;
0118 T[R,Z]←T[R,Z]-B*RAD/(C*(R+1/2)+A*(R+1/4));
0119 RADSUM←RADSUM+RAD;
0120 IF R<X THEN T[R,Z]←T[R,Z]+(B*Q*(R+1/4)/(X↑2))/
0121 (C*(R+1/2)+A*(R+1/4));
0122 GO TO NEWON;
0123 L4 : T[R,Z]←B*(C*(R-1/2)*T[R-1,Z]+C*(R+1/2)*T[R+1,Z]
0124 +2*A*R*T[R,Z+1])/(2*(A+C)*R)+(1-B)*T[R,Z];
0125 GO TO NEWON;

```



```

0126 L5 : T[R,Z] ← B*(2*C*(R-1/2)*T[R-1,Z] + A*(R-1/4)*(T[R,Z-1]
0127           + T[R,Z+1])) / (2*C*(R-1/2) + 2*A*(R-1/4)
0128           + (1-B)*T[R,Z]);
0129 GO TO NEWON;
0130 L6 : T[R,Z] ← B*(C*(R-1/2)*T[R-1,Z] + A*(R+1/4)*T[R,Z+1]) /
0131           (C*(R-1/2) + A*(R+1/4)) + (1-B)*T[R,Z];
0132 GO TO NEWON;
0133 L7 : T[R,Z] ← B*(C*(R-1/2)*T[R-1,Z] + A*(R-1/4)*T[R,Z-1]) /
0134           (C*(R-1/2) + A*(R-1/4)) + (1-B)*T[R,Z];
0135 RAD ← (D*(R-1/4)/W)*SB*TT;
0136 T[R,Z] ← T[R,Z] - B*RAD / (C*(R-1/2) + A*(R-1/4));
0137 RADSUM ← RADSUM + RAD;
0138 IF X=N-1 THEN T[R,Z] ← T[R,Z] + (B*Q*(R-1/4)/(X↑2)) /
0139           (C*(R-1/2) + A*(R-1/4));
0140 GO TO NEWON;
0141 L8 : T[R,Z] ← B*(2*C*(R-1/2)*T[R-1,Z] + 2*C*(R+1/2)*T[R+1,Z]
0142           + 2*A*R*(T[R,Z-1] + T[R,Z+1])) / (4*(A+C)*R)
0143           + (1-B)*T[R,Z];
0144 GO TO NEWON;
0145 L9 : T[R,Z] ← B*(2*C*(R+1/2)*T[R+1,Z] + A*(R+1/4)*(T[R,Z-1]
0146           + T[R,Z+1])) / (2*C*(R+1/2) + 2*A*(R+1/4))
0147           + (1-B)*T[R,Z];
0148 GO TO NEWON;
0149 L10: T[R,Z] ← B*(C*(R-1/2)*T[R-1,Z] + C*(R+1/2)*T[R+1,Z]
0150           + 2*A*R*T[R,Z-1] + 2*D*R*TC) / (2*(A+C+D)*R)
0151           + (1-B)*T[R,Z];
0152 GO TO NEWON;
0153 L11: T[R,Z] ← B*(C*(R-1/2)*T[R-1,Z] + C*(R+1/2)*T[R+1,Z]
0154           + 2*A*R*T[R,Z+1] + 2*D*R*TC) / (2*(A+C+D)*R)
0155           + (1-B)*T[R,Z];
0156 GO TO NEWON;
0157 L12: T[R,Z] ← B*(2*C*(R-1/2)*T[R-1,Z] + A*(R-1/4)*(T[R,Z-1]
0158           + T[R,Z+1]) + 2*E*R*TC) / (2*C*(R-1/2)
0159           + 2*A*(R-1/4) + 2*E*R) + (1-B)*T[R,Z];
0160 GO TO NEWON;
0161 L13: T[R,Z] ← B*(C*(R-1/2)*T[R-1,Z] + A*(R-1/4)*T[R,Z+1]
0162           + E*R*TC) / (C*(R-1/2) + A*(R-1/4) + E*R)
0163           + (1-B)*T[R,Z];
0164 GO TO NEWON;
0165 L14: T[R,Z] ← B*(C*(R-1/2)*T[R-1,Z] + A*(R-1/4)*T[R,Z+1]
0166           + D*(R-1/4)*TC) / (C*(R-1/2) + (A+D)*(R-1/4))
0167           + (1-B)*T[R,Z];
0168 GO TO NEWON;
0169 L15: T[R,Z] ← B*(C*(R-1/2)*T[R-1,Z] + A*(R-1/4)*T[R,Z+1]
0170           + 2*(E+D)*R*TC) / (C*(R-1/2) + A*(R-1/4) + 2*(E
0171           + D)*R) + (1-B)*T[R,Z];
0172 GO TO NEWON;
0173 L16: T[R,Z] ← B*(C*(R-1/2)*T[R-1,Z] + A*(R-1/4)*T[R,Z-1]
0174           + D*(R-1/4)*TC) / (C*(R-1/2) + (A+D)*(R-1/4))
0175           + (1-B)*T[R,Z];
0176 GO TO NEWON;
0177 L17: T[R,Z] ← B*(C*(R-1/2)*T[R-1,Z] + A*(R-1/4)*T[R,Z-1]
0178           + E*R*TC) / (C*(R-1/2) + A*(R-1/4) + E*R)
0179           + (1-B)*T[R,Z];
0180 IF X=N-1 THEN T[R,Z] ← T[R,Z] + (B*Q*(R-1/4)/(X↑2)) /
0181           (C*(R-1/2) + A*(R-1/4) + E*R);
0182 GO TO NEWON;
0183 L18: T[R,Z] ← B*(C*(R-1/2)*T[R-1,Z] + A*(R-1/4)*T[R,Z-1]
0184           + 2*(E+D)*R*TC) / (C*(R-1/2) + A*(R-1/4) + 2*(E+D)
0185           *R) + (1-B)*T[R,Z];
0186 GO TO NEWON;

```



```

0187 L19: T[R,Z]←B*(2*C*(R-1/2)*T[R-1,Z]+C*(R+1/2)*T[R+1,Z]
0188      +2*A*R*T[R,Z+1]+A*(R-1/4)*T[R,Z-1]+E*R*TC
0189      +D*(R+1/4)*TC)/(C*(3*R-1/2)+A*(3*R-1/4)
0190      +E*R+D*(R+1/4))+(1-B)*T[R,Z];
0191      GO TO NEWON;
0192 L20: T[R,Z]←B*(2*C*(R-1/2)*T[R-1,Z]+C*(R+1/2)*T[R+1,Z]
0193      +2*A*R*T[R,Z-1]+A*(R-1/4)*T[R,Z+1]+E*R*TC
0194      +D*(R+1/4)*TC)/(C*(3*R-1/2)+A*(3*R-1/4)
0195      +E*R+D*(R+1/4))+(1-B)*T[R,Z];
0196      GO TO NEWON;
0197 L21: T[R,Z]←B*((C/2)*T[R+1,Z]+(A/4)*T[R,Z+1]+(D/4)*TC)/
0198      (C/2+A/4+D/4)+(1-B)*T[R,Z];
0199      GO TO NEWON;
0200 L22: T[R,Z]←B*((C*T[R+1,Z]+(A/4)*(T[R,Z+1]+T[R,Z-1]))/
0201      (C+A/2))+(1-B)*T[R,Z];
0202      GO TO NEWON;
0203 L23: T[R,Z]←B*((C/2)*T[R+1,Z]+(A/4)*T[R,Z-1]+Q/
0204      (4*(X↑2)))/(C/2+A/4)+(1-B)*T[R,Z];
0205      RAD←(D/(4*W))*SB*TT;
0206      T[R,Z]←T[R,Z]-B*RAD/(C/2+A/4);
0207      RADSUM←RADSUM+RAD;
0208      GO TO NEWON;
0209 L24: T[R,Z]←B*((C/2)*T[R+1,Z]+(A/4)*T[R,Z+1])/
0210      (C/2+A/4)+(1-B)*T[R,Z];
0211      GO TO NEWON;
0212 L25: T[R,Z]←1000000; GO TO NEWON;
0213 NEWON: END;
0214 GO TO START;
0215 FINAL:
0216 WRITE(LUO,#(X,I5),COUNT);
0217 WRITE(LUO,#(6(X,I3)),FOR R←0 TO N DO
0218 FOR Z←0 TO M DO T[R,Z]);
0219 ENDS

```


REFERENCES

Abbreviations :

NIM	Nuclear Instruments & Methods
JRaC	Journal of Radio-analytical Chemistry
AC	Analytical Chemistry
IEEE	IEEE Transactions on Nuclear Science
Liege '67	Proceedings of 3rd Conference on Accelerator Targets Designed for the Production of Neutrons Liege, Sept. 1967 Euratom EUR 3895 d-f-e

1. ADAMS & HOSTE : Atomic Energy Review 4 (1966) 2 , 113
2. HOSTE et al. : 'Instrumental & Radiochemical Activation
Analysis' CRC
3. AMSEL : JRaC 17 (1973) 15
4. SIPPEL & GLOVER : NIM 2 (1960) 37
5. WOLICKI : 'New Uses of Ion Accelerators' (Ziegler , ed.)
6. PIERCE, PECK & CUFF : The Analyst 92 (1967) 143
7. BUTLER : U.S. Naval Research Laboratory NRL Report 5282 (1959)
8. AJZENBERG-SELOVE & LAURITSEN : Nuclear Physics 11 (1959) 1
9. ENDT & van der LEUN : Nuclear Physics 34 (1962) 1
10. GOLICHEFF, LOEUILLET & ENGELMANN : JRaC 12 (1972) 233
11. DECONNINCK : JRaC 12 (1972) 157
12. RUBIN, PASSELL & BAILEY : AC 29 (1957) 736
13. PIERCE, PECK & HENRY : The Analyst 90 , 339
14. ENGLAND, ASHE, WILLIAMS, MORGAN & BLAKE :
Transactions of the American Nuclear Society 10 (1967) 86
15. AMSEL & SAMUEL : AC 39 (1967) 1689
16. AMSEL, BERANGER, de GELAS & LACOMBE :
Journal of Applied Physics 39 (1968) 5 , 2246

17. MAUREL, DIEUMEGARD & AMSEL :
Journal of the Electrochemical Society 119 (1972) 1717
18. ANDERS : AC 38 (1966) 1442
19. MOLLER, NILSSON & STARFELT : NIM 50 (1967) 270
20. RICCI & HAHN : AC 37 (1965) 742
21. MACKLIN, GIBBONS, RICCI, HANDLEY & CUNEO :
Nuclear Applications 5 (1968) 269
22. HENSHAW : Ph.D Thesis (1974) University of Birmingham
23. DIEUMEGARD : Doctoral Thesis , University of Paris (Orsay)
24. CHEN : Ph.D Thesis (1969) University of Birmingham
25. BEWERS & FLACK : The Analyst 94 (1969) I
26. POINT : Proceedings of 1st (UNESCO) International Conference
on Radio-isotopes in Scientific Research (1957)
27. PIERCE, PECK & HENRY : Nature 204 (1964) 571
28. PIERCE, PECK & CUFF : NIM 67 (1969) I
29. DECONNINCK & DEMORTIER : JRaC 12 (1972) 189
30. BODART & DEMORTIER : JRaC 12 (1972) 209
31. AMSEL & SAMUEL : Journal of the Physical Chemistry of Solids
23 (1962) 1707
32. PALMER : NIM 38 (1965) 187
33. WHITTON, MITCHELL & WINTERBON : Canadian Journal of Physics
49 (1971) 1225
34. DERRY, LEES & CALVERT : Proceedings of the British Ceramic Society
19 (1971) 77
35. NEILD, WISE & BARNES : Journal of Physics D 5 (1972) 2292
36. ZIEGLER, COLE & BAGLIN : Journal of Applied Physics 43 (1972) 3809
37. ZIEGLER & BAGLIN : Journal of Applied Physics 42 (1971) 2031
38. WORMLEY : Ph.D Thesis (1972) University of Birmingham
39. MANDLER, MOLLER, RAISEN & RAJAN :
'Ion Beam Surface Layer Analysis' (1974 ; Elsevier, Lausanne) 165
40. MOLLER & STARFELT : NIM 50 (1967) 225

41. VILATHONG : M.Sc Thesis (1971) University of Aston
42. O'CONNELL : Ph.D Thesis (1976) University of Aston
43. GOLICHEFF & ENGELMANN : JRaC 16 (1973) 503
44. AMSEL, NADAI, d'ARTEMARE, DAVID, GIRARD & MOULIN : NIM 92 (1971) 481
45. DUNNING, HUBLER, COMAS, LUCKE & HUGHES :
 'Ion Beam Surface Layer Analysis' (1974 ; Elsevier, Lausanne) I45
46. CHEMIN, ROTURIER, SABOYA & PETIT : NIM 97 (1971) 97
47. 'Target Design' in Radiation Review 4 , I (Nov. 1964)
48. HANLEY, HABERL & TAYLOR : IEEE NS-I4 , 3 (1967) 933
49. SEILER, CLELAND & WEGNER : IEEE NS-I4 , 3 (1967) 943
50. RETHMEIER & van der MEULEN : NIM 24 (1963) 349
51. SMITH : 'Life of Tritium Targets Under Deuteron Bombardment'
 Liege '67
52. ALLARD : 'Cibles a Haut Rendement Neutronique pour un Accelérateur
 Lineaire a Electrons (Faisceau a puissance moyenne elevee
 de l'ordre de 10 kW)' ; Liege '67
53. BOOTH : IEEE NS-I4 , 3 (1967) 938
54. COSSUTA : 'A Rotating Target Assembly for 10 n/sec' ; Liege '67
55. WILLIAMSON : 'A Design Study for a Gas Target using a Rotating
 Foil' ; Liege '67
56. DUMOND, WATSON & HICKS : Review of Scientific Instruments
 NS-6 (1935) I83
57. SPAA : Journal of Scientific Instruments 35 (1958) I75
58. HOURST & ROCHE : NIM 92 (1971) 589
59. GRIFFITHS : M.Sc Thesis (1971) University of Birmingham
60. KAS & NOVAK : NIM 99 (1972) 359
61. PENNER : IEEE NS-I4 , 3 (1967) 908
62. DUSINBERRE : Numerical Analysis of Heat Flow
63. DUSINBERRE : Heat Transfer Calculations by Finite Differences
64. CLAUSING : 'Numerical Methods in Heat Transfer' in
 Advanced Heat Transfer (Chao, ed.) Univ. of Illinois 1969

65. Modern Computing Methods chap. 10

NPL 1957 H.M. Stationery Office

66. NOBLE : Numerical Methods I (1964) Oliver & Boyd

67. GLASSTONE & SESONKE : 'Nuclear Reactor Engineering' chap. 6

68. HUNT, POPE, EVANS & HANCOCK : British Journal of Applied Physics
2 (1958) 443

TABLES

TABLE I

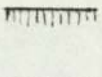
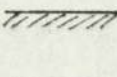
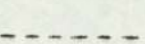
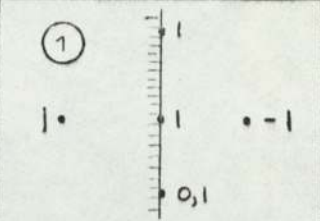
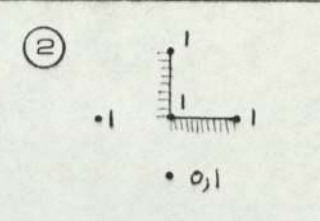
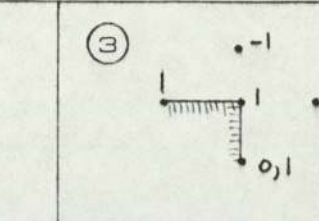
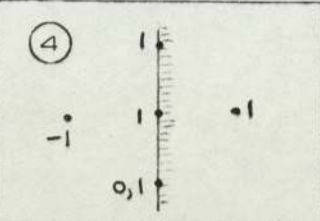
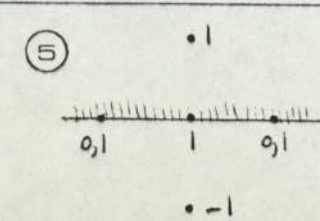
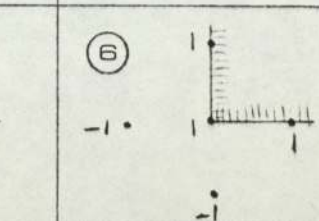
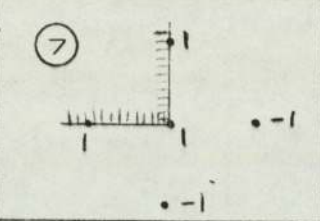
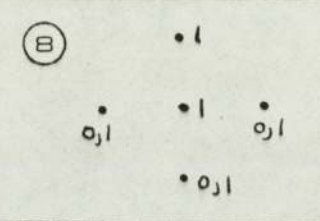
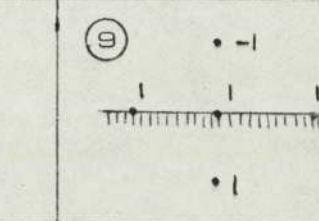
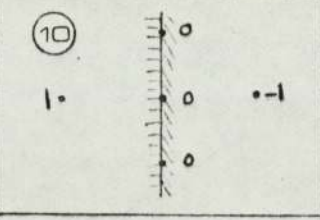
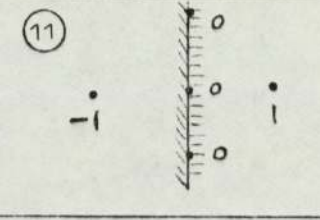
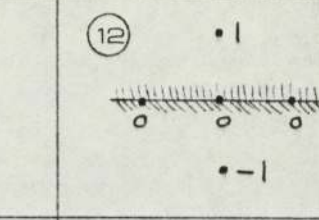
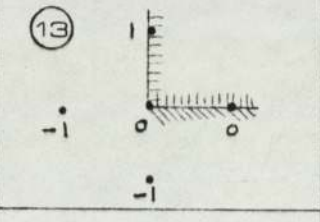
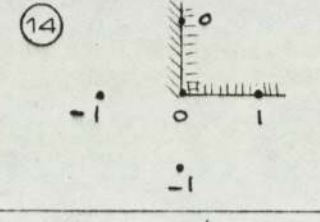
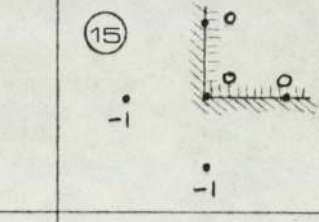
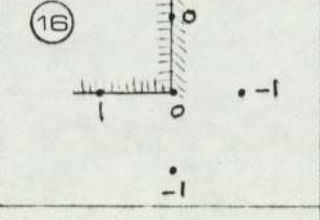
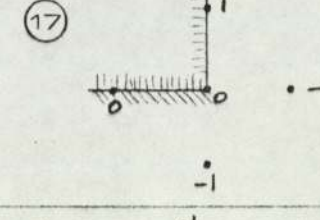
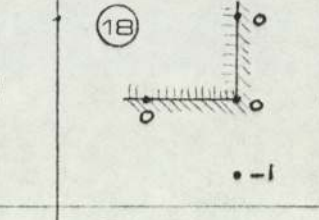
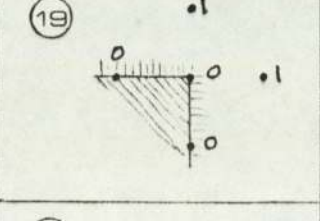
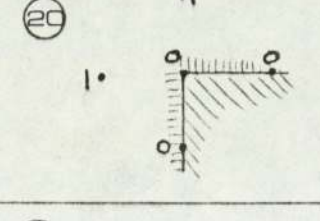
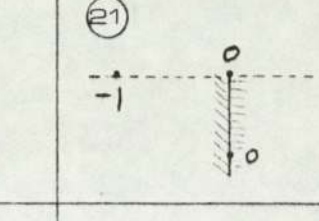
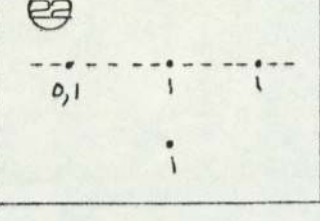
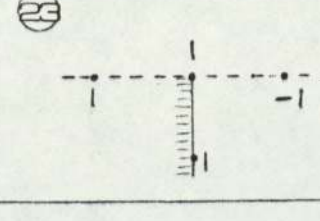
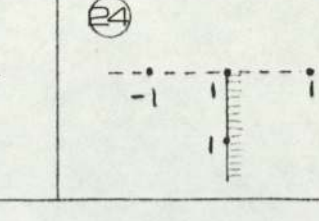
	 SOLID BOUNDARY	 LIQUID BOUNDARY	 AXIS ($R=0$)
①			
④			
⑦			
⑩			
⑬			
⑯			
⑲			
⑳			

TABLE 2

I :	$T_{r_1 z}$	$= (\pi K(R+\frac{1}{2}) \Delta Z \cdot T_{r+1 z} + \pi K(R-\frac{1}{2}) \Delta Z \cdot T_{r-1 z} + 2\pi K R \frac{\Delta R^2}{\Delta Z} \cdot T_{r_1 z}) / (2\pi K R \cdot \Delta Z + 2\pi K R \frac{\Delta R^2}{\Delta Z})$
2 :	$T_{r_2 z}$	$= (2\pi K(R+\frac{1}{2}) \cdot \Delta Z \cdot T_{r+1 z} + 2\pi K R \frac{\Delta R^2}{\Delta Z} \cdot T_{r_1 z}) / (2\pi K(R+\frac{1}{2}) \Delta Z + 2\pi K R \frac{\Delta R^2}{\Delta Z})$
3 :	$T_{r_3 z}$	$= (\pi K(R+\frac{1}{2}) \Delta Z \cdot T_{r+1 z} + \pi K(R+\frac{1}{4}) \cdot \frac{\Delta R^2}{\Delta Z} \cdot T_{r_1 z}) / (\pi K(R+\frac{1}{2}) \Delta Z + \pi K(R+\frac{1}{4}) \frac{\Delta R^2}{\Delta Z})$
4 :	$T_{r_4 z}$	$= (\pi K(R+\frac{1}{2}) \Delta Z \cdot T_{r+1 z} + \pi K(R-\frac{1}{2}) \Delta Z \cdot T_{r-1 z} + 2\pi K R \frac{\Delta R^2}{\Delta Z} \cdot T_{r_1 z}) / (\pi K(R+\frac{1}{2}) \cdot \Delta Z + \pi K(R-\frac{1}{2}) \cdot \Delta Z + 2\pi K R \frac{\Delta R^2}{\Delta Z})$
5 :	$T_{r_5 z}$	$= (2\pi K(R-\frac{1}{2}) \Delta Z \cdot T_{r-1 z} + \pi K(R-\frac{1}{4}) \frac{\Delta R^2}{\Delta Z} \cdot T_{r_1 z}) / (T_{r_1 z} + T_{r_3 z}) / (2\pi K(R-\frac{1}{2}) \Delta Z + 2\pi K(R-\frac{1}{4}) \frac{\Delta R^2}{\Delta Z})$
6 :	$T_{r_6 z}$	$= (\pi K(R-\frac{1}{2}) \cdot \Delta Z \cdot T_{r-1 z} + K(R-\frac{1}{4}) \frac{\Delta R^2}{\Delta Z} \cdot T_{r_1 z}) / (\pi K(R-\frac{1}{2}) \Delta Z + \pi K(R-\frac{1}{4}) \frac{\Delta R^2}{\Delta Z})$
7 :	$T_{r_7 z}$	$= (\pi K(R-\frac{1}{2}) \Delta Z \cdot T_{r-1 z} + \pi K(R-\frac{1}{4}) \frac{\Delta R^2}{\Delta Z} \cdot T_{r_1 z}) / (\pi K(R-\frac{1}{2}) \Delta Z + \pi K(R-\frac{1}{4}) \frac{\Delta R^2}{\Delta Z})$
8 :	$T_{r_8 z}$	$= (2\pi K(R+\frac{1}{2}) \Delta Z \cdot T_{r+1 z} + 2\pi K R \frac{\Delta R^2}{\Delta Z} \cdot T_{r_1 z} + 2\pi K R \frac{\Delta R^2}{\Delta Z} (T_{r_1 z} + T_{r_3 z})) / (2\pi K(R+\frac{1}{2}) \Delta Z + 2\pi K(R-\frac{1}{2}) \Delta Z + 4\pi K R \frac{\Delta R^2}{\Delta Z})$
9 :	$T_{r_9 z}$	$= (2\pi K(R+\frac{1}{2}) \Delta Z \cdot T_{r+1 z} + \pi K(R+\frac{1}{4}) \frac{\Delta R^2}{\Delta Z} \cdot T_{r_1 z}) / (T_{r_1 z} + T_{r_3 z}) / (2\pi K(R+\frac{1}{2}) \cdot \Delta Z + 2\pi K(R+\frac{1}{4}) \frac{\Delta R^2}{\Delta Z})$
10 :	$T_{r_{10} z}$	$= (\pi K(R+\frac{1}{2}) \cdot \Delta Z \cdot T_{r+1 z} + \pi K(R-\frac{1}{2}) \cdot \Delta Z \cdot T_{r-1 z} + 2\pi K R \frac{\Delta R^2}{\Delta Z} \cdot T_{r_1 z} + 2\pi H R \cdot \Delta R \cdot T_c) / (\pi K(R+\frac{1}{2}) \Delta Z + \pi K(R-\frac{1}{2}) \Delta Z + 2\pi H R \frac{\Delta R^2}{\Delta Z} + 2\pi H R \Delta R)$
II :	$T_{r_1 z}$	$= (\pi K(R+\frac{1}{2}) \Delta Z \cdot T_{r+1 z} + \pi K(R-\frac{1}{2}) \Delta Z \cdot T_{r-1 z} + 2\pi K R \frac{\Delta R^2}{\Delta Z} \cdot T_{r_1 z} + 2\pi H R \cdot \Delta R \cdot T_c) / (2\pi K R \cdot \Delta Z + 2\pi K R \frac{\Delta R^2}{\Delta Z} + 2\pi H R \cdot \Delta R)$
12 :	$T_{r_2 z}$	$= (2\pi K(R-\frac{1}{2}) \Delta Z \cdot T_{r-1 z} + \pi K(R-\frac{1}{4}) \frac{\Delta R^2}{\Delta Z} \cdot T_{r_1 z}) / (T_{r_1 z} + T_{r_3 z}) + \pi H R \cdot \Delta R \cdot T_c / (2\pi K(R-\frac{1}{2}) \cdot \Delta Z + 2\pi K(R-\frac{1}{4}) \frac{\Delta R^2}{\Delta Z} + \pi H R \Delta R)$
13 :	$T_{r_3 z}$	$= (\pi K(R-\frac{1}{2}) \Delta Z \cdot T_{r-1 z} + \pi K(R-\frac{1}{4}) \frac{\Delta R^2}{\Delta Z} \cdot T_{r_1 z} + \frac{1}{2} \pi H R \Delta R \cdot T_c) / (\pi K(R-\frac{1}{2}) \Delta Z + \pi K(R-\frac{1}{4}) \frac{\Delta R^2}{\Delta Z} + \frac{1}{2} \pi H R \Delta R)$
14 :	$T_{r_4 z}$	$= (\pi K(R-\frac{1}{2}) \Delta Z \cdot T_{r-1 z} + \pi K(R-\frac{1}{4}) \frac{\Delta R^2}{\Delta Z} \cdot T_{r_1 z} + \pi H(R-\frac{1}{4}) \Delta R \cdot T_c) / (\pi K(R-\frac{1}{2}) \Delta Z + \pi K(R-\frac{1}{4}) \frac{\Delta R^2}{\Delta Z} + \pi H(R-\frac{1}{4}) \Delta R)$
15 :	$T_{r_5 z}$	$= (\pi K(R-\frac{1}{2}) \Delta Z \cdot T_{r-1 z} + \pi K(R-\frac{1}{4}) \frac{\Delta R^2}{\Delta Z} \cdot T_{r_1 z} + \frac{1}{2} \pi H R \Delta R \cdot T_c + \pi H \Delta R^2 (R-\frac{1}{4}) T_c) / (\pi K(R-\frac{1}{2}) \Delta Z + \pi K(R-\frac{1}{4}) \frac{\Delta R^2}{\Delta Z} + \frac{1}{2} \pi H R \Delta R + \pi H(R-\frac{1}{4}) \Delta R)$

- I6 : $T_{r_3} = \left(\pi K(R-\frac{1}{2}) \Delta Z \cdot T_{r_3} + \pi K(R-\frac{1}{2}) \frac{\Delta R}{\Delta Z} \cdot T_{r_3-1} + \pi H(R-\frac{1}{2}) \Delta R \cdot T_c \right) / \left(\pi K(R-\frac{1}{2}) \Delta Z + \pi K(R-\frac{1}{2}) \frac{\Delta R}{\Delta Z} + \pi H(R-\frac{1}{2}) \Delta R \right)$
- I7 : $T_{r_3} = \left(\pi K(R-\frac{1}{2}) \Delta Z \cdot T_{r_3} + \pi K(R-\frac{1}{2}) \frac{\Delta R}{\Delta Z} \cdot T_{r_3-1} + \frac{1}{2} \pi HR \Delta R \cdot \Delta Z \cdot T_c \right) / \left(\pi K(R-\frac{1}{2}) \Delta Z + \pi K(R-\frac{1}{2}) \frac{\Delta R}{\Delta Z} + \frac{1}{2} \pi HR \Delta R \right)$
- I8 : $T_{r_3} = \left(\pi K(R-\frac{1}{2}) \Delta Z \cdot T_{r_3} + \pi K(R-\frac{1}{2}) \frac{\Delta R}{\Delta Z} \cdot T_{r_3-1} + \frac{1}{2} \pi HR \Delta R \cdot \Delta Z \cdot T_c + \pi H \Delta R \left(R-\frac{1}{2} \right) \cdot T_c \right) / \left(\pi K(R-\frac{1}{2}) \Delta Z + \pi K(R-\frac{1}{2}) \frac{\Delta R}{\Delta Z} + \frac{1}{2} \pi HR \Delta R \cdot \Delta Z + \pi H(R-\frac{1}{2}) \Delta R \right)$
- I9 : $T_{r_3} = \left(\pi K(R+\frac{1}{2}) \Delta Z \cdot T_{r_3} + 2\pi K(R-\frac{1}{2}) \Delta Z \cdot T_{r_3} + 2\pi KR \frac{\Delta R}{\Delta Z} \cdot T_{r_3+1} + \pi K(R-\frac{1}{2}) \frac{\Delta R}{\Delta Z} \cdot T_{r_3-1} + \pi H(R+\frac{1}{2}) \Delta R \cdot T_c \right) / \left(2\pi R \Delta Z + 2\pi KR \frac{\Delta R}{\Delta Z} + \pi K(R-\frac{1}{2}) \frac{\Delta R}{\Delta Z} + \pi H(R+\frac{1}{2}) \Delta R + \frac{1}{2} \pi HR \Delta R \right)$
- 20 : $T_{r_3} = \left(\pi K(R+\frac{1}{2}) \Delta Z \cdot T_{r_3} + 2\pi K(R-\frac{1}{2}) \Delta Z \cdot T_{r_3} + \pi K(R-\frac{1}{2}) \frac{\Delta R}{\Delta Z} \cdot T_{r_3+1} + 2\pi KR \frac{\Delta R}{\Delta Z} \cdot T_{r_3-1} + \pi H(R+\frac{1}{2}) \Delta R \cdot T_c + \frac{1}{2} \pi HR \Delta R \cdot T_c \right) / \left(\pi K(R+\frac{1}{2}) \Delta Z + 2\pi K(R-\frac{1}{2}) \Delta Z + \pi K(R-\frac{1}{2}) \frac{\Delta R}{\Delta Z} + 2\pi KR \frac{\Delta R}{\Delta Z} + \pi H(R+\frac{1}{2}) \Delta R + \frac{1}{2} \pi HR \Delta R \right)$
- 21 : $T_{r_3} = \left(\frac{1}{2} \pi K \Delta Z \cdot T_{r_3} + \frac{1}{4} \pi K \frac{\Delta R}{\Delta Z} \cdot T_{r_3+1} + \frac{1}{4} \pi H \Delta R \cdot T_c \right) / \left(\frac{1}{2} \pi K \Delta Z + \frac{1}{4} \pi K \frac{\Delta R}{\Delta Z} + \frac{1}{4} \pi H \Delta R \right)$
- 22 : $T_{r_3} = \left(\pi K \Delta Z \cdot T_{r_3} + \frac{1}{2} \pi K \frac{\Delta R}{\Delta Z} \cdot (T_{r_3+1} + T_{r_3-1}) \right) / \left(\pi K \Delta Z + \frac{1}{2} \pi K \frac{\Delta R}{\Delta Z} \right)$
- 23 : $T_{r_3} = \left(\frac{1}{2} \pi K \Delta Z \cdot T_{r_3} + \frac{1}{4} \pi K \frac{\Delta R}{\Delta Z} \cdot T_{r_3-1} \right) / \left(\frac{1}{2} \pi K \Delta Z + \frac{1}{4} \pi K \frac{\Delta R}{\Delta Z} \right)$
- 24 : $T_{r_3} = \left(\frac{1}{2} \pi K \Delta Z \cdot T_{r_3} + \frac{1}{4} \pi K \frac{\Delta R}{\Delta Z} \cdot T_{r_3+1} \right) / \left(\frac{1}{2} \pi K \Delta Z + \frac{1}{4} \pi K \frac{\Delta R}{\Delta Z} \right)$

DIAGRAMS

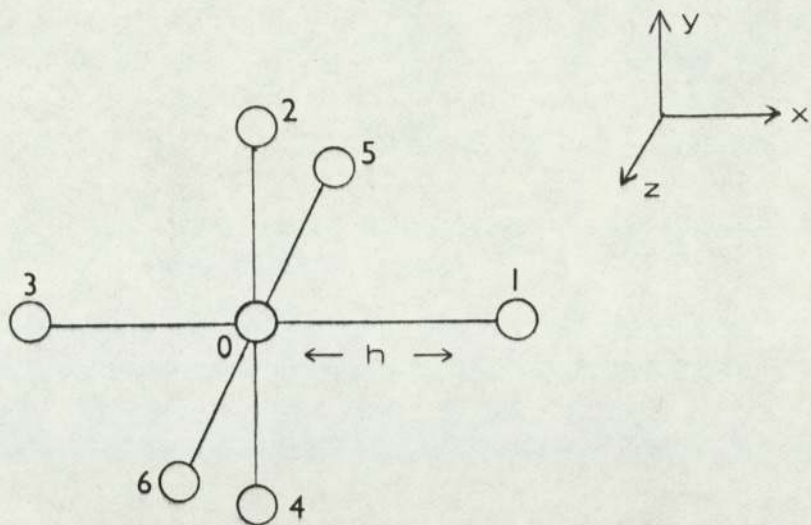


FIG. 1

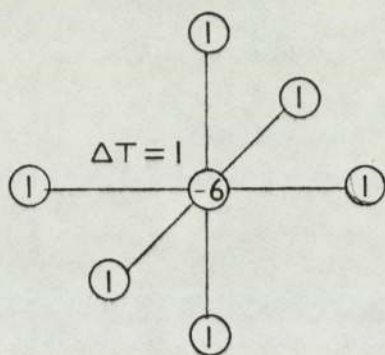


FIG. 2

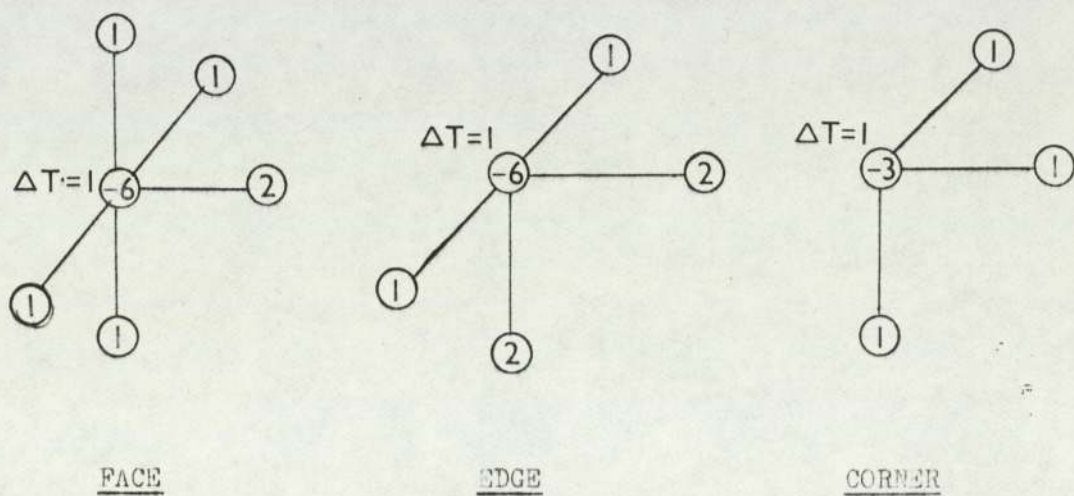


FIG. 3

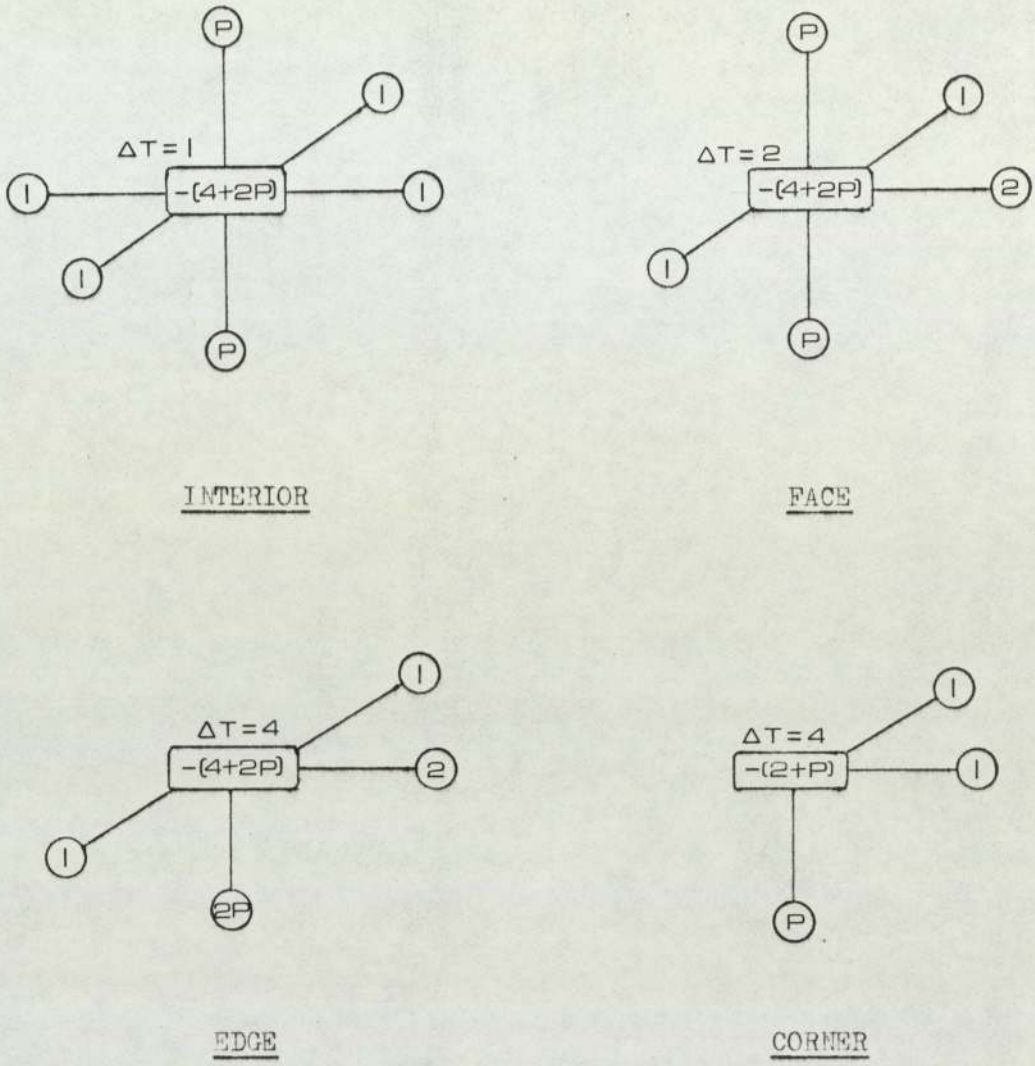


FIG. 4

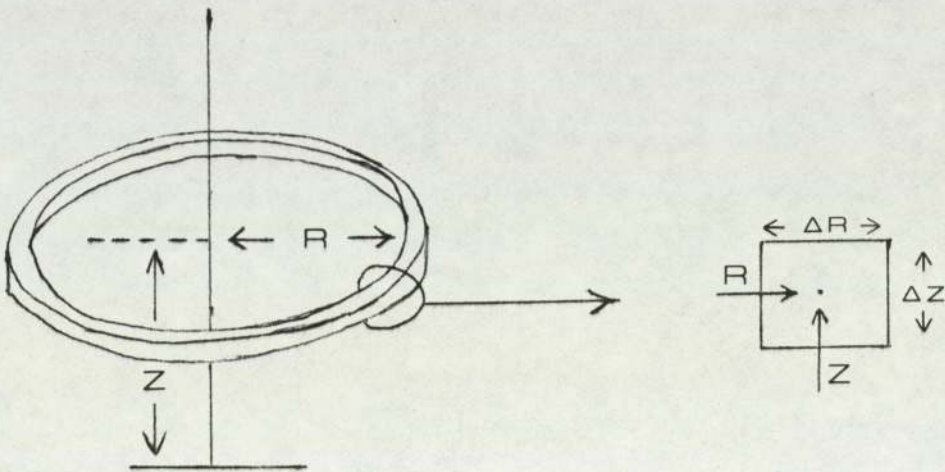


FIG. 5

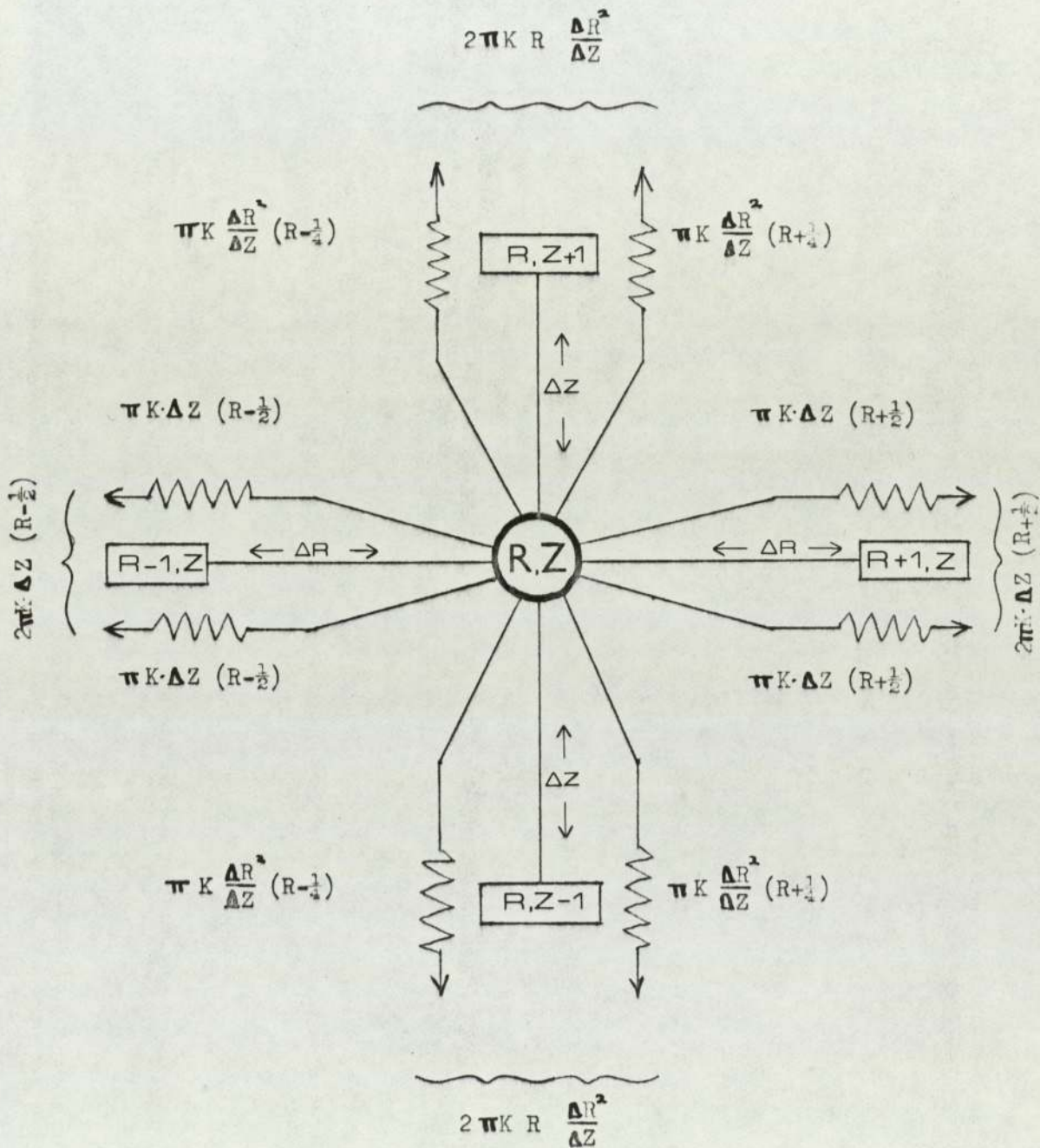


FIG. 6

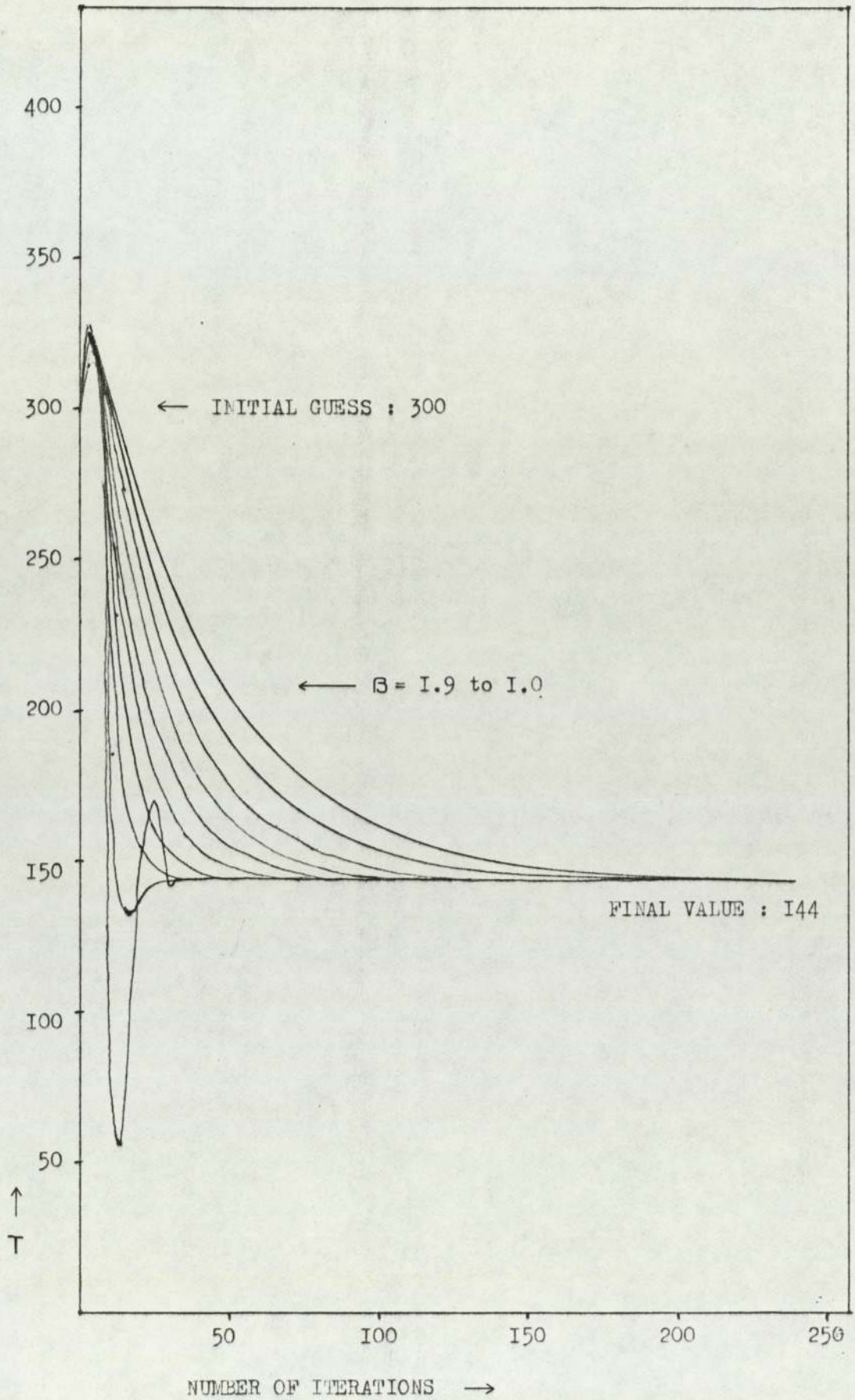


FIG. 7 : EFFECT OF RELAXATION COEFFICIENT

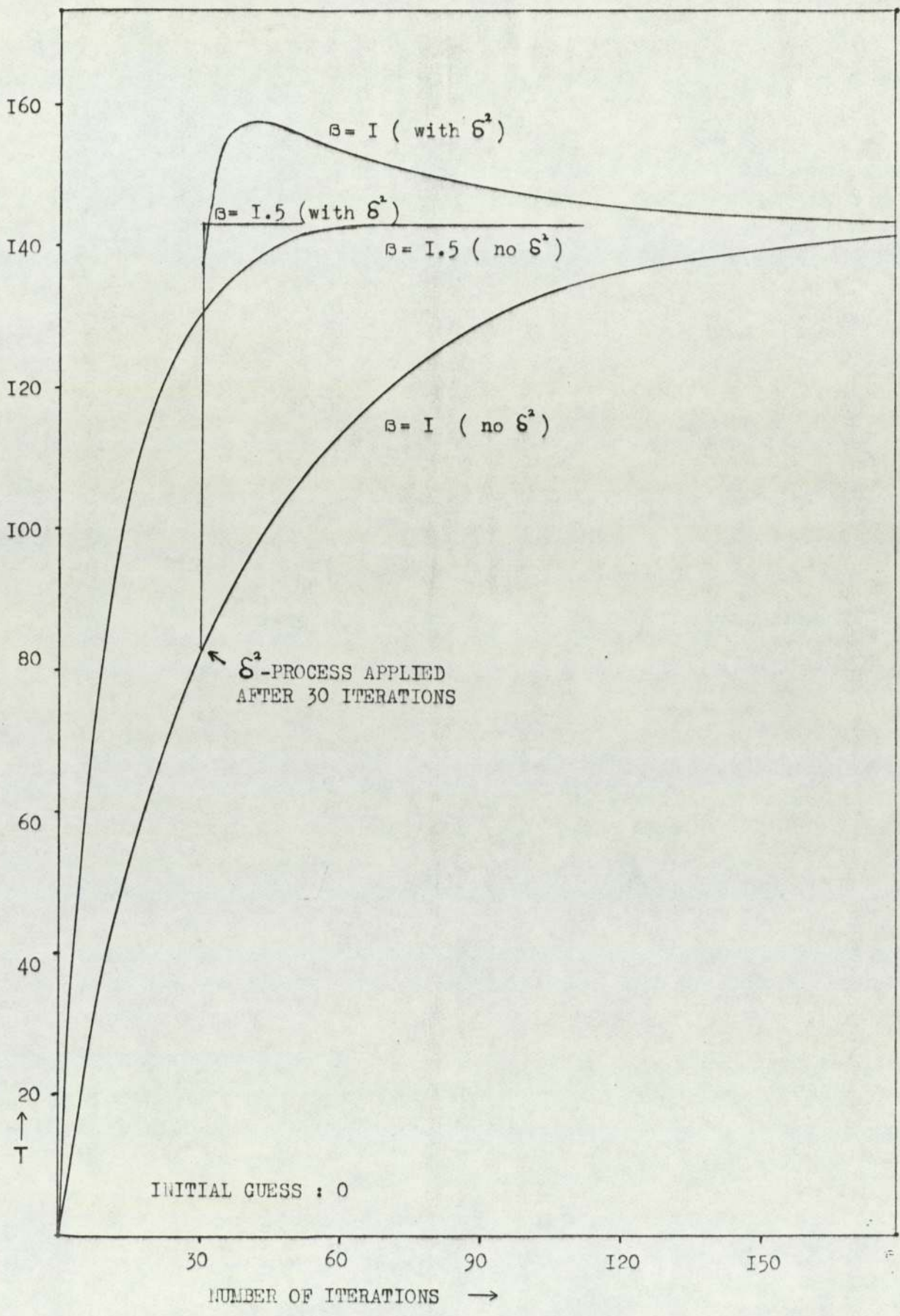


FIG. 8 : EFFECT OF AITKEN δ^2 -PROCESS

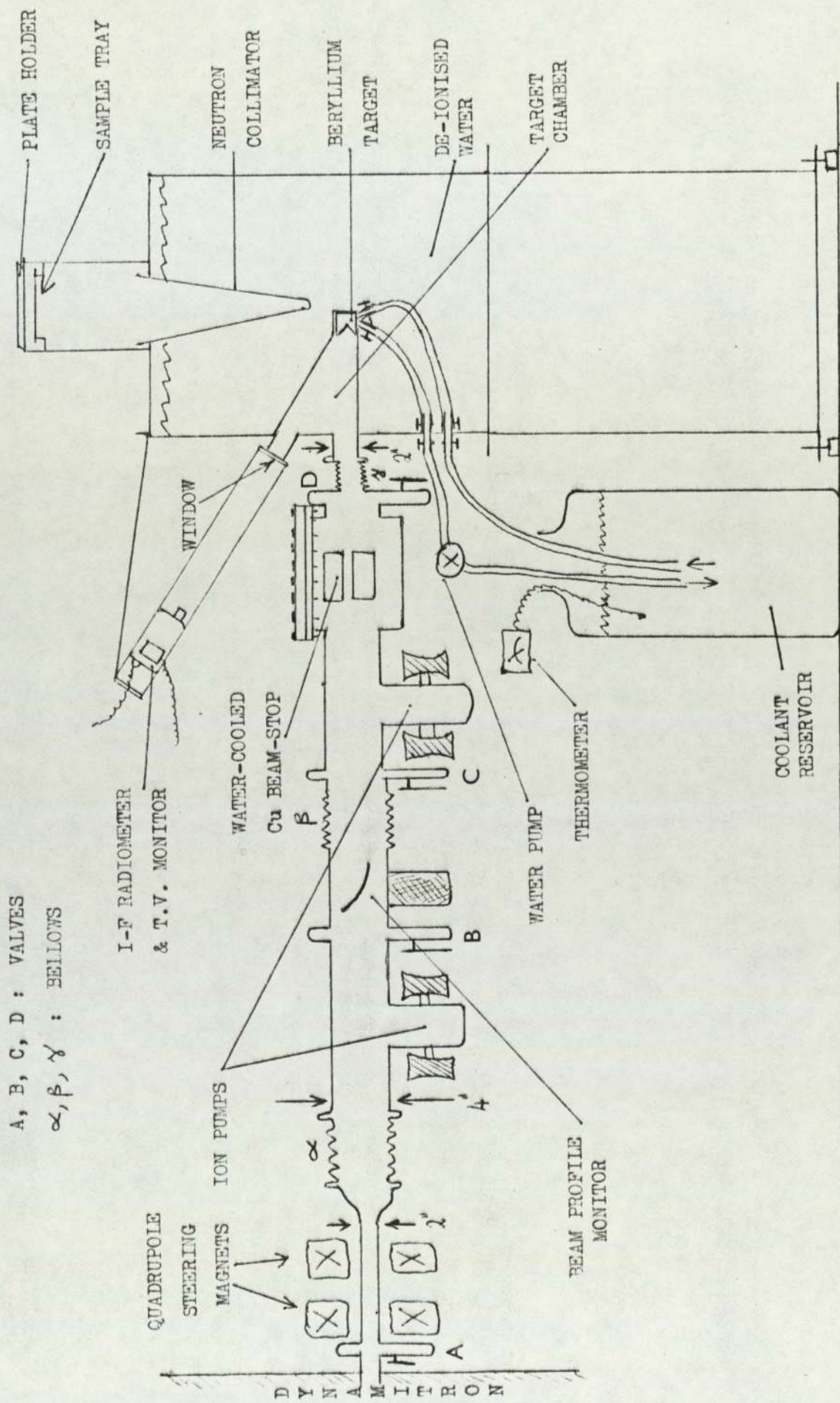
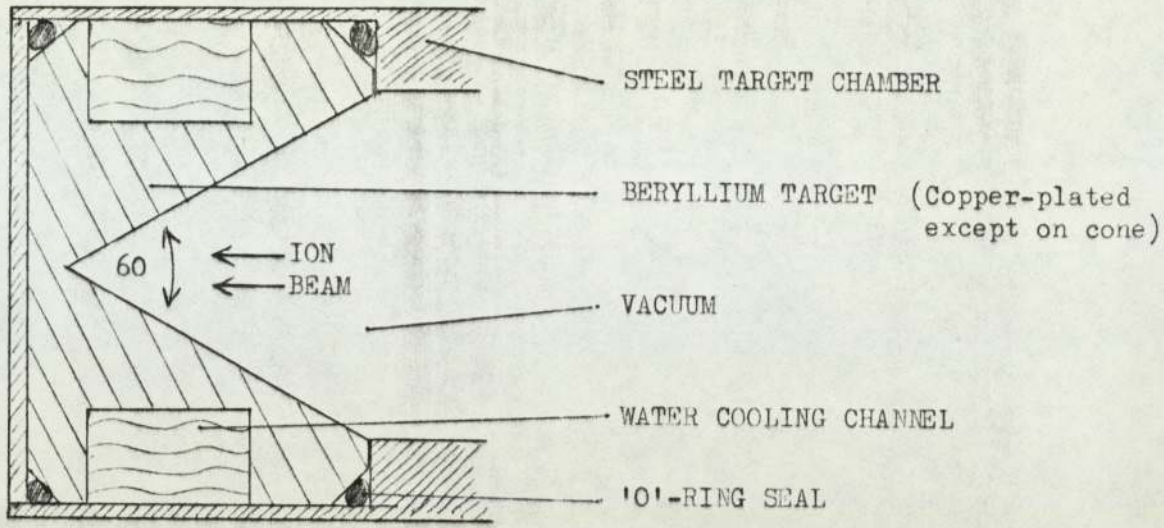


FIG. 9



1 cm.

FIG. 10 : NEUTRON-GENERATING TARGET

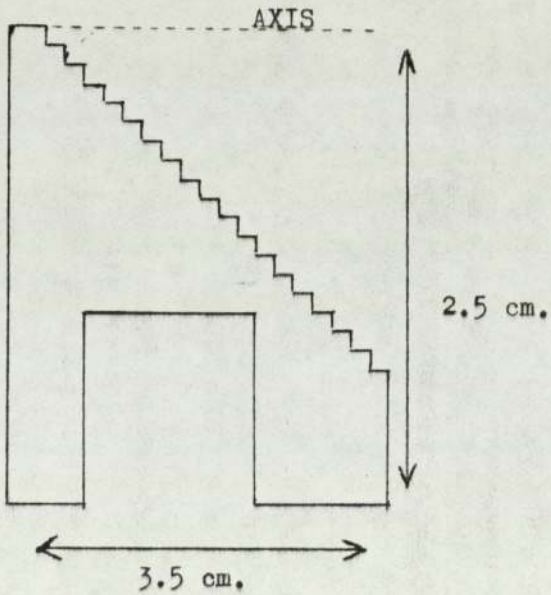


FIG. 11 : COMPUTER SCHEMATIC OF FIG. 10
(Cf. FIG. 27)

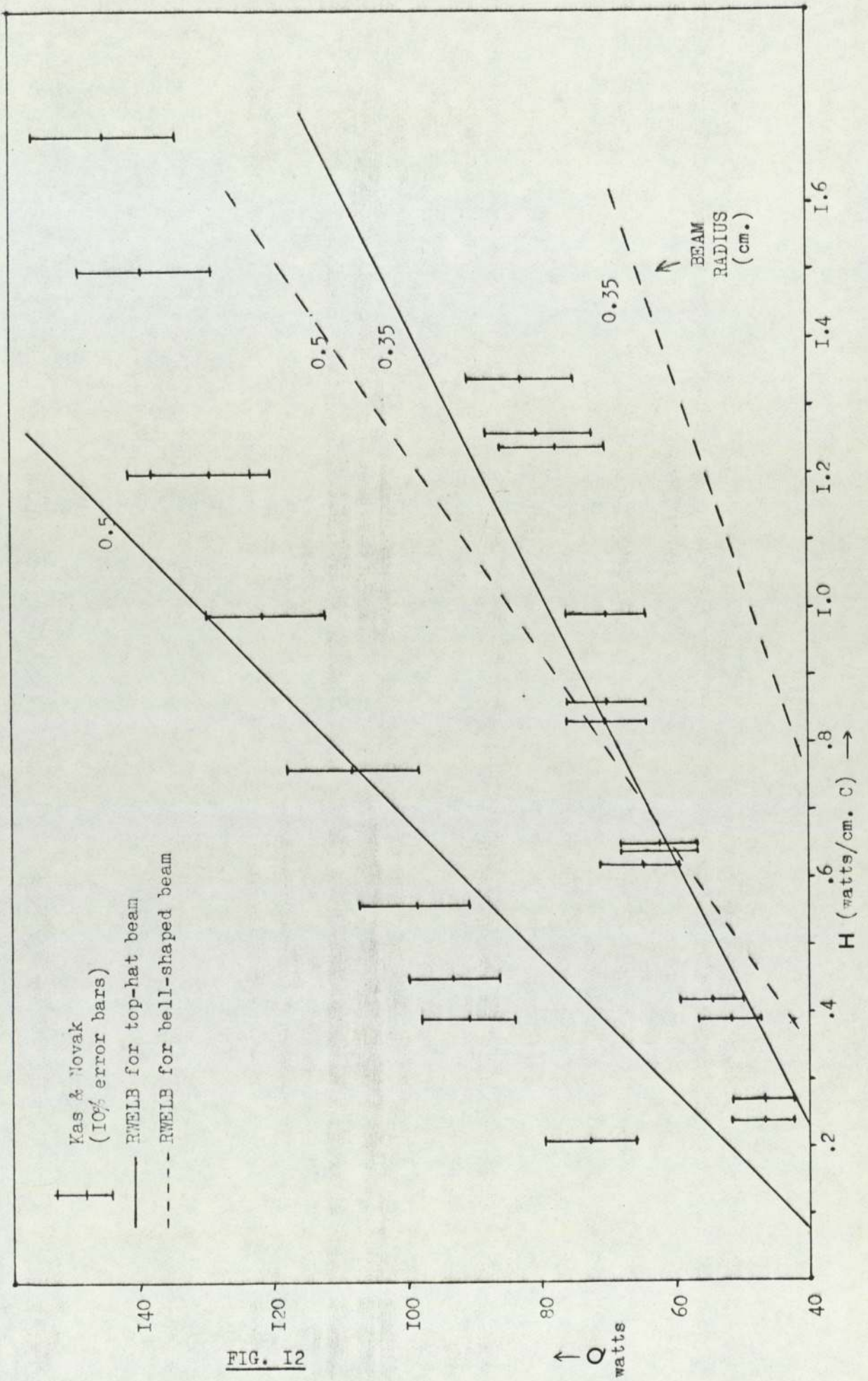


FIG. 12

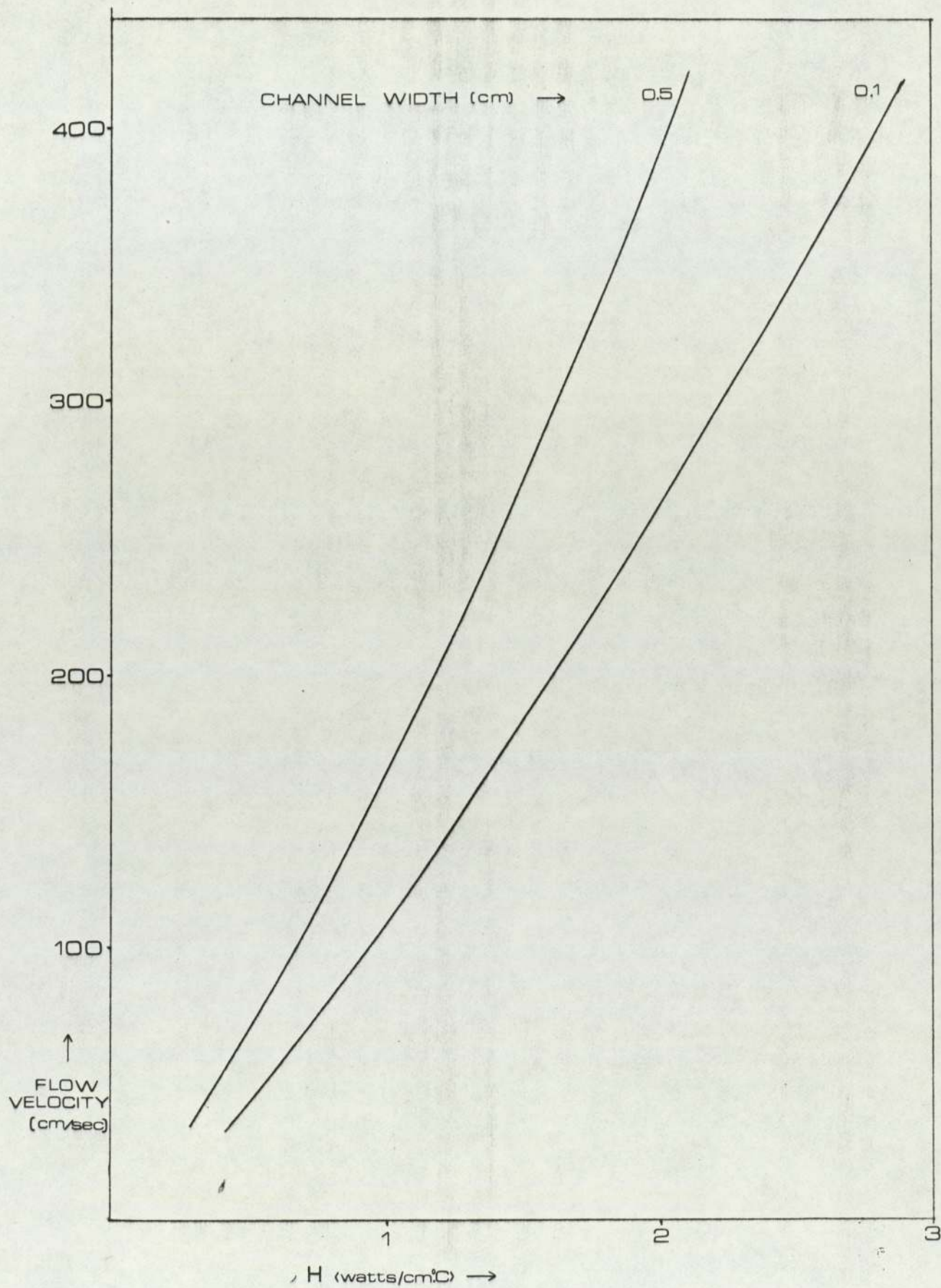


FIG. 13 : HEAT TRANSFER COEFFICIENT FOR WATER

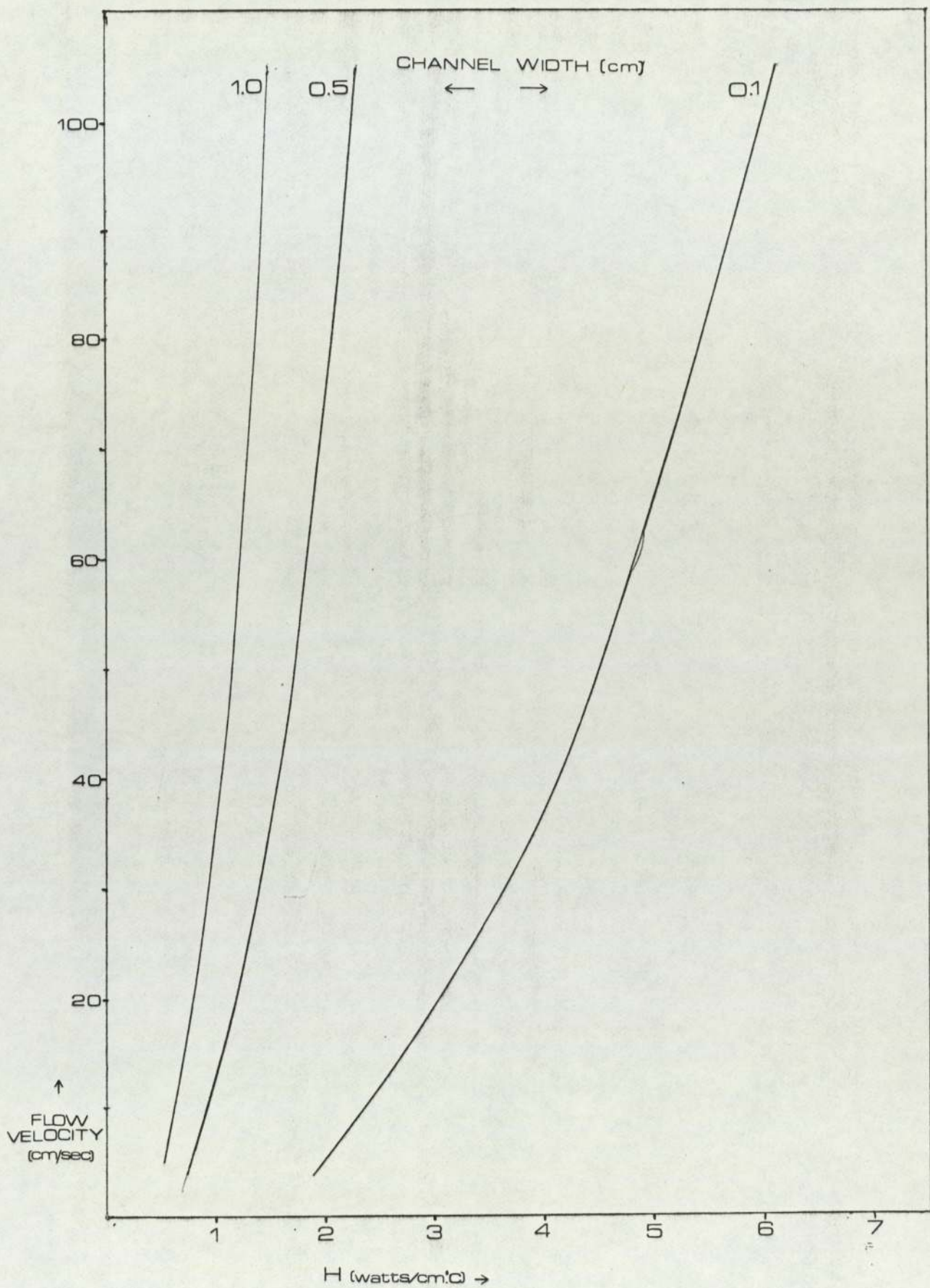


FIG.14: H for NaK

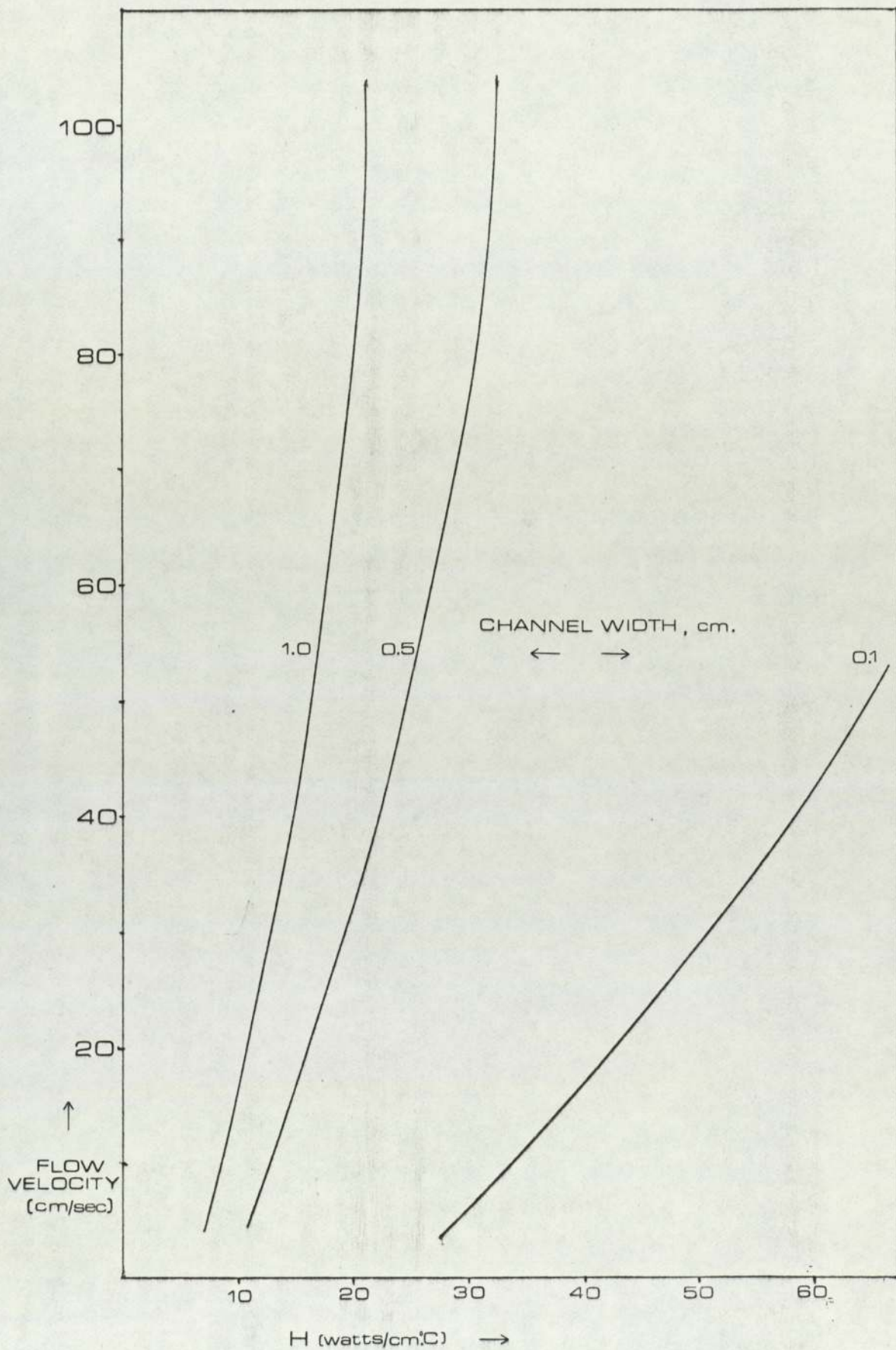


FIG. 15: H for Mercury.

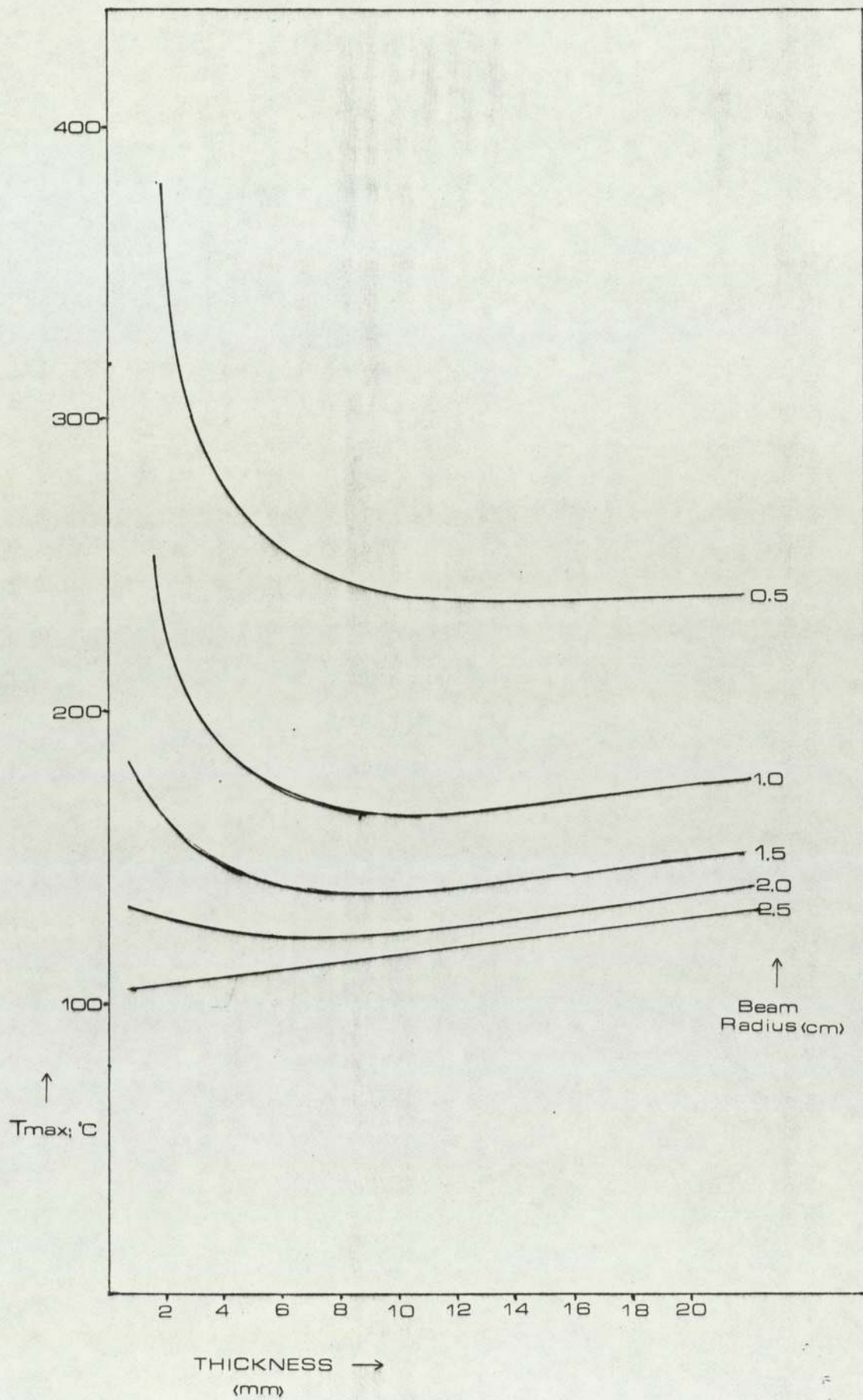


FIG. 16a: Back-cooled Copper Target

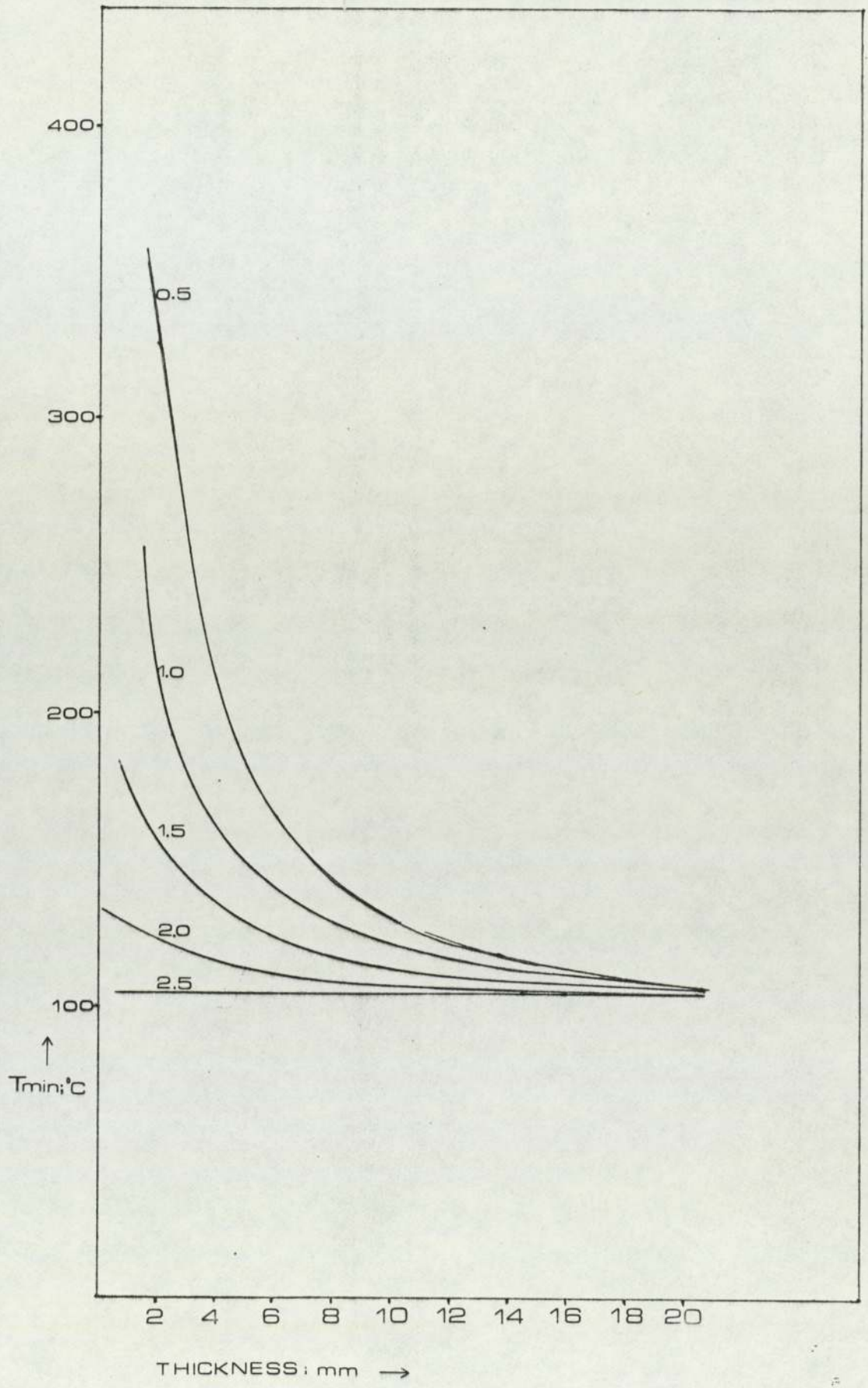


FIG. 16 b: Back-cooled Copper Target

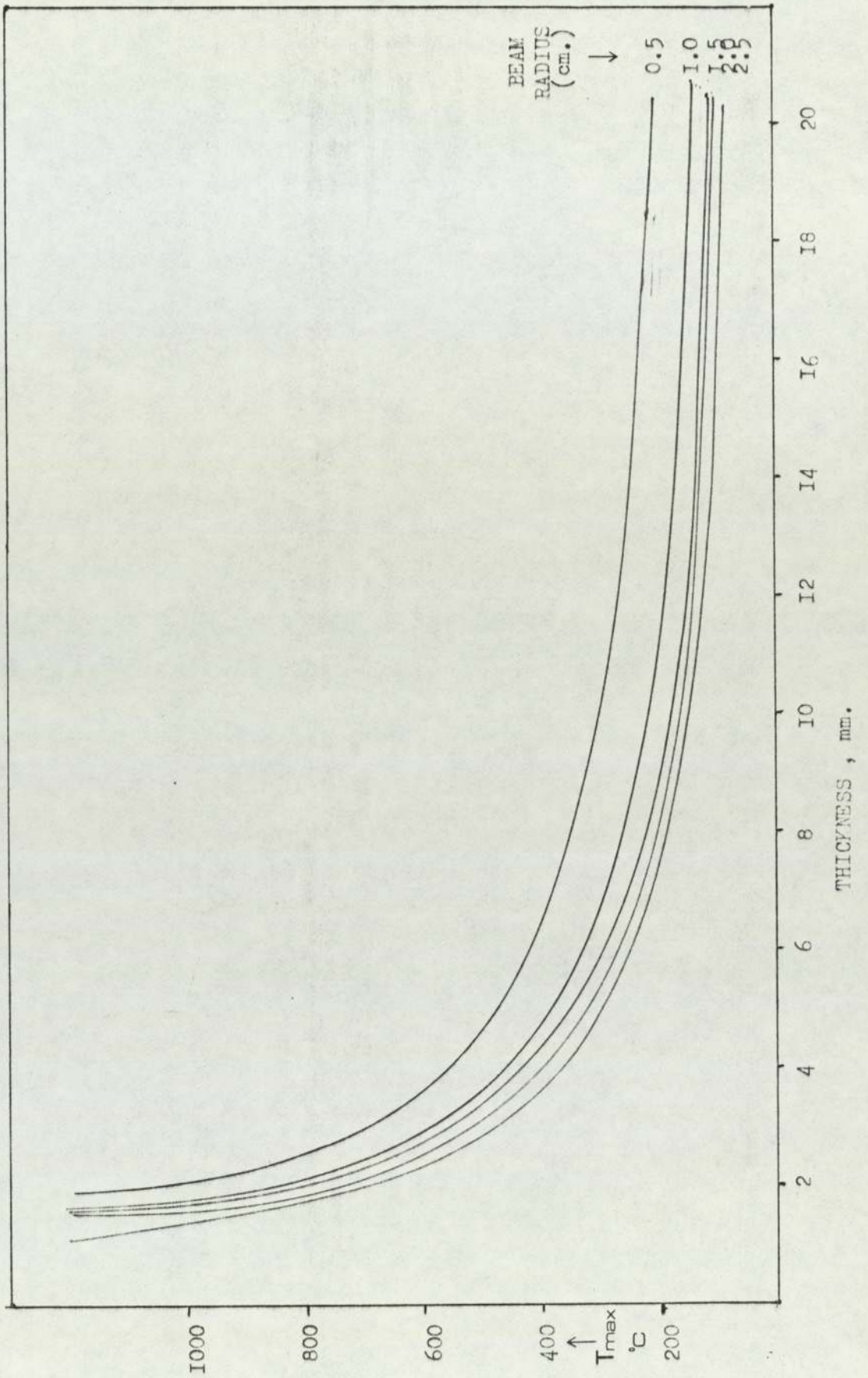


FIG. 17a : Edge-cooled Copper Target

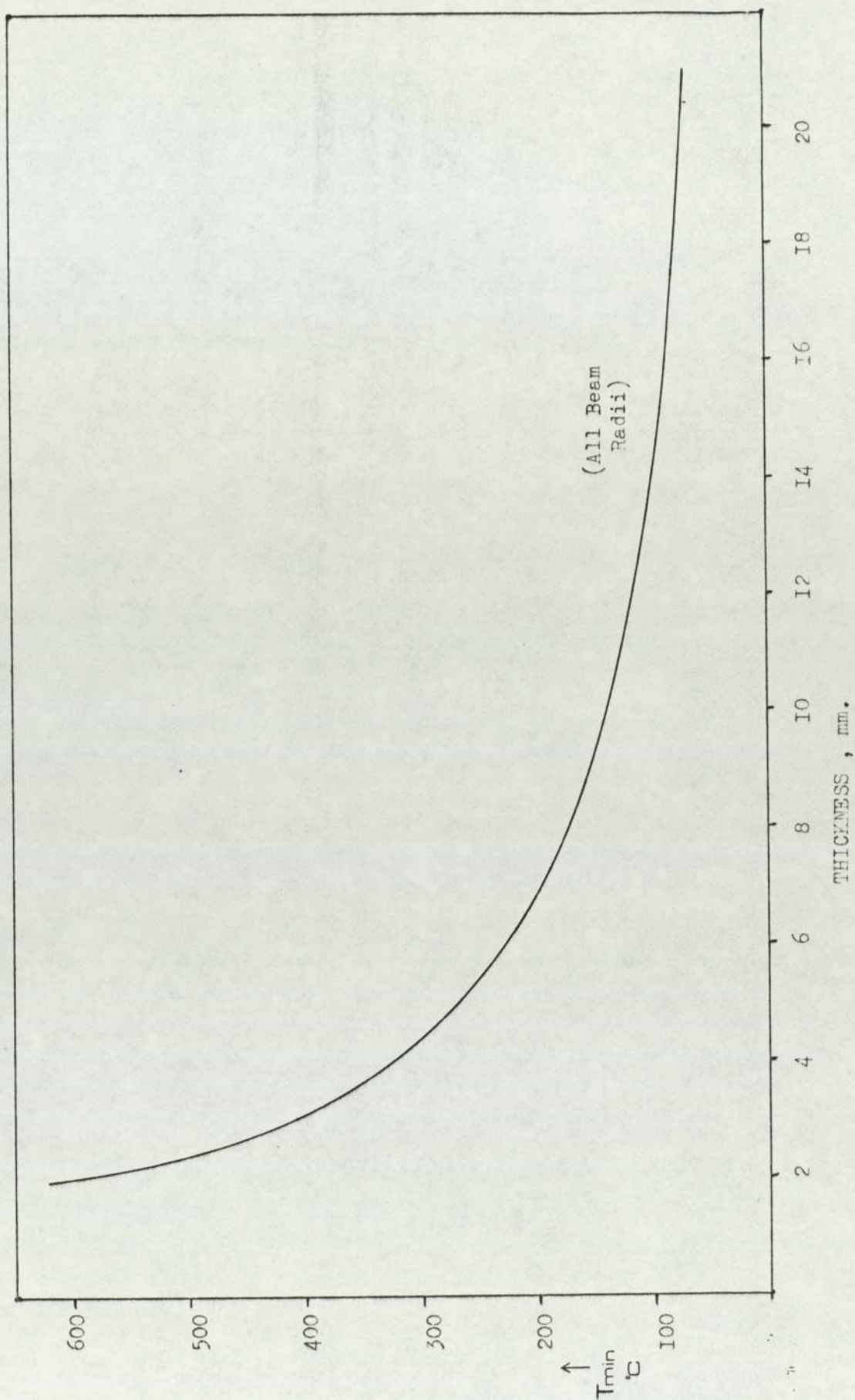


FIG. 17b : Edge-cooled Copper Target

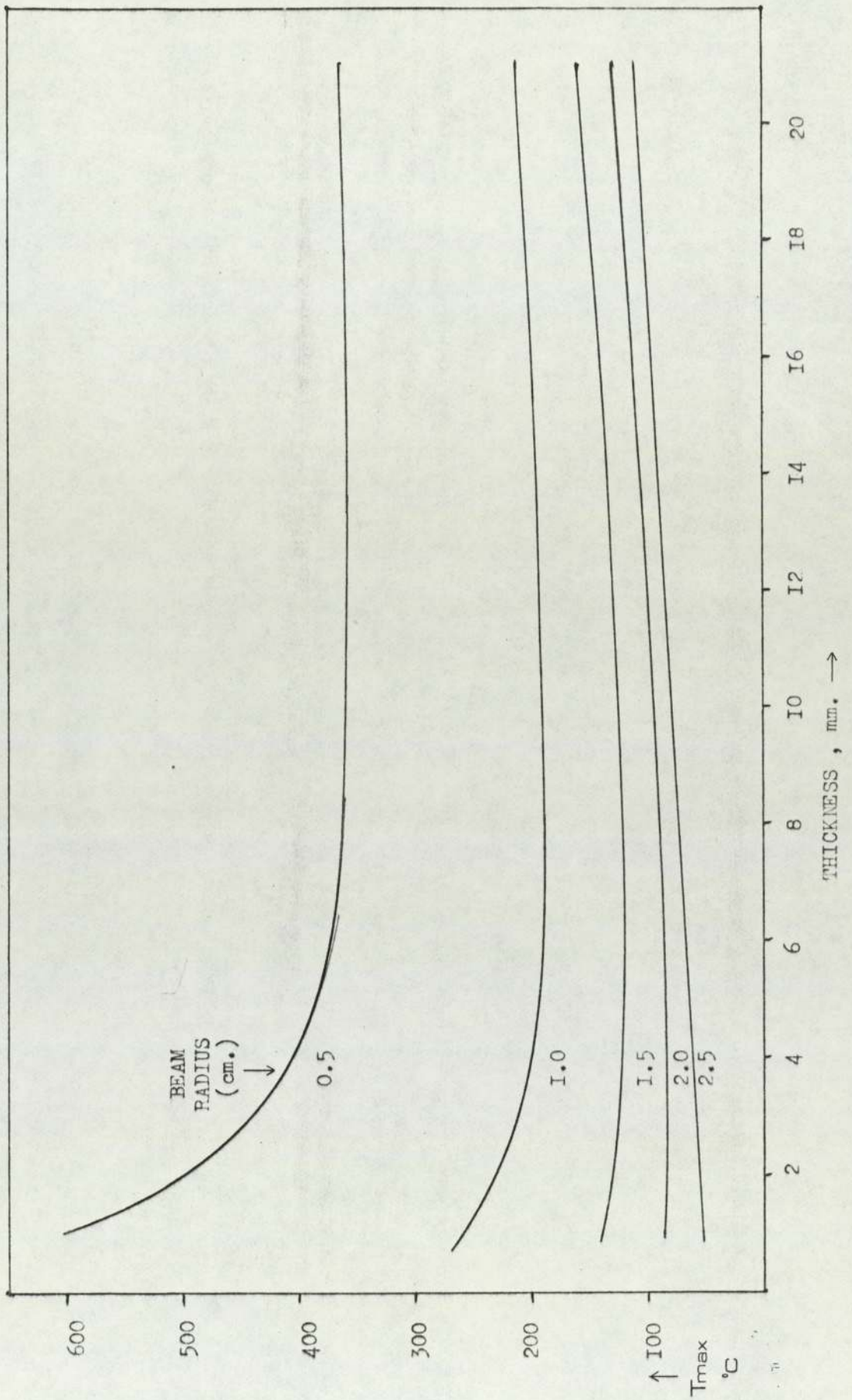


FIG. 18a : Back-cooled Tungsten Target

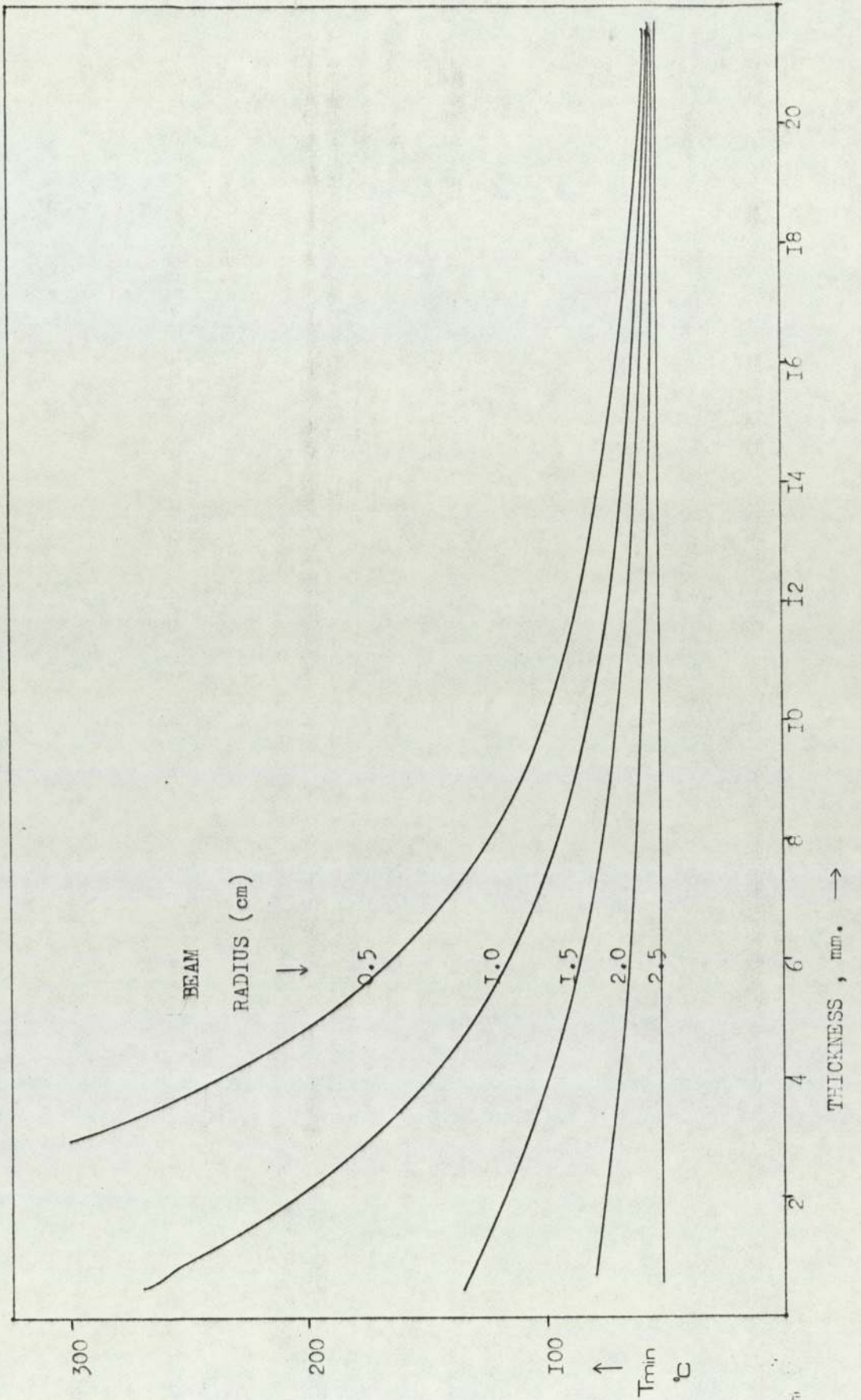


FIG. 18b : for Back-cooled Tungsten Target.

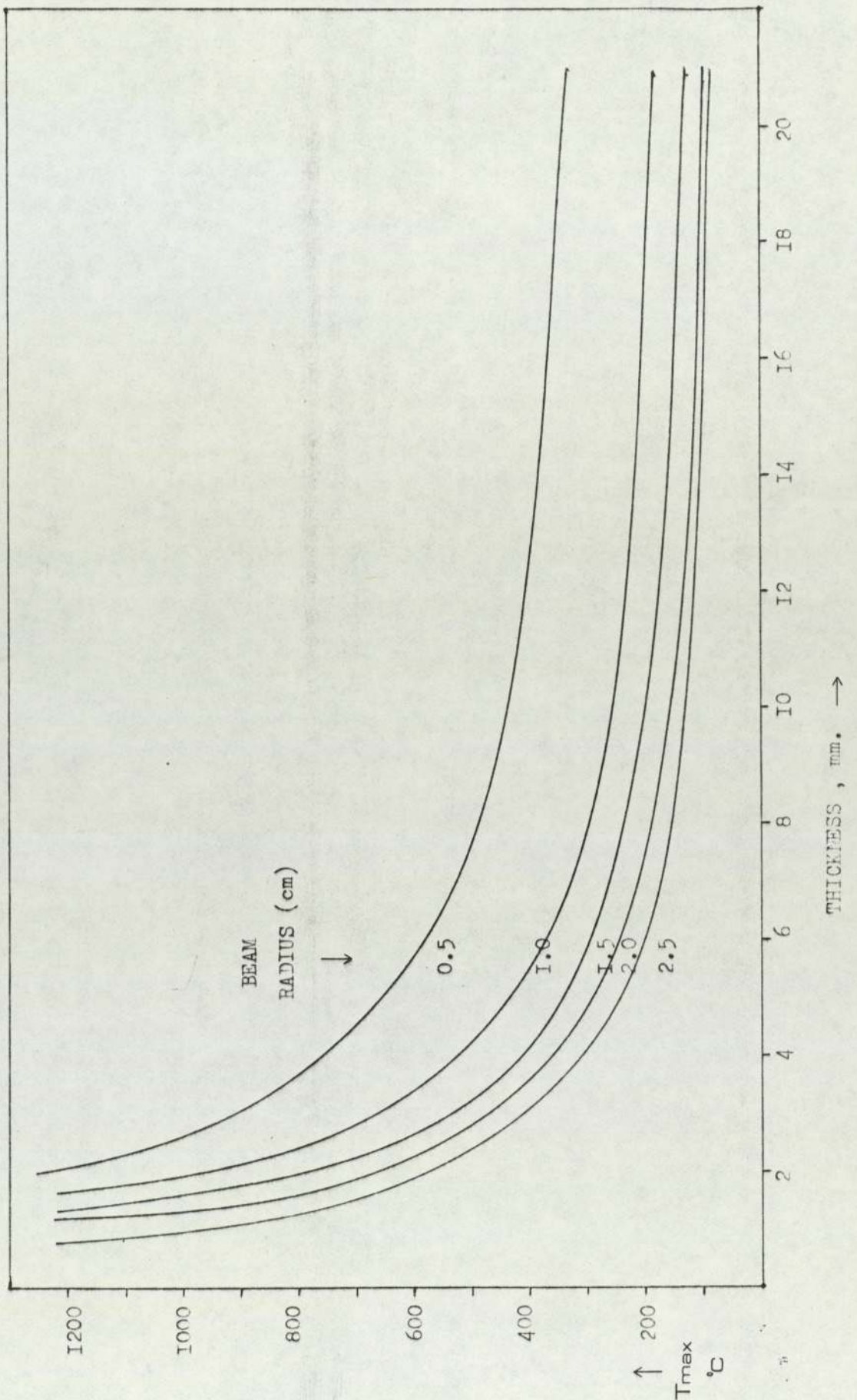


FIG. 19a : for Edge-cooled Tungsten Target.

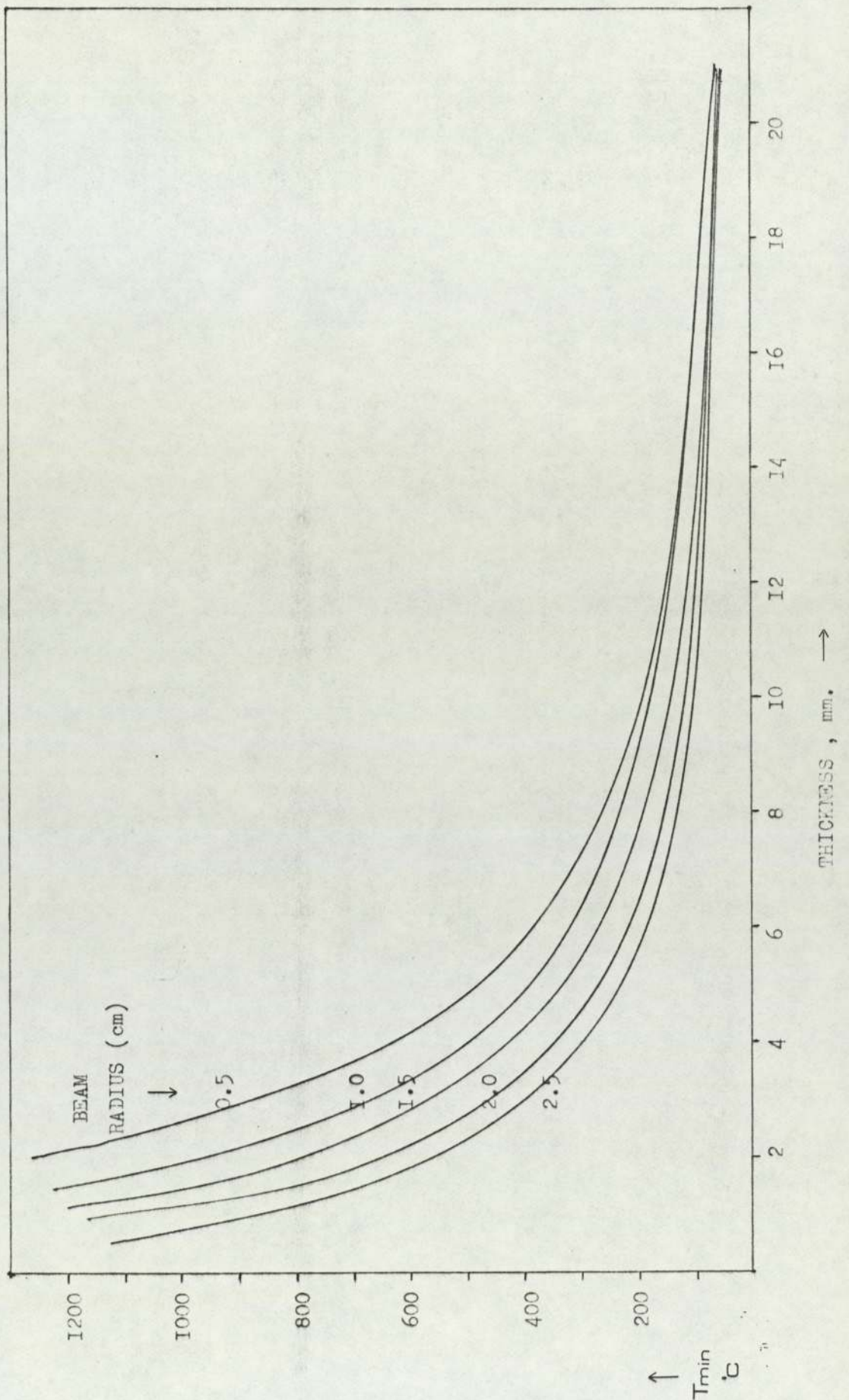


FIG. 19b : for Edge-cooled Tungsten Target.

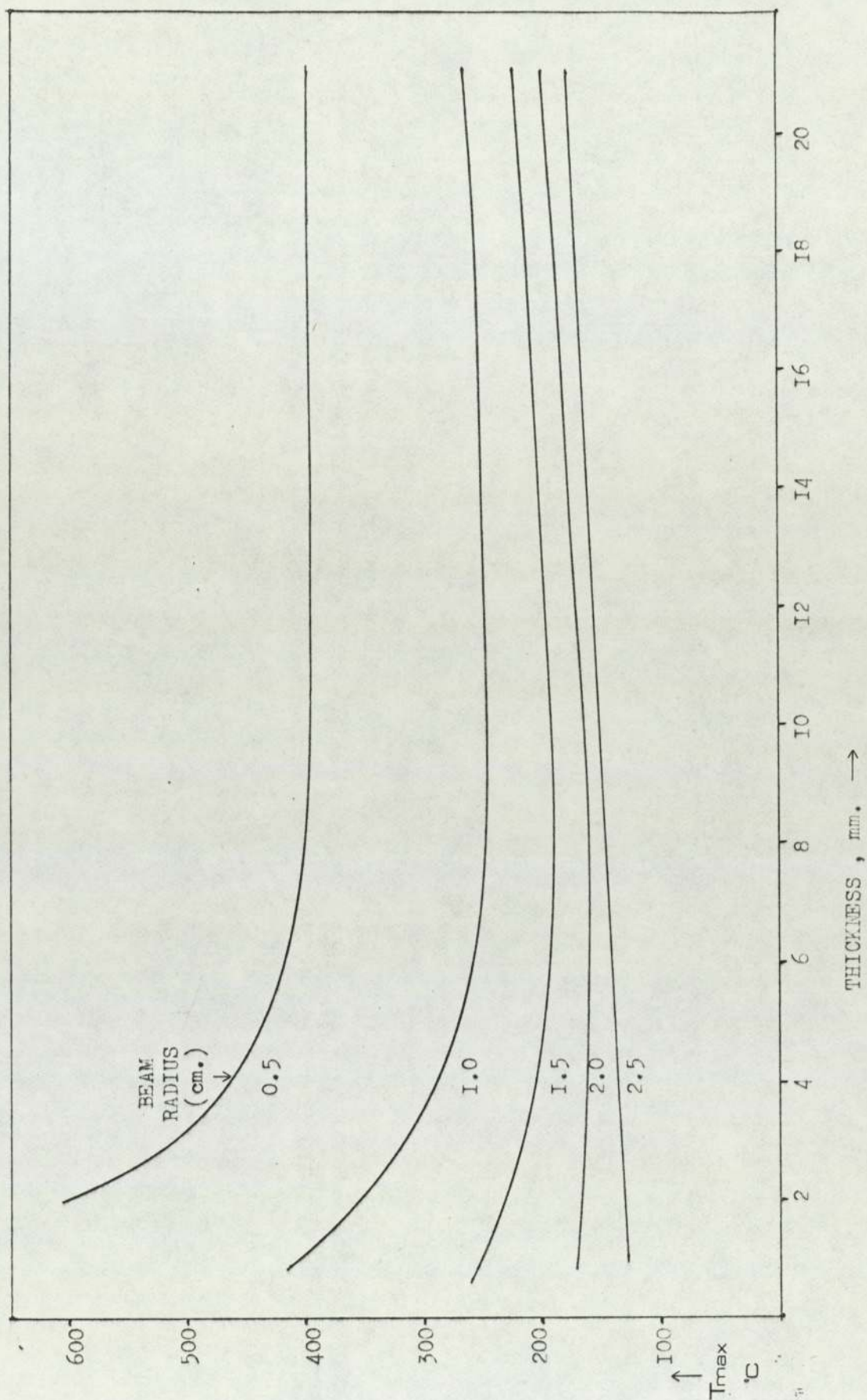


FIG. 20a : Back-cooled Beryllium Target ; $H = 0.4$

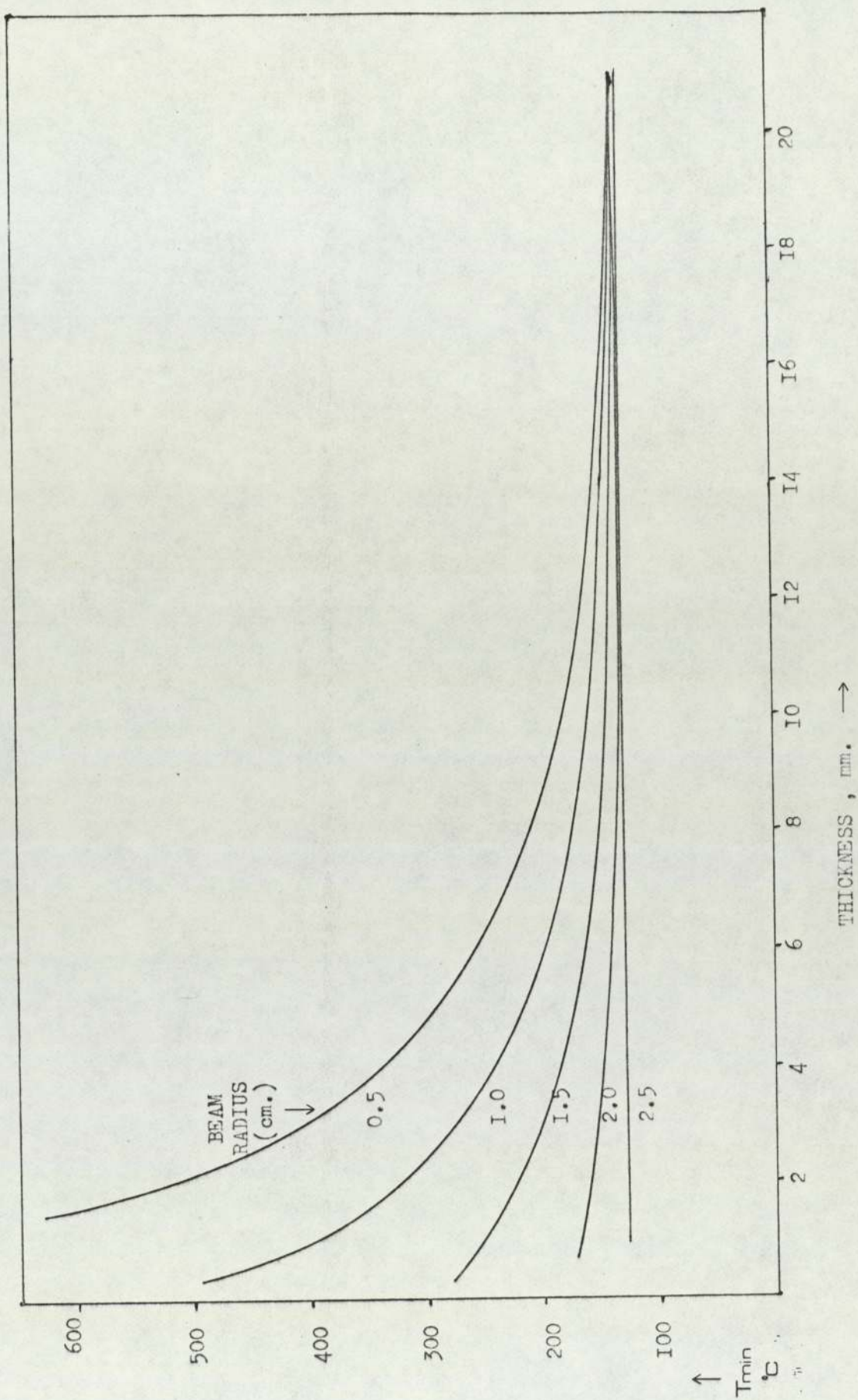


FIG. 20b : Back-cooled Beryllium Target ; $H = 0.4$

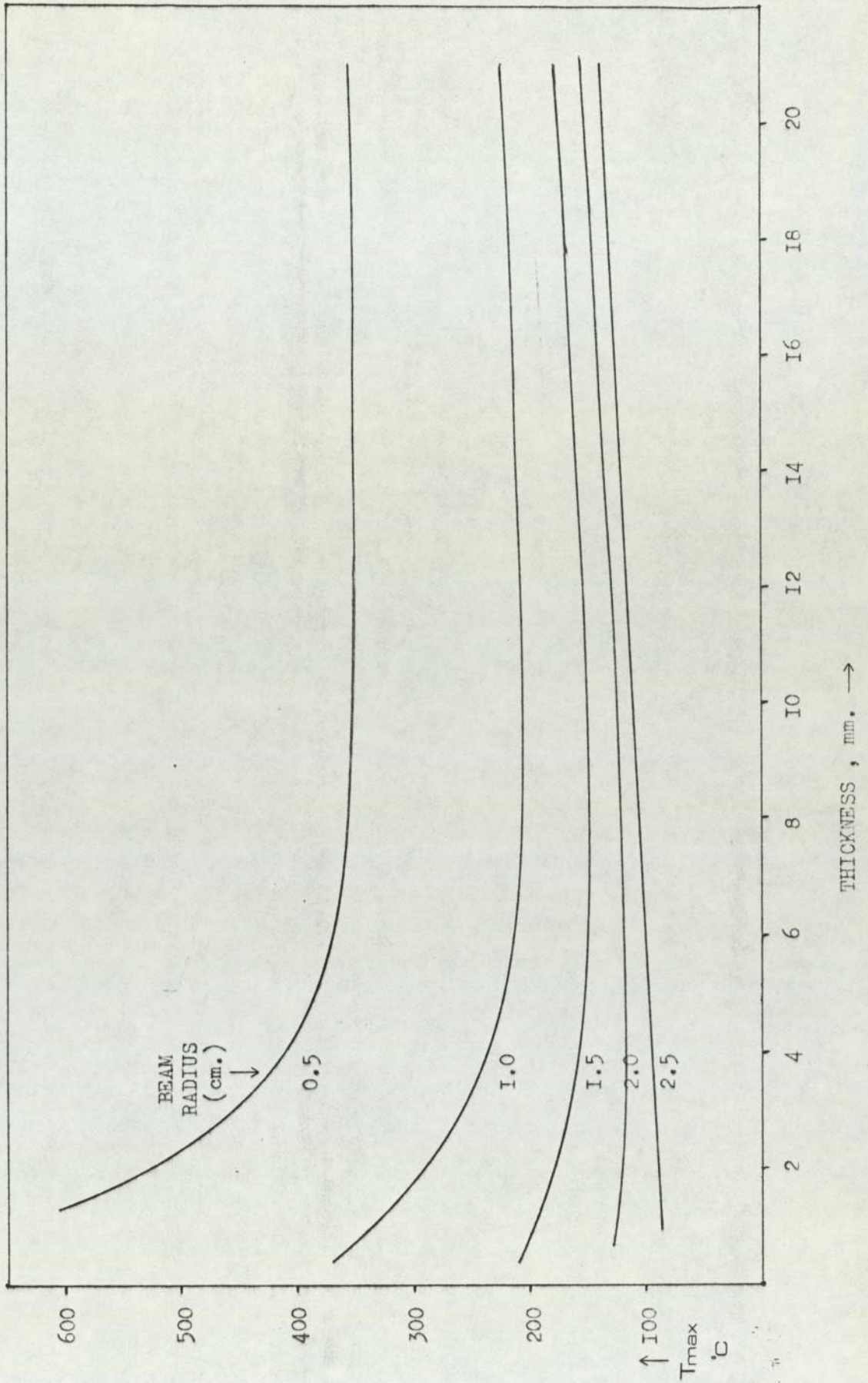


FIG. 20c : Back-cooled Beryllium Target ; $H = 0.6$

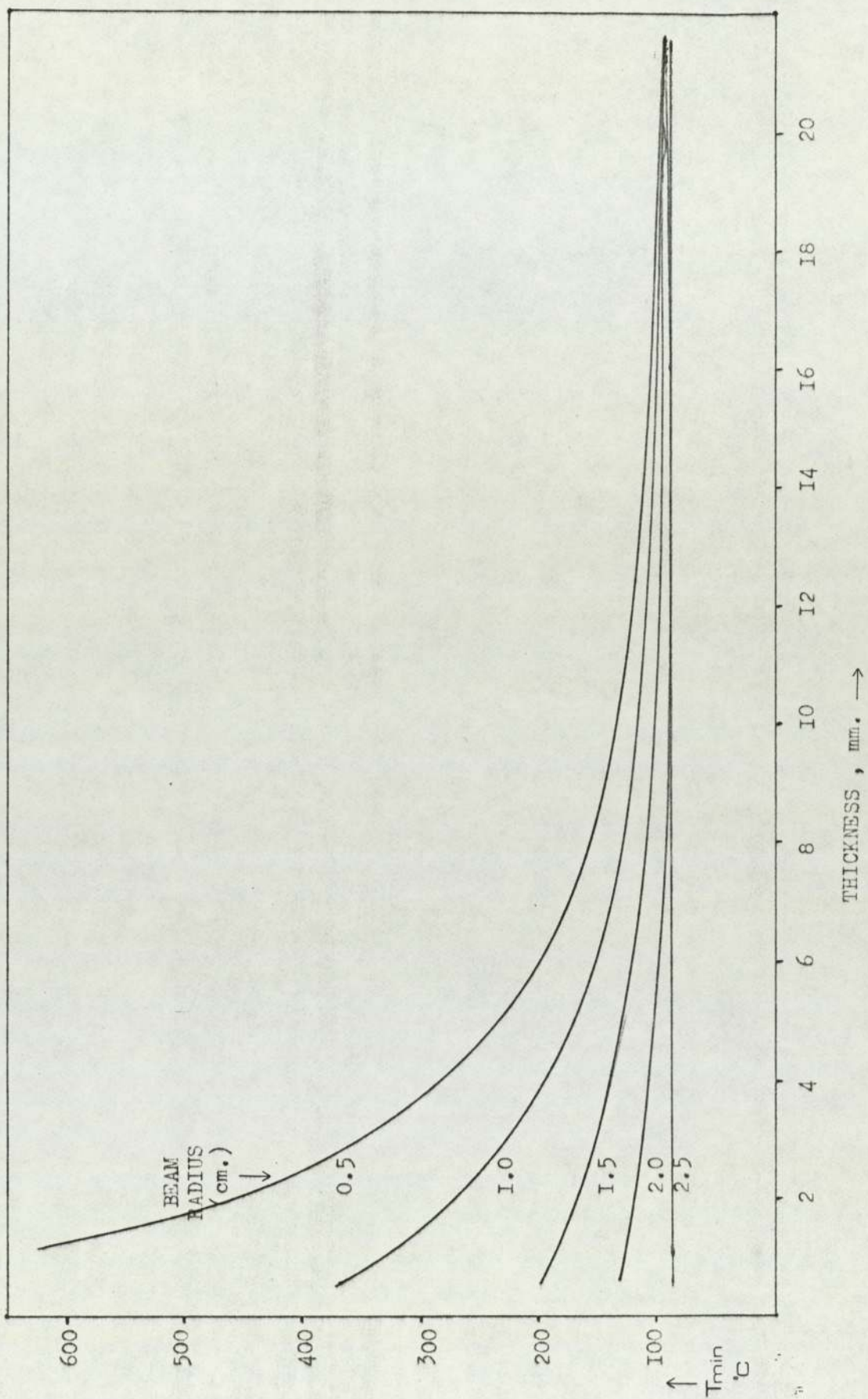


FIG. 20d : Back-cooled Beryllium Target ; $H = 0.6$

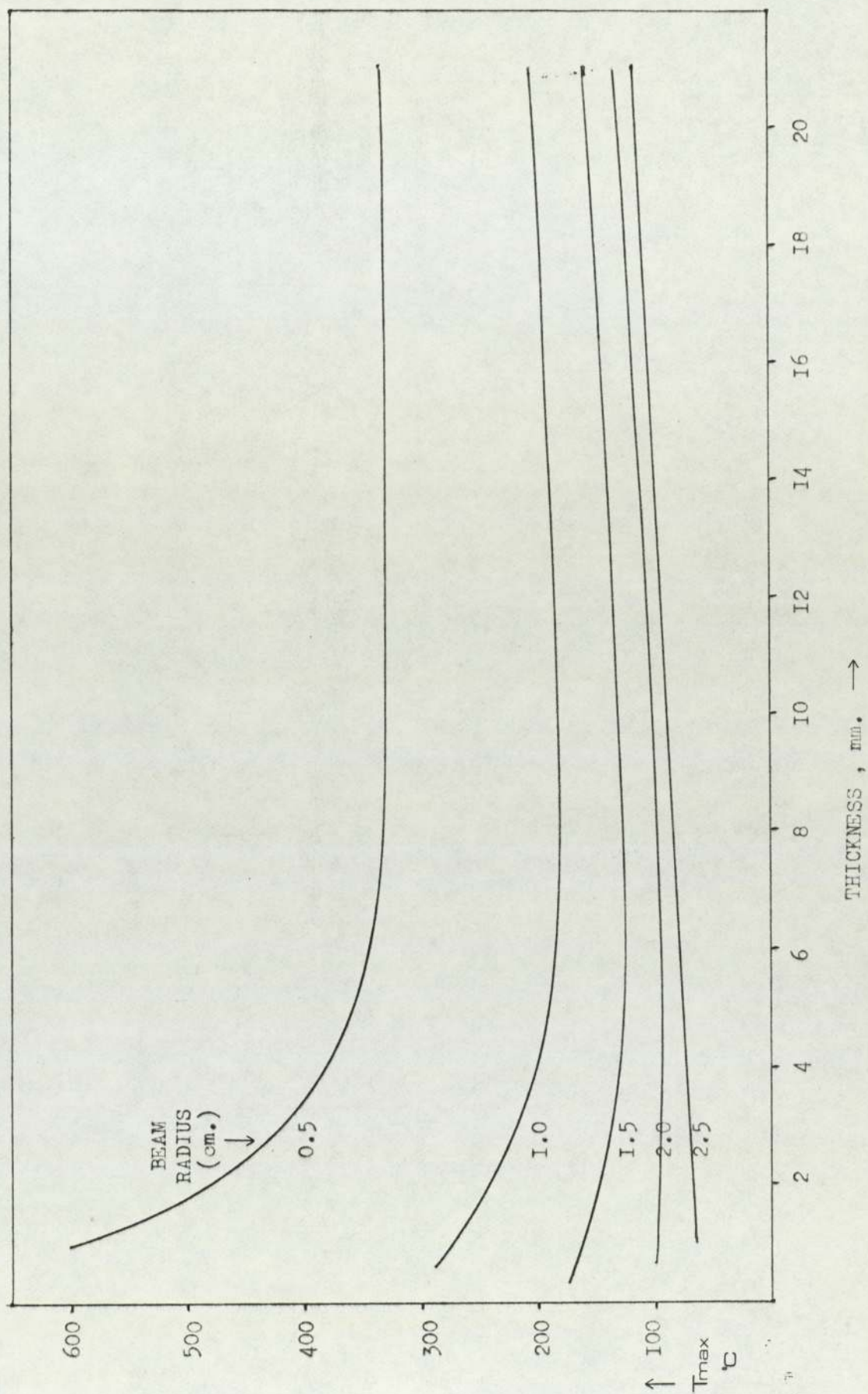


FIG. 20e : Back-cooled Beryllium Target ; $H = 0.8$

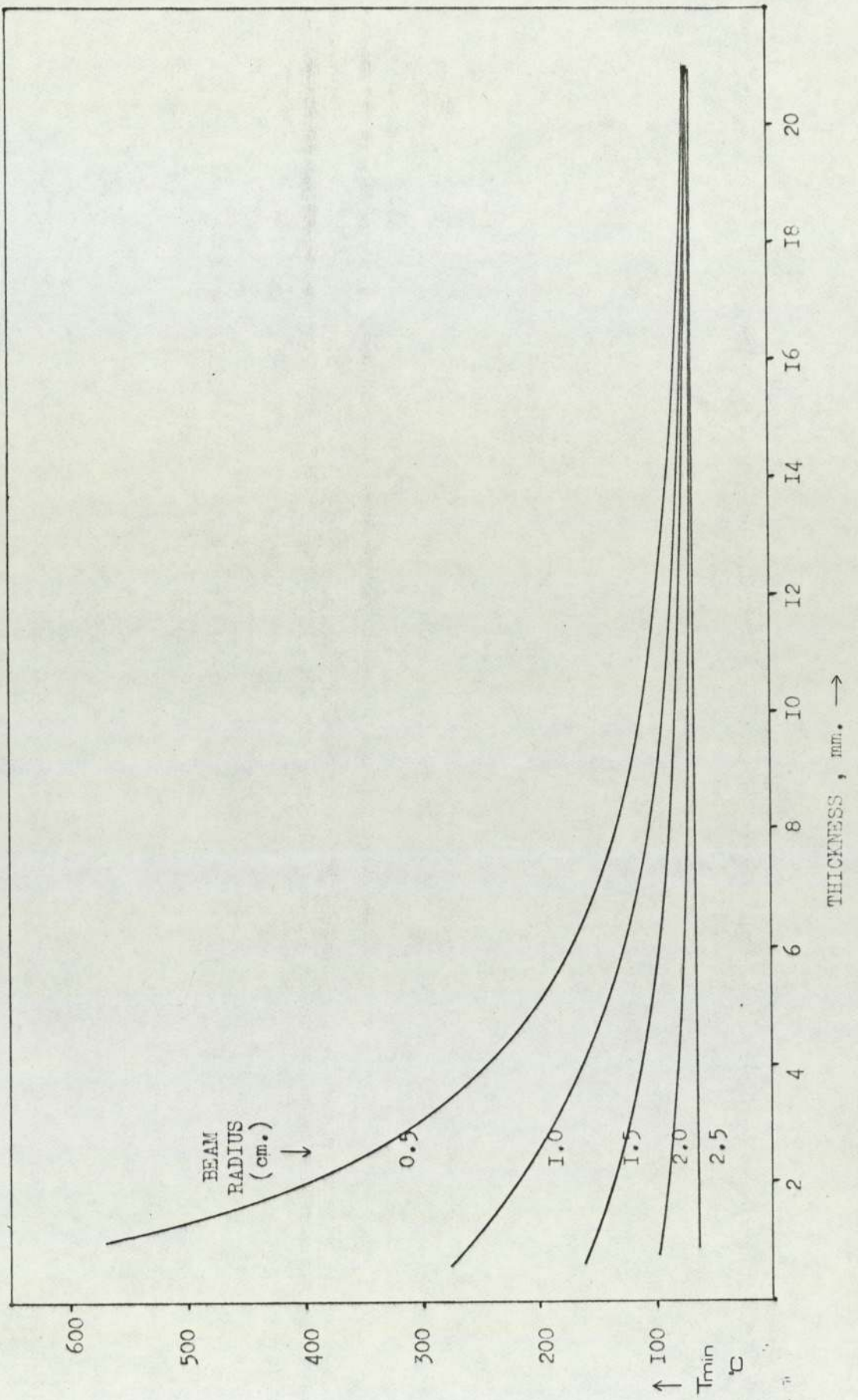


FIG. 20f : Back-cooled Beryllium Target ; $H = 0.8$

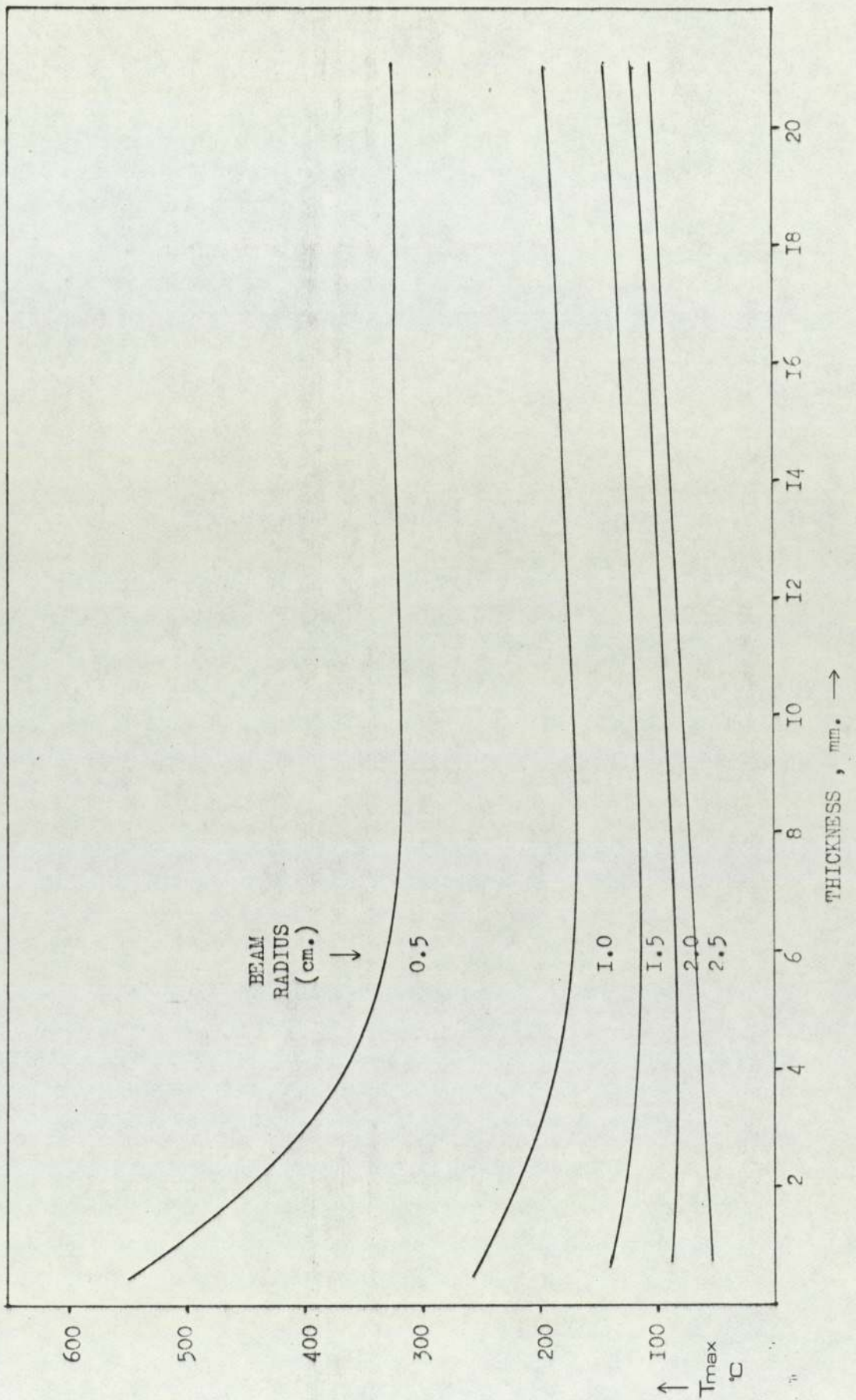


FIG. 20g : Back-cooled Beryllium Target ; $H = 1.0$

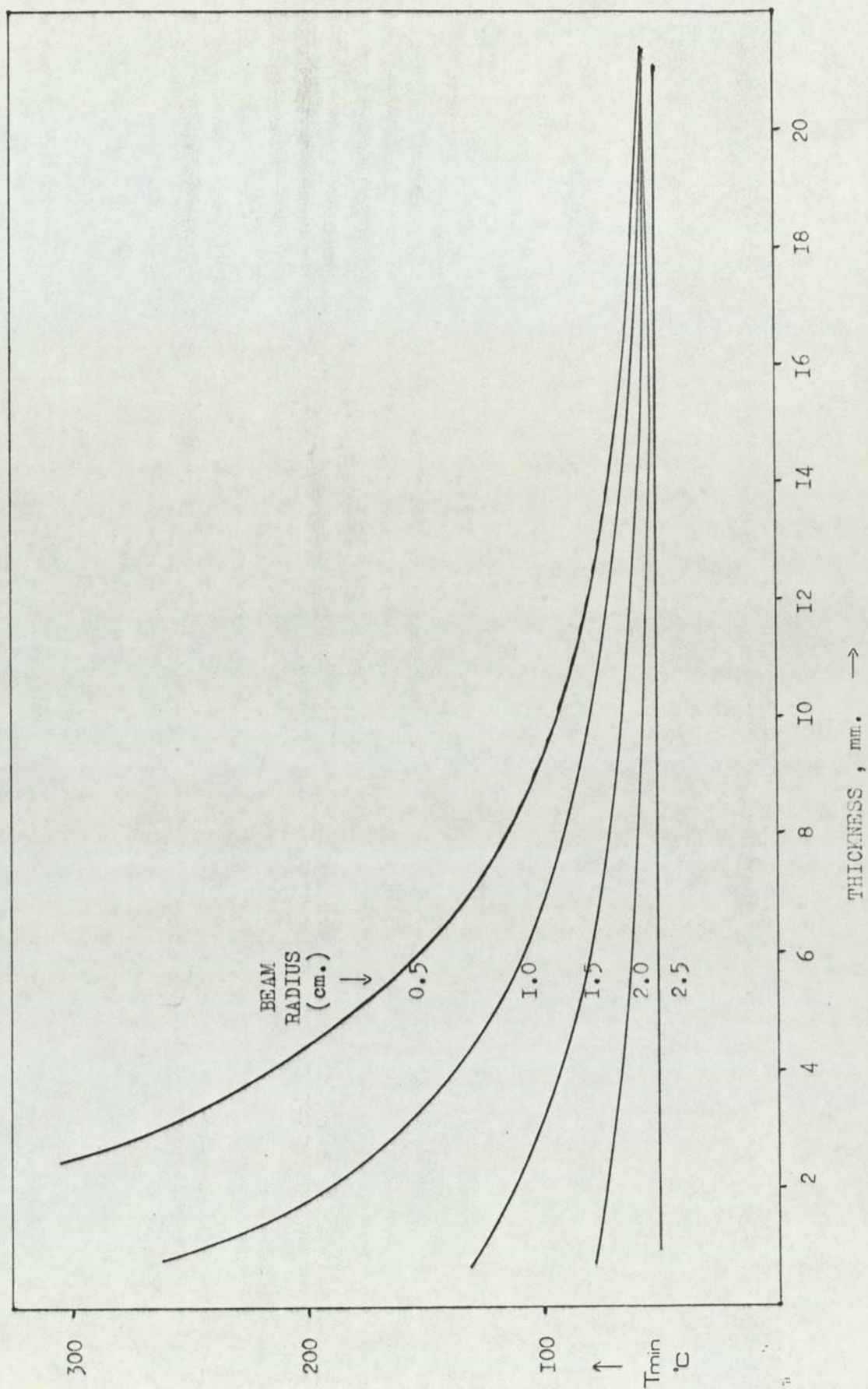


FIG. 20h : Back-cooled Beryllium Target ; $H = 1.0$

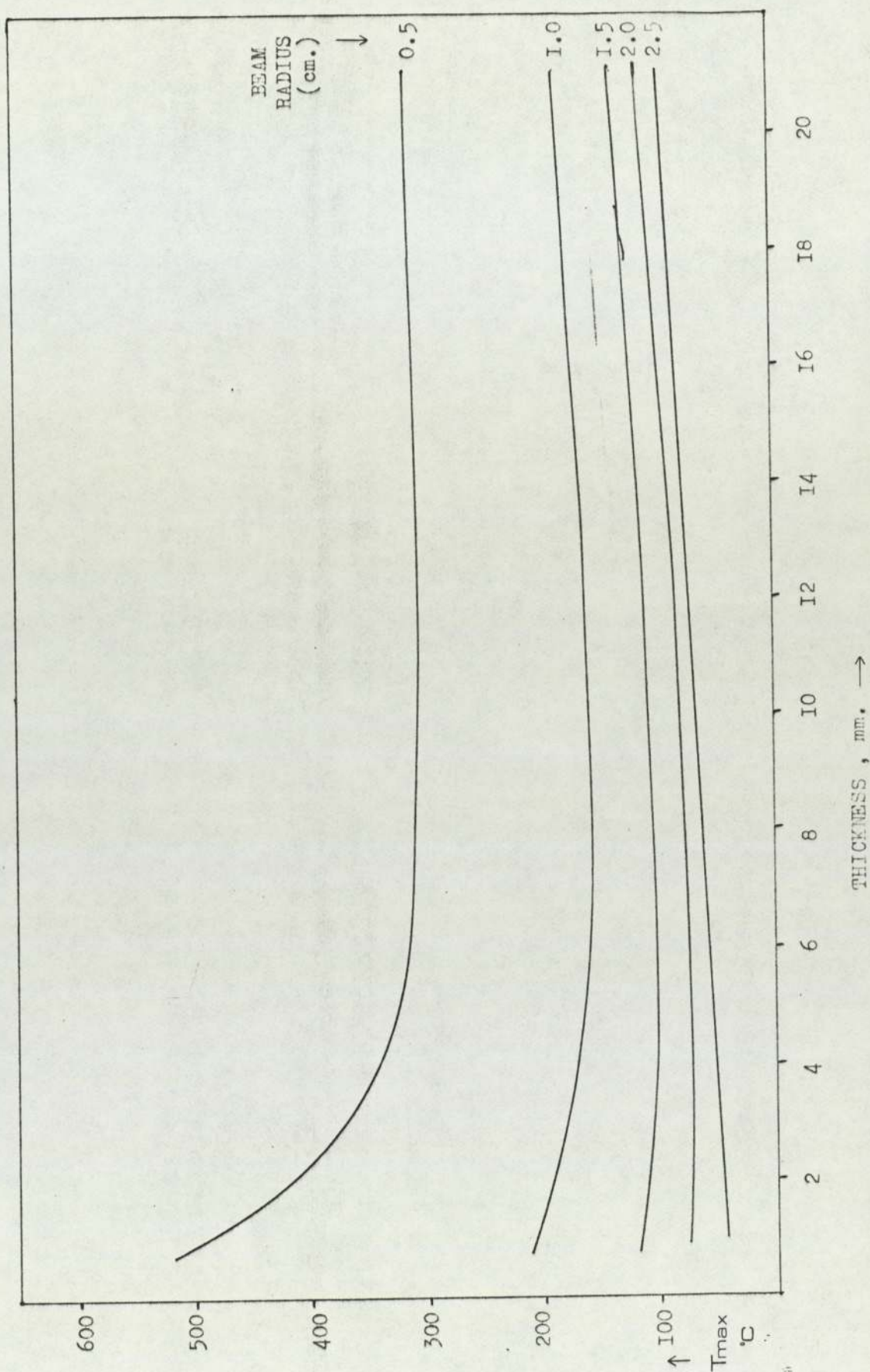


FIG. 20i : Back-cooled Beryllium Target ; $H = 1.2$

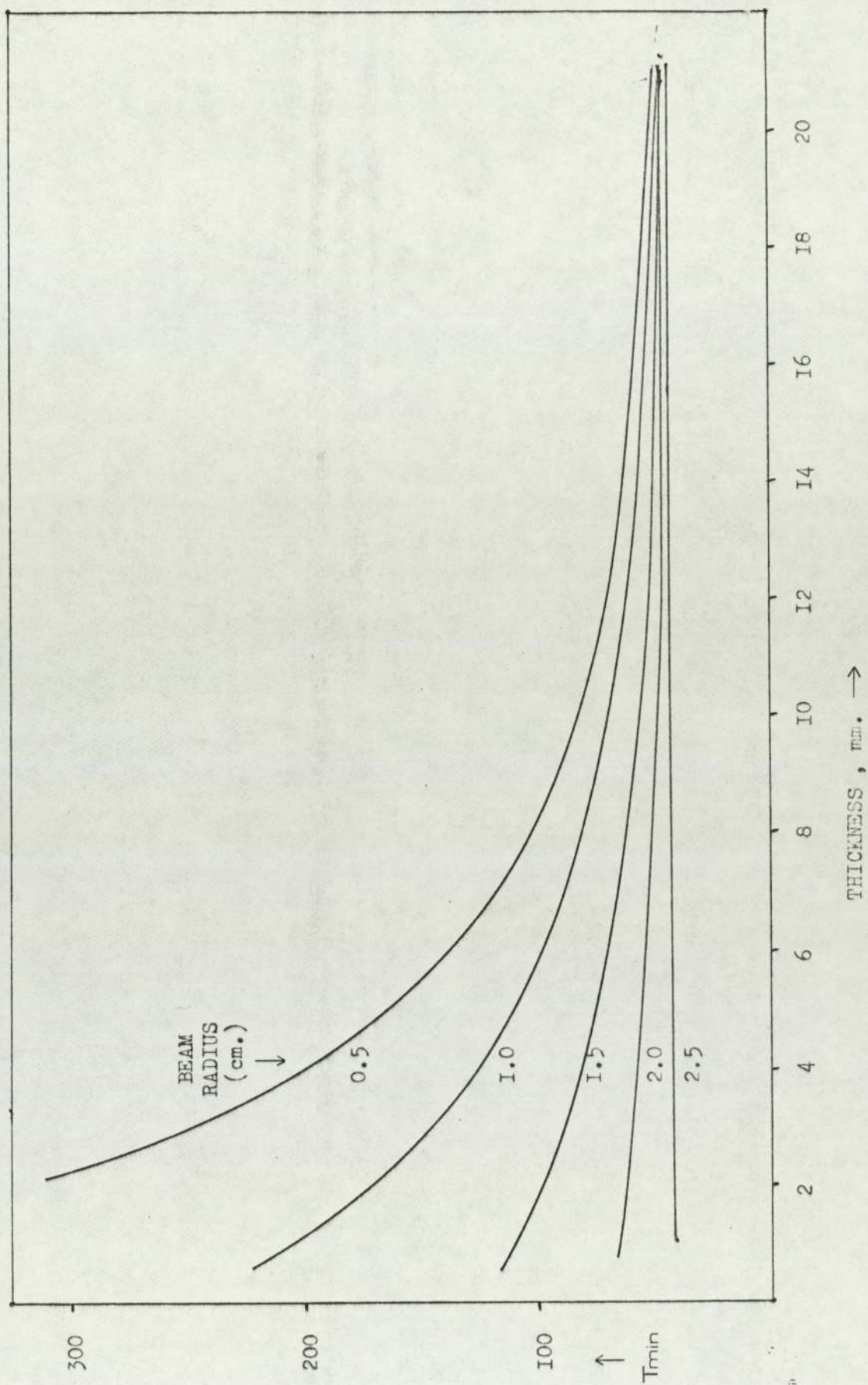


FIG. 20j ; Back-cooled Beryllium Target ; $H = 1.2$

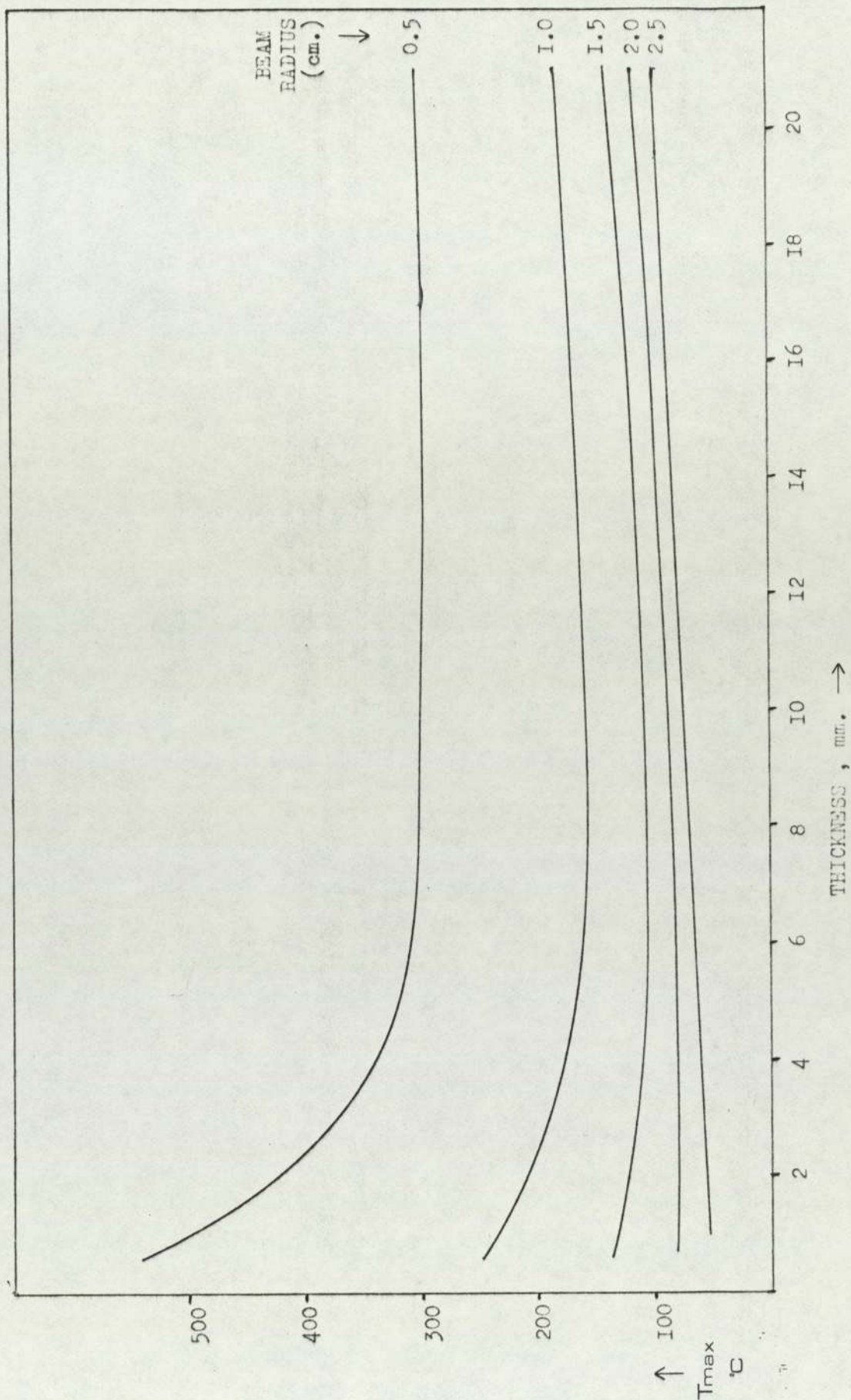


FIG. 2Ia : Back-cooled Aluminium Target ;

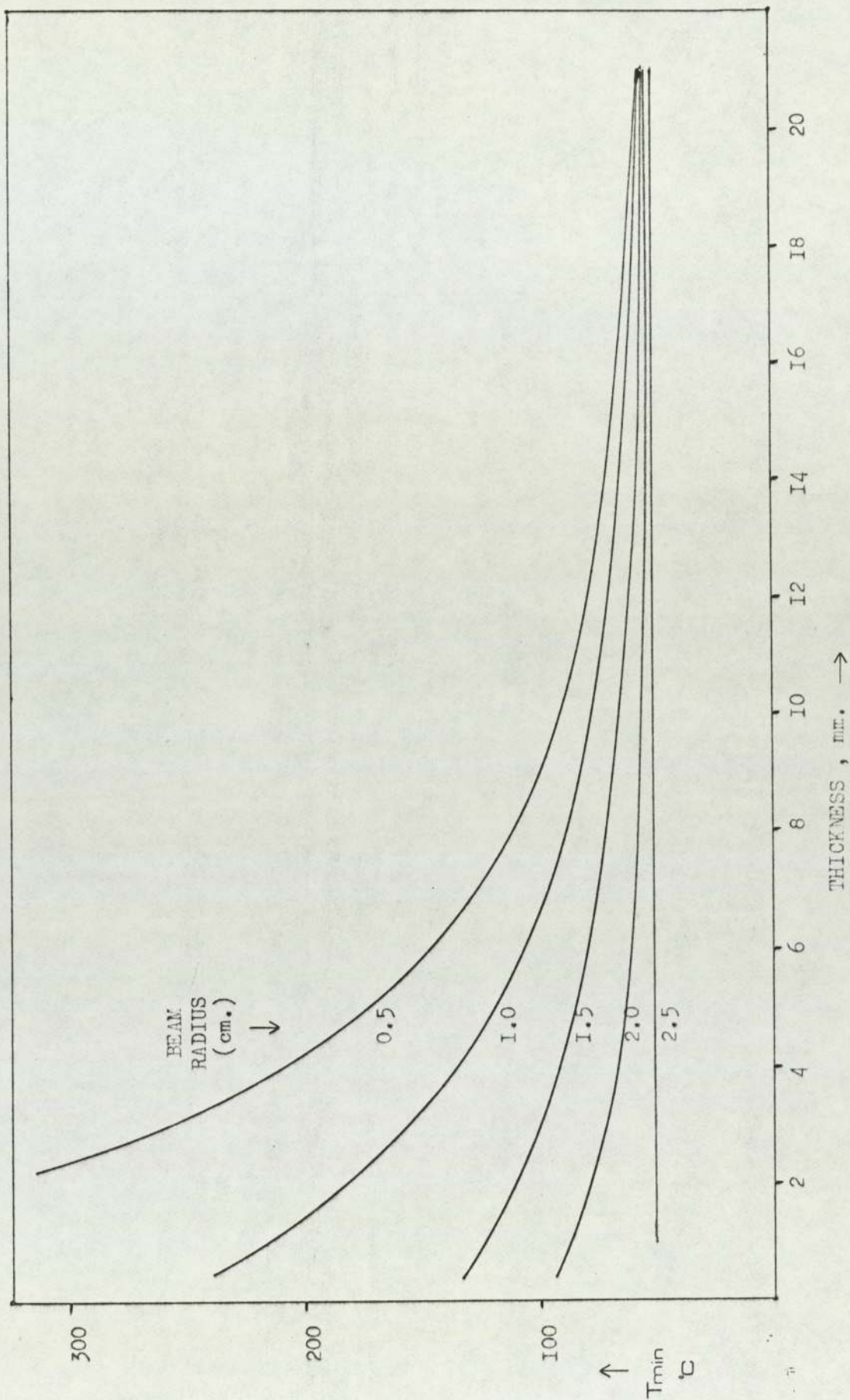


FIG. 21b : Back-cooled Aluminium Target

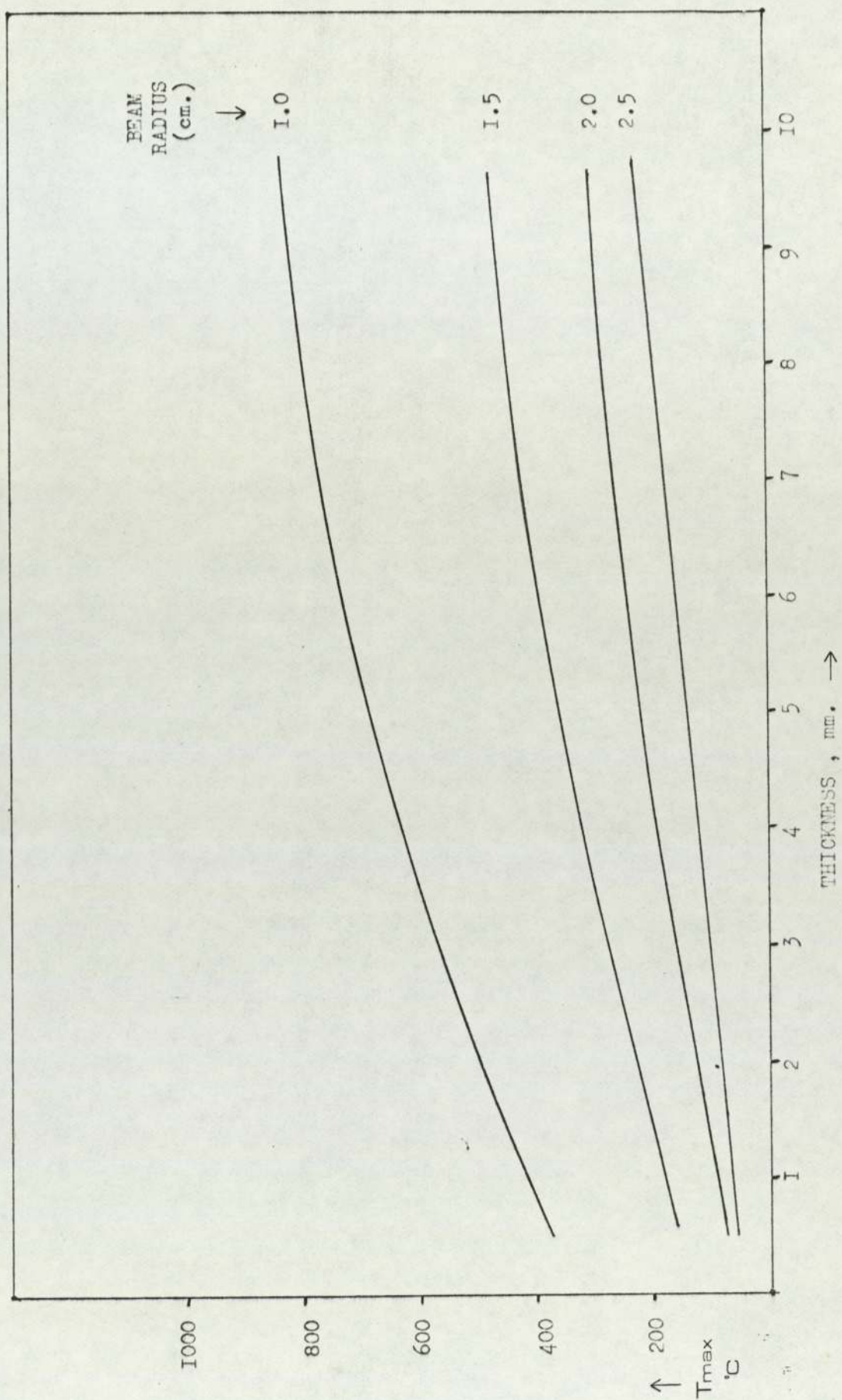


FIG. 22a : Back-cooled Uranium Target

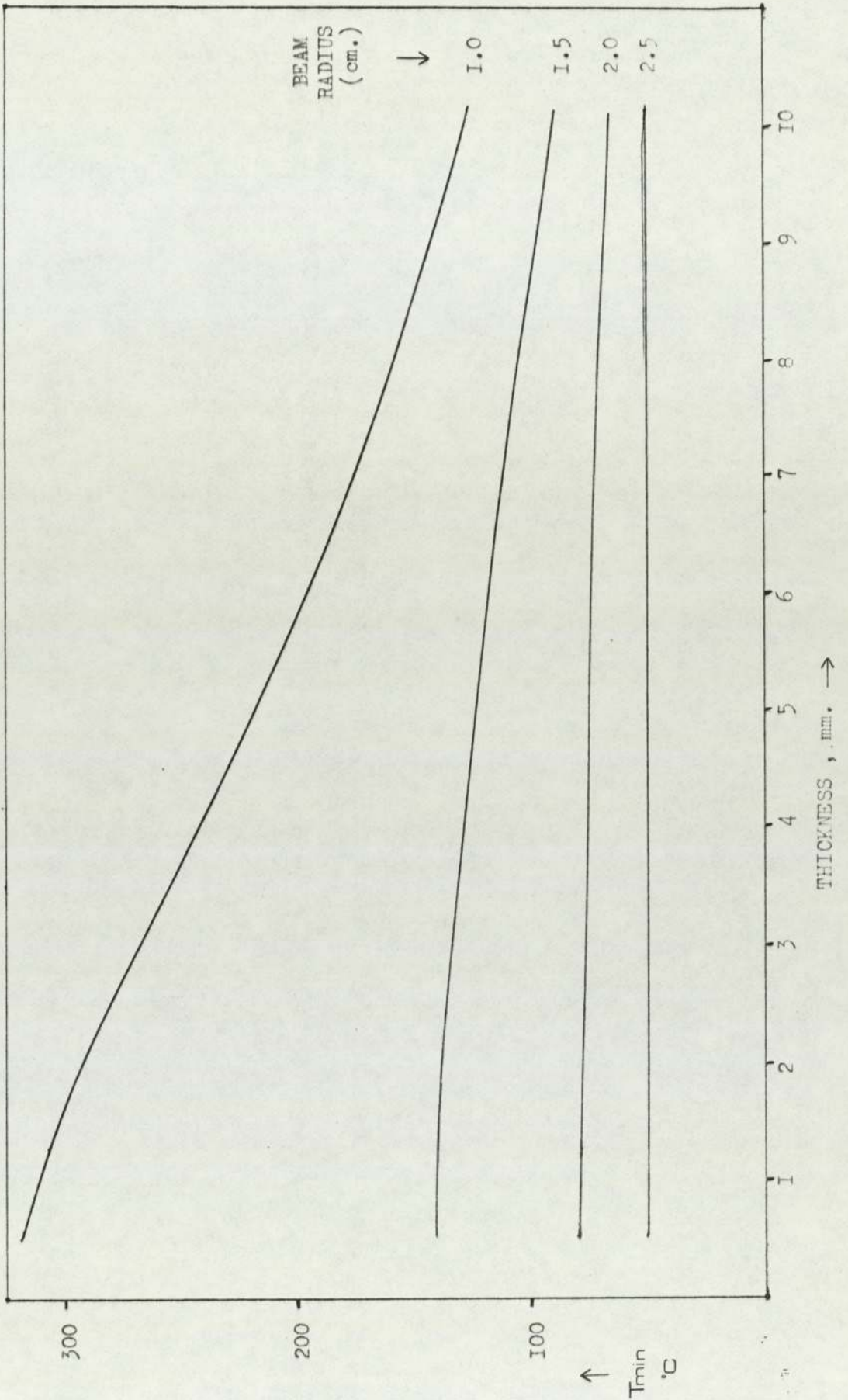


FIG. 22b : Back-cooled Uranium Target

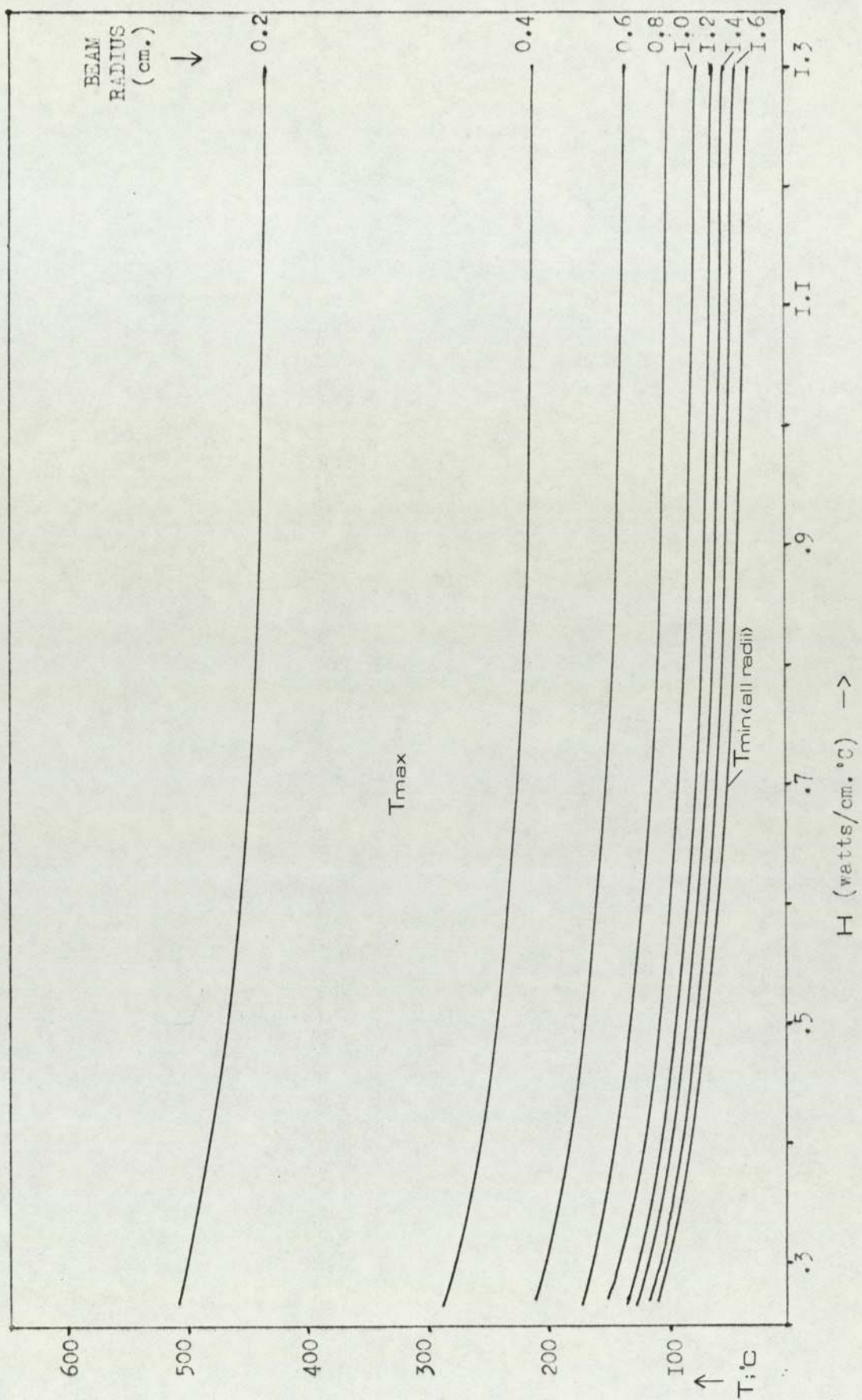


FIG. 23 : BERYLLIUM NEUTRON-GENERATING TARGET

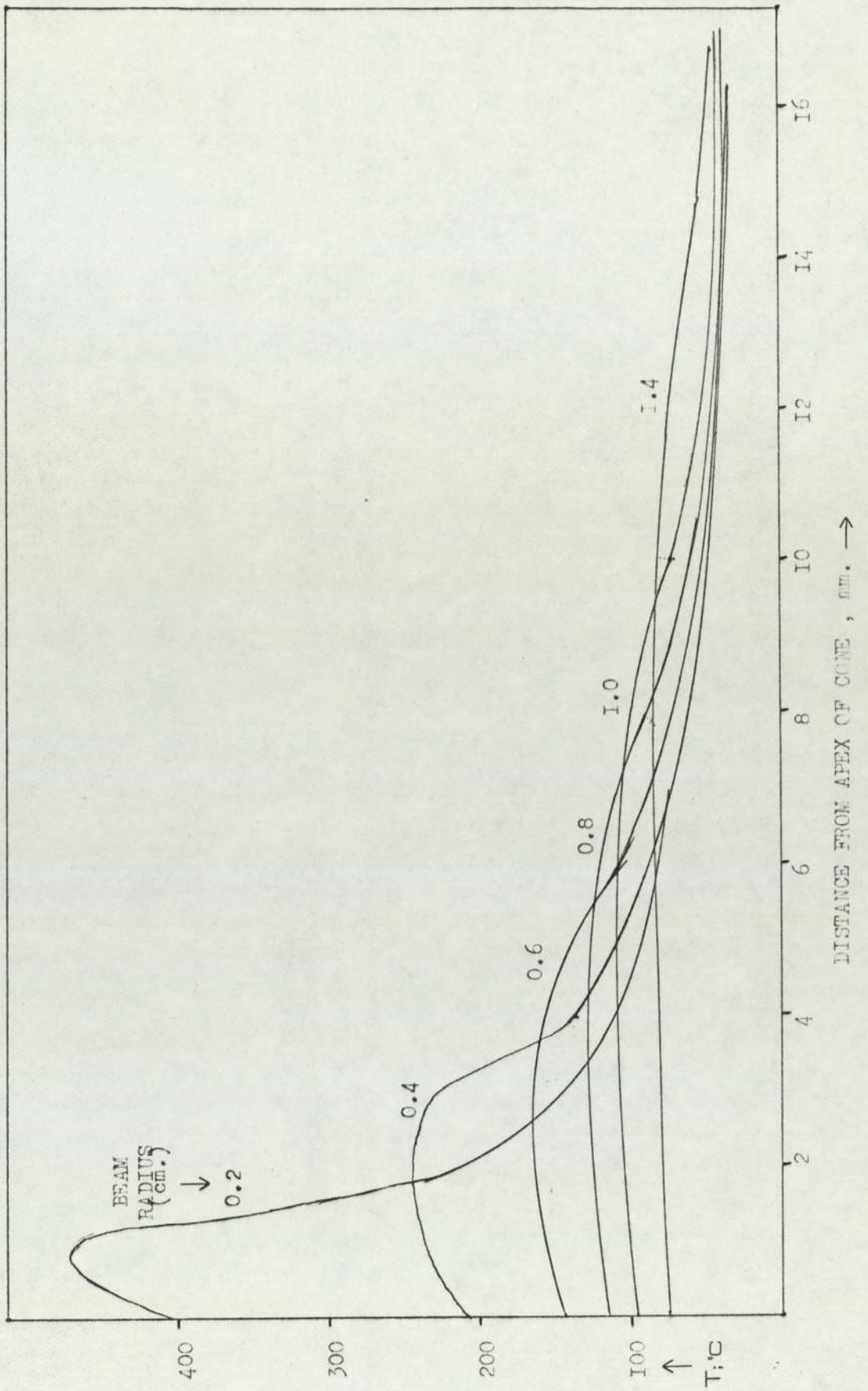


FIG. 24 : Surface Temperature of Beryllium Target

-I	0	I	I	I	I	I	-I	25	2I	22	22	22	22	23	25
-I	0	I	I	I	I	I	-I	25	II	8	8	8	8	I	25
-I	0	I	I	I	I	I	-I	25	II	8	8	8	8	I	25
-I	0	I	I	I	I	I	-I	25	II	8	8	8	8	I	25
-I	0	I	I	I	I	I	-I	25	II	8	8	8	8	I	25
-I	0	I	I	I	I	I	-I	25	II	8	8	8	8	I	25
-I	0	I	I	I	I	I	-I	25	II	8	8	8	8	I	25
-I	0	I	I	I	I	I	-I	25	II	8	8	8	8	I	25
-I	0	I	I	I	I	I	-I	25	II	8	8	8	8	I	25
-I	0	I	I	I	I	I	-I	25	II	8	8	8	8	I	25
-I	0	I	I	I	I	I	-I	25	II	8	8	8	8	I	25
-I	0	I	I	I	I	I	-I	25	I4	5	5	5	5	7	25
-I	-I	-I	-I	-I	-I	-I	-I	25	25	25	25	25	25	25	25

A : G(R,Z)

B : H(R,Z)

FIG. 25 : BACK-COOLED TARGET

-I	I	I	I	I	I	I	-I	25	24	22	22	22	22	23	25
-I	I	I	I	I	I	I	-I	25	4	8	8	8	8	I	25
-I	I	I	I	I	I	I	-I	25	4	8	8	8	8	I	25
-I	I	I	I	I	I	I	-I	25	4	8	8	8	8	I	25
-I	I	I	I	I	I	I	-I	25	4	8	8	8	8	I	25
-I	I	I	I	I	I	I	-I	25	4	8	8	8	8	I	25
-I	I	I	I	I	I	I	-I	25	4	8	8	8	8	I	25
-I	I	I	I	I	I	I	-I	25	4	8	8	8	8	I	25
-I	I	I	I	I	I	I	-I	25	4	8	8	8	8	I	25
-I	I	I	I	I	I	I	-I	25	4	8	8	8	8	I	25
-I	0	0	0	0	0	0	-I	25	I3	I2	I2	I2	I2	I7	25
-I	-I	-I	-I	-I	-I	-I	-I	25	25	25	25	25	25	25	25

A : G(R,Z)

B : H(R,Z)

FIG. 26 : EDGE-COOLED TARGET

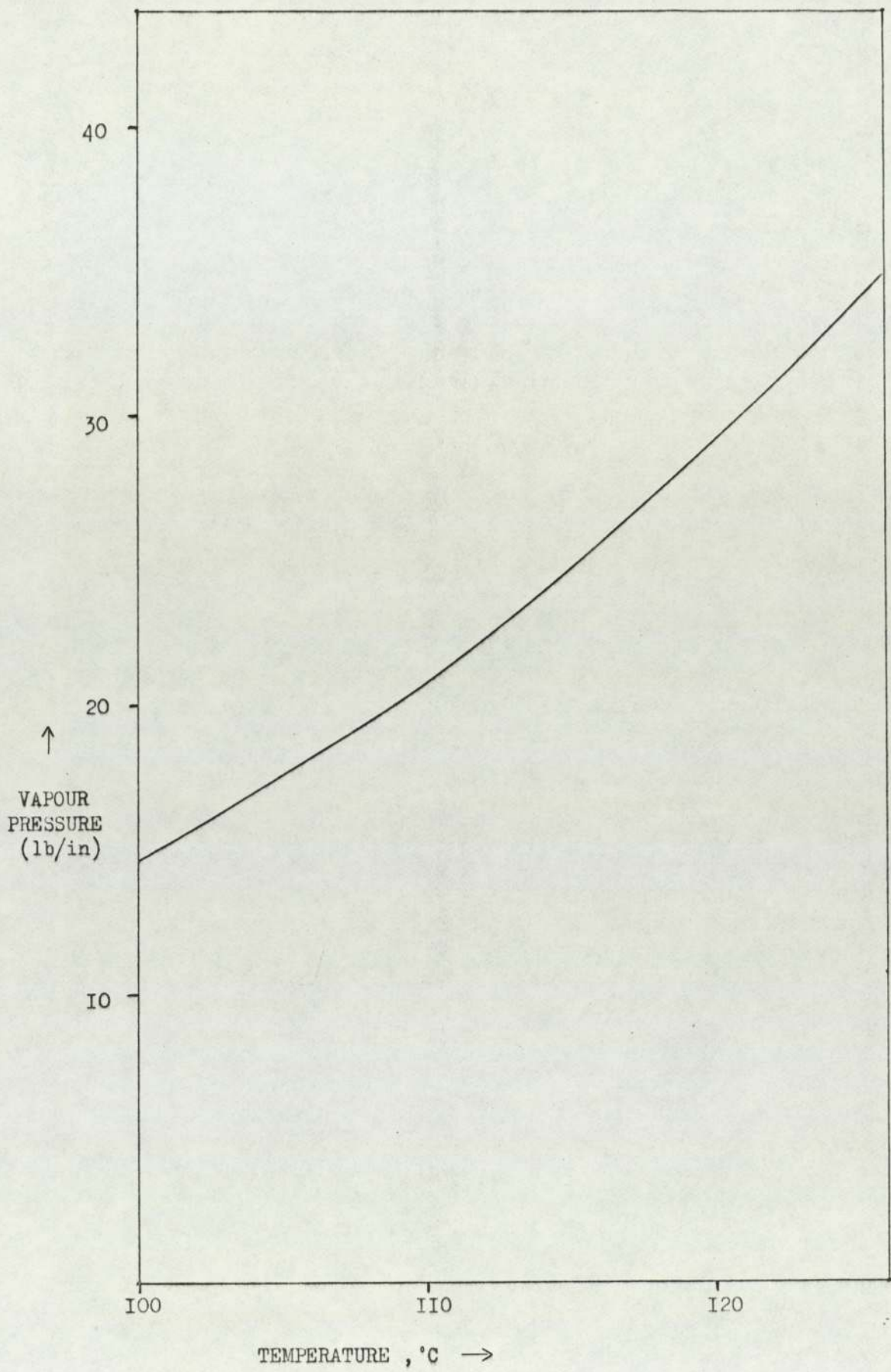


FIG. 28 : Vapour Pressure of Water v. Temperature

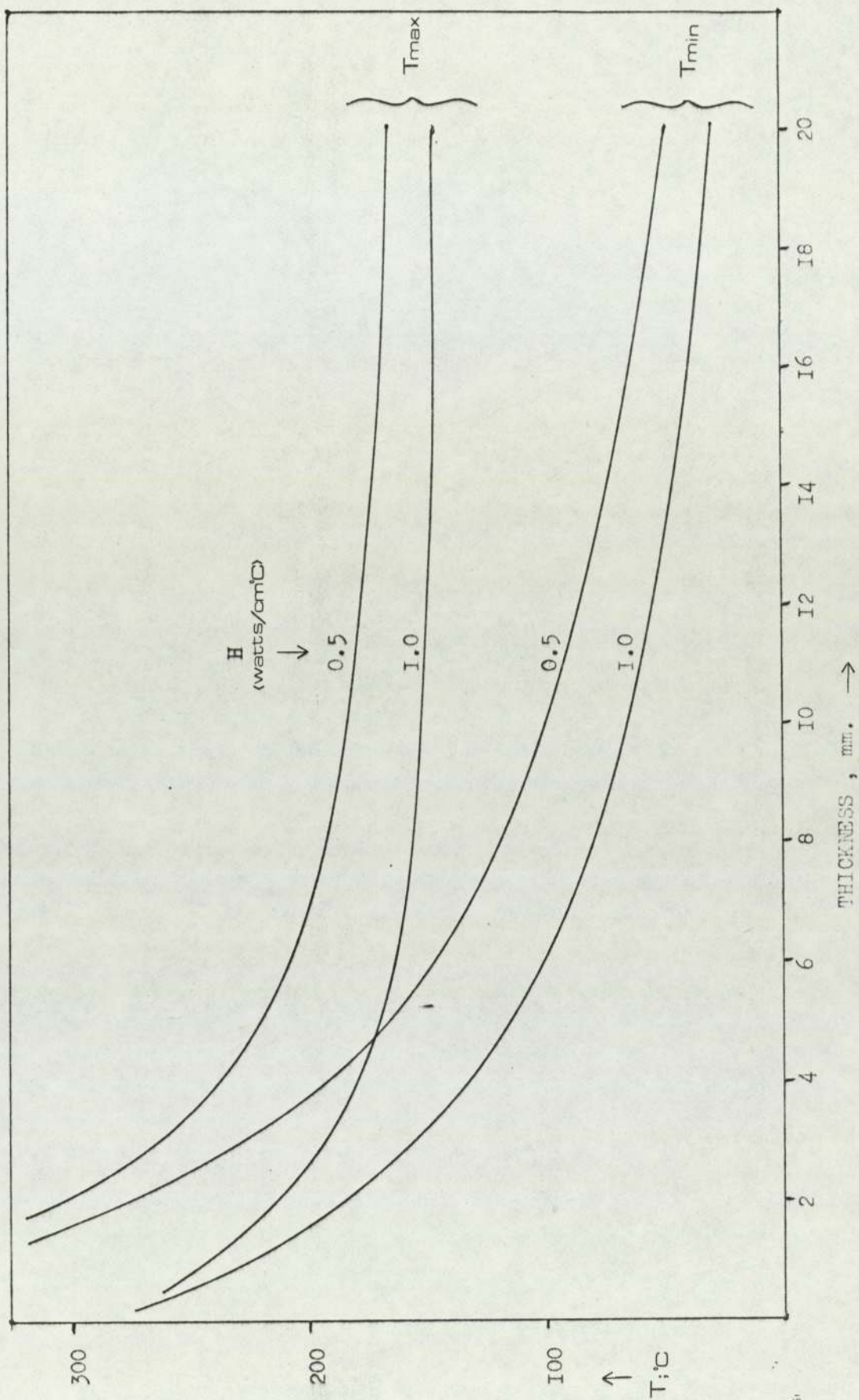


FIG. 29 : Beryllium Target

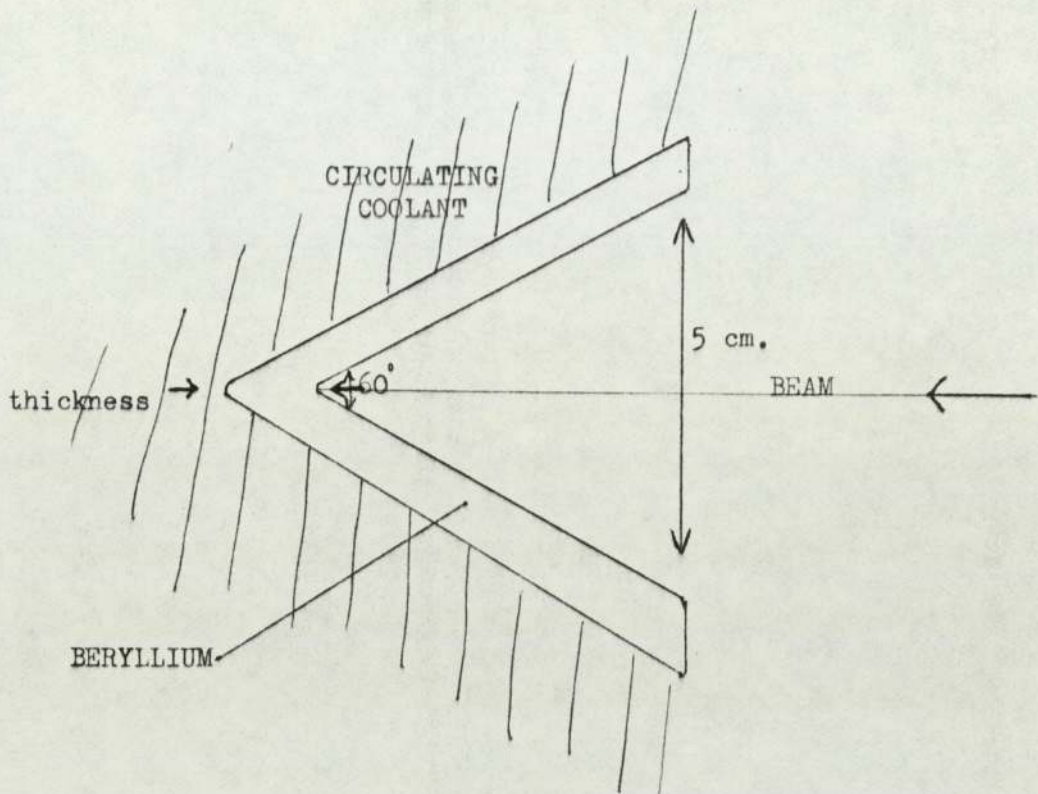


FIG. 30

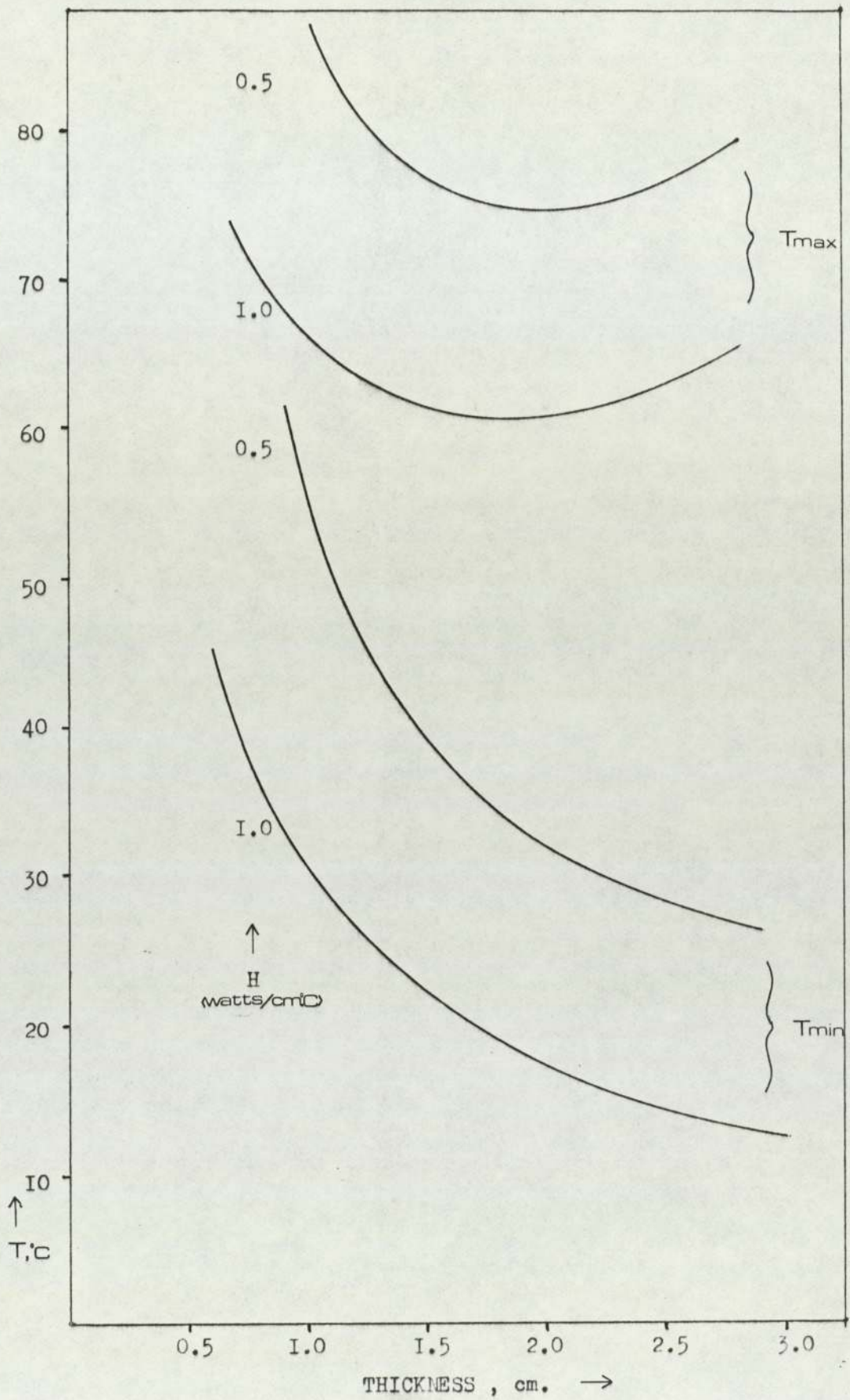


FIG. 31 : Conical Beryllium Target

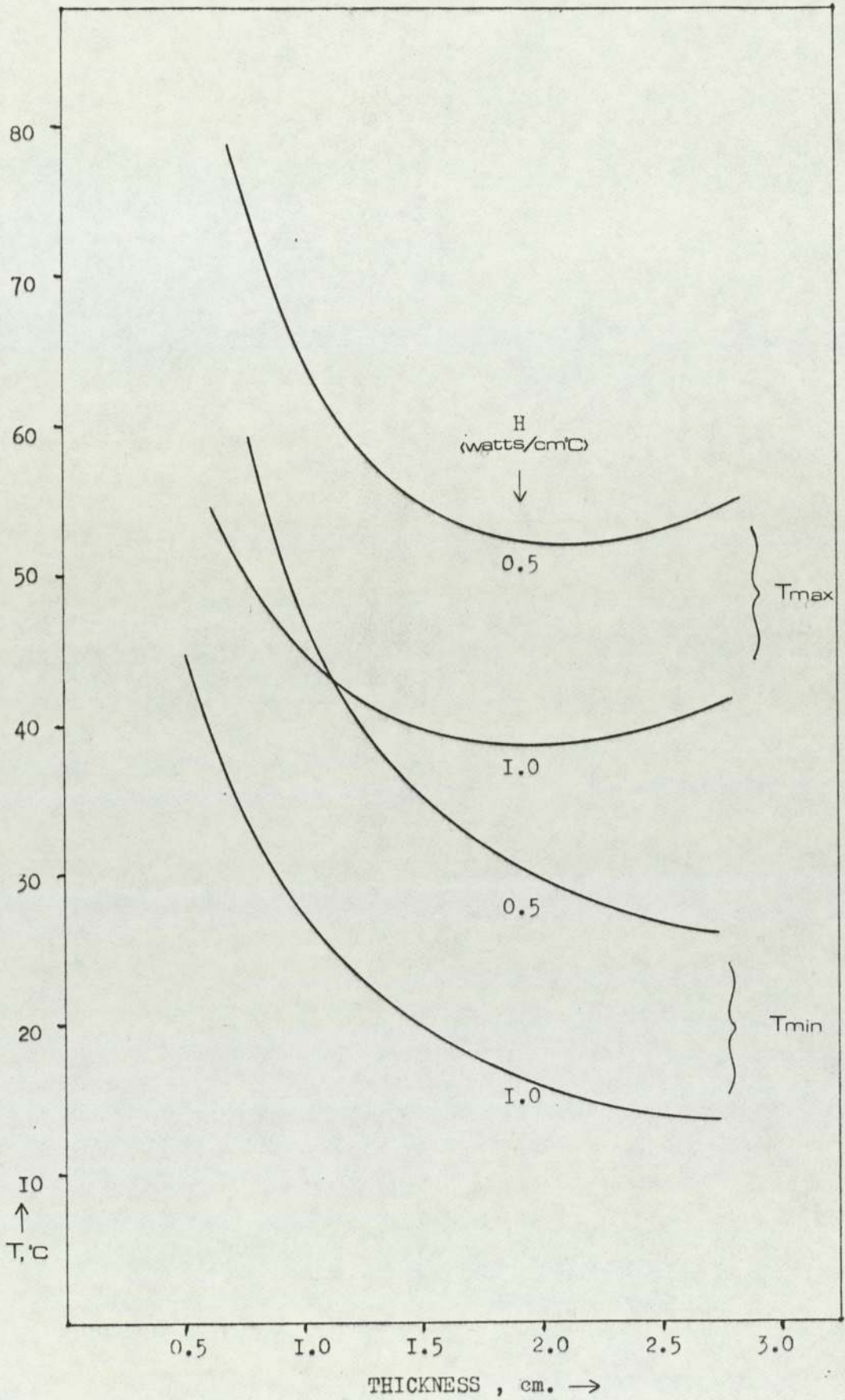


FIG. 32 : Conical Copper Target